

## Refined Permian–Triassic floristic timeline reveals early collapse and delayed recovery of south polar terrestrial ecosystems

# Chris Mays<sup>1,†</sup>, Vivi Vajda<sup>1</sup>, Tracy D. Frank<sup>2</sup>, Christopher R. Fielding<sup>2</sup>, Robert S. Nicoll<sup>3</sup>, Allen P. Tevyaw<sup>2</sup>, and Stephen McLoughlin<sup>1</sup>

<sup>1</sup>Swedish Museum of Natural History, Box 50007 S-104 05 Stockholm, Sweden

<sup>2</sup>Department of Earth & Atmospheric Sciences, University of Nebraska-Lincoln, 126 Bessey Hall, Lincoln, NE 68588-0340, USA <sup>3</sup>72 Ellendon Street, Bungendore, NSW 2621, Australia

### **ABSTRACT**

The collapse of late Permian (Lopingian) Gondwanan floras, characterized by the extinction of glossopterid gymnosperms, heralded the end of one of the most enduring and extensive biomes in Earth's history. The Sydney Basin, Australia, hosts a nearcontinuous, age-constrained succession of high southern paleolatitude (~65-75°S) terrestrial strata spanning the end-Permian extinction (EPE) interval. Sedimentological, stable carbon isotopic, palynological, and macrofloral data were collected from two cored coal-exploration wells and correlated. Six palynostratigraphic zones, supported by ordination analyses, were identified within the uppermost Permian to Lower Triassic succession, corresponding to discrete vegetation stages before, during, and after the EPE interval. Collapse of the glossopterid biome marked the onset of the terrestrial EPE and may have significantly predated the marine mass extinctions and conodont-defined Permian-Triassic Boundary. Apart from extinction of the dominant Permian plant taxa, the EPE was characterized by a reduction in primary productivity, and the immediate aftermath was marked by high abundances of opportunistic fungi, algae, and ferns. This transition is coeval with the onset of a gradual global decrease in  $\delta^{13}C_{\text{org}}$  and the primary extrusive phase of Siberian Traps Large Igneous Province magmatism. The dominant gymnosperm groups of the Gondwanan Mesozoic (peltasperms, conifers, and corystosperms) all appeared soon after the collapse but remained rare throughout the immediate post-EPE succession. Faltering recovery was due to a succession of rapid and severe climatic stressors until at least the late Early Triassic. Immediately prior to the

†chris.mays@nrm.se.

GSA Bulletin;

Smithian-Spathian boundary (ca. 249 Ma), indices of increased weathering, thick redbeds, and abundant pleuromeian lycophytes likely signify marked climate change and intensification of the Gondwanan monsoon climate system. This is the first record of the Smithian-Spathian floral overturn event in high southern latitudes.

### INTRODUCTION

Several mass extinction intervals in Earth's history have been linked to rapid warming driven by elevated levels of greenhouse gases (Bond and Wignall, 2014), e.g., the end-Triassic extinction (McElwain et al., 1999; Steinthorsdottir et al., 2011) and Toarcian oceanic anoxic event (McElwain et al., 2005; Suan et al., 2010). The end-Permian mass extinction (EPE), an episode of Earth history associated with the single greatest loss of biodiversity, is no exception. Extreme warming driven by greenhouse gas emissions from the Siberian Traps Large Igneous Province has been implicated as a proximate cause of this cataclysm (Brand et al., 2012; Payne and Clapham, 2012; Song et al., 2014; Burgess et al., 2017). Approximately 50% of marine invertebrate families were eliminated during this episode of extinctions (Raup and Sepkoski, 1982; Alroy et al., 2008), ~81% of marine fossil species disappeared (Stanley, 2016), and it is the only mass extinction interval with a similar impact on both marine and terrestrial faunas (Benton, 1995; Labandeira, 2005).

The global fossil record of terrestrial floras reveals a greater species turnover between the Permian and Triassic than any other interval in Earth's history (McElwain and Punyasena, 2007; Cascales-Miñana et al., 2016). Although it has been argued that floral diversity changes across the EPE were modest compared to animals (e.g., Schneebeli-Hermann et al., 2017; Nowak et al., 2019), a major terrestrial ecosystem collapse is represented by the apparently synchronous

disappearance of coals across Gondwana (Retallack et al., 1996), the extinction of the primary coal-forming glossopterid gymnosperms (Class Dictyopteridiopsida; McLoughlin, 2011), and the disappearance of key herbaceous to arborescent accessory taxa including a range of sphenophytes, ferns, cordaitaleans, and conifers (Hill et al., 1999). Glossopterids constituted an overwhelming proportion of the Lopingian (late Permian) terrestrial biomass across Gondwana (e.g., Miller et al., 2016) and were the keystones of Lopingian component communities incorporating a broad range of invertebrates, vertebrates, and fungi (Zavada and Mentis, 1992; Prevec et al., 2009; Slater et al., 2012, 2015). Consequently, the loss of these primary producers would have had an unprecedented impact on herbivore populations (van de Schootbrugge and Gollner, 2013) even if gross plant diversity changes were modest.

Systematic analysis of the amplitude and timing of floral productivity changes across the Permian-Triassic will elucidate the progressive patterns of environmental change and the catastrophic diversity losses at higher trophic levels. Moreover, previous reports of a few glossopterids post-dating the initial stages of the EPE interval in Gondwana (see Bomfleur et al., 2018) require testing to assess the timing and significance of relictual communities that might have harbored plant groups that seeded subsequent taxonomic radiations in the Triassic. It is particularly relevant to establish the pace and extent of extinction and recovery in high-latitude biomes, which may have provided the optimal settings for the persistence of thermophobic and hygrophilic plant communities preferring cool and moist environments, while illuminating the adaptations promoting their survival. In this paper, we document the floristic changes from the end-Permian ecological collapse through the stepwise pattern of vegetation recovery in the southern high-latitude Lower Triassic succession of the Sydney Basin, eastern Australia. This floristic succession

https://doi.org/10.1130/B35355.1; 12 figures; Data Repository item 2020024.

provides context for the interpretation of climatic shifts and other global events through the latest Permian and Early Triassic.

## Timing of the End-Permian Extinction and Permian-Triassic Boundary

In continental settings, the EPE has traditionally been interpreted as a single, rapid destabilization and collapse of the terrestrial biosphere (e.g., Visscher et al., 1996), whereas in the marine realm at least two prominent stages of extinction have been identified, e.g., at the Permian-Triassic boundary (PTB)type section at Meishan, southern China (Jin et al., 2000; Yin et al., 2012; Song et al., 2013). These extinction pulses, and their associated sharp carbon isotope excursions, are separated by ~60 k.y. (Burgess et al., 2014) and have been employed to define an "extinction interval." Furthermore, the marine record shows a long-term carbon isotope excursion that predates the primary extinction phase and the PTB by more than one million years, which could indicate a prolonged disruption of the global carbon cycle (Korte and Kozur, 2010). Complex, multi-stage extinctions are consistent with the leading hypothesized cause of the EPE: massive, sustained, or episodic outgassing from Siberian Traps Large Igneous Province magmatism (Benton and Newell, 2014; Cui and Kump, 2015; Burgess et al., 2017). Although the onset of a terrestrial "extinction interval" can be readily identified by the abrupt loss of peat-forming plants (e.g., Retallack et al., 1996), the timing and patterns of terrestrial extinction and recovery are far less well constrained than those of the marine record at present.

The identification of the PTB in continental strata has been confounded because: (1) the system boundary is defined by the first appearance of a marine conodont index taxon, Hindeodus parvus (Mei et al., 1998; Metcalfe and Nicoll, 2007), and (2) this bioevent is not coeval with the initial stage of the end-Permian extinction interval (Song et al., 2013; Burgess et al., 2014). Attempts to place the PTB in terrestrial successions have generally employed a combination of palynostratigraphic, lithostratigraphic, and magnetostratigraphic markers (e.g., southern Africa, Smith and Botha-Brink, 2014, Gastaldo et al., 2015; Antarctica, Retallack et al., 2005, Lindström and McLoughlin, 2007; China, Bercovici et al., 2015, Bercovici and Vajda, 2016; Russia, Taylor et al., 2009; Svalbard, Hounslow and Nawrocki et al., 2008). However, there are no regionally extensive event beds or fossil indices available for consistent, broad geographic correlation of the PTB in terrestrial settings, in contrast to the widely distributed and well-delineated boundary clay of the end-Cretaceous event (Schulte et al.,

2010; Esmeray-Senlet et al., 2017). Consequently, terrestrial biostratigraphic studies have proposed widely disparate placements of the system boundary, especially in regions remote from the stratotype section. For example, some have placed the PTB in stratigraphical proximity to the terrestrial EPE (e.g., Laurie et al., 2016), whereas others have favored its placement much higher in the stratigraphic successions (e.g., Looy et al., 2001; Lindström and McLoughlin, 2007; Gastaldo et al., 2015; Zhang et al., 2016). Independent proxies have been increasingly employed to correlate both the PTB and EPE over broad regions, such as U-Pb radiogenic-isotope ages (Burgess et al., 2014; Metcalfe et al., 2015), stable carbon isotope trends (e.g., Morante, 1996; Korte and Kozur, 2010), and/or other geochemical signatures (e.g., Grice et al., 2005; Williams et al., 2012, 2017). The combination of radioisotopic geochronology, chemostratigraphy, and highresolution biostratigraphy currently provides the most robust method for dating and correlating the key terrestrial bioevents associated with the Permian-Triassic transition and other complex ecological turnovers in Earth's history.

### Permian-Triassic Palynostratigraphy of Gondwana

The Permian-Triassic palynostratigraphic schemes most widely employed across Gondwana were established on Australian successions (Foster, 1982; Helby et al., 1987; Price, 1997; Mantle et al., 2010; Fig. 1). Independent correlation proxies in eastern Australia have resulted in arguably the best age-constrained terrestrial Permian to Lower Triassic palynostratigraphic scheme in the world (Stephenson, 2018). These proxies have included stable carbon isotopes (Morante, 1996; Williams et al., 2017), lithostratigraphic markers (Michaelsen, 2002; Wheeler et al., 2019), and recent radiogenic-isotope ages from U-Pb chemical abrasion-isotope dilution-thermal ionization mass spectrometry (CA-ID-TIMS) of zircons (Metcalfe et al., 2015; Ayaz et al., 2016; Phillips et al., 2018; Fielding et al., 2019). These data support approximately synchronous Lopingian (upper Permian) to Lower Triassic palynological zones across eastern Australia (Laurie et al., 2016). Despite this, the precise stratigraphic positions of the PTB and EPE have remained ambiguous owing to a paucity of absolute age constraints for strata overlying the uppermost Permian coals.

The bio- and lithostratigraphic events long-considered concurrent with the PTB boundary (e.g., loss of glossopterid floras: Balme, 1969; Foster et al., 1997; cessation of peat-forming conditions: Retallack et al., 1996) are now considered to be indicators of the terrestrial EPE,

which occurred long before the system boundary *sensu stricto* based on correlations with the stratotype section at Meishan, South China. With recent improved chronostratigraphic controls on the Sydney-Gunnedah-Bowen basin succession (Metcalfe et al., 2015; Laurie et al., 2016; Fielding et al., 2019), the Lopingian to Lower Triassic palynozones of eastern Australia have been recalibrated herein (Fig. 1). This refined timeline provides the context for interpreting the stageby-stage extinctions and recoveries of the latest Permian to Early Triassic south polar floras.

### **Geological Setting**

During the Permian and Triassic, the Sydney Basin was situated at ~65–75°S (Veevers, 2006), and it was the southernmost component of the Sydney-Gunnedah-Bowen basin complex. This large foreland basin system and the continental volcanic belt to its east, the New England Orogen, developed in association with active subduction of Panthalassan oceanic crust along the eastern margin of Gondwana (Fig. 2A; Waschbusch et al., 2009). The modern onshore Sydney Basin is in eastern New South Wales, Australia (Fig. 2B) and forms a broad synclinorium with an onshore areal extent of >60,000 km2. It hosts a >5000-m-thick Cisuralian-Middle Triassic succession (Tadros, 1995); the Early-Middle Triassic succession alone comprises 1350 m of strata in the axis of the basin near Sydney (Herbert, 1997a). The upper Permian succession is especially significant in hosting numerous bituminous coal seams that represent some of the world's largest steaming- and coking-coal resources (Agnew et al., 1995). Coastal exposures of the Permian-Triassic transition occur in the northern (near Catherine Hill Bay) and southern (near Wollongong) parts of the basin (Fig. 2C).

The Illawarra and Newcastle coal measures constitute the Lopingian successions of the southern and northern Sydney Basin, respectively. These units are characterized by intercalated sandstone, mudstone, and conglomerate facies typical of coastal-plain and deltaic deposits. Fining-upward cycles within these deposits are typically capped by prominent coal seams that represent the development of thick forest mires on floodplains flanking predominantly large, sandy-bed fluvial channels (Brakel, 1986; Bamberry et al., 1995; Tadros, 1995; Herbert, 1997b). The overlying Narrabeen Group spans almost the entirety of the Lower Triassic (Metcalfe et al., 2015). This unit is characterized by laterally extensive, sandstone-dominated, fining-upward alluvial plain deposits lacking coals but containing significant packages of gray, green, and red mudrocks (Emerson and Branagan, 2011). A predominantly southward drainage pattern with

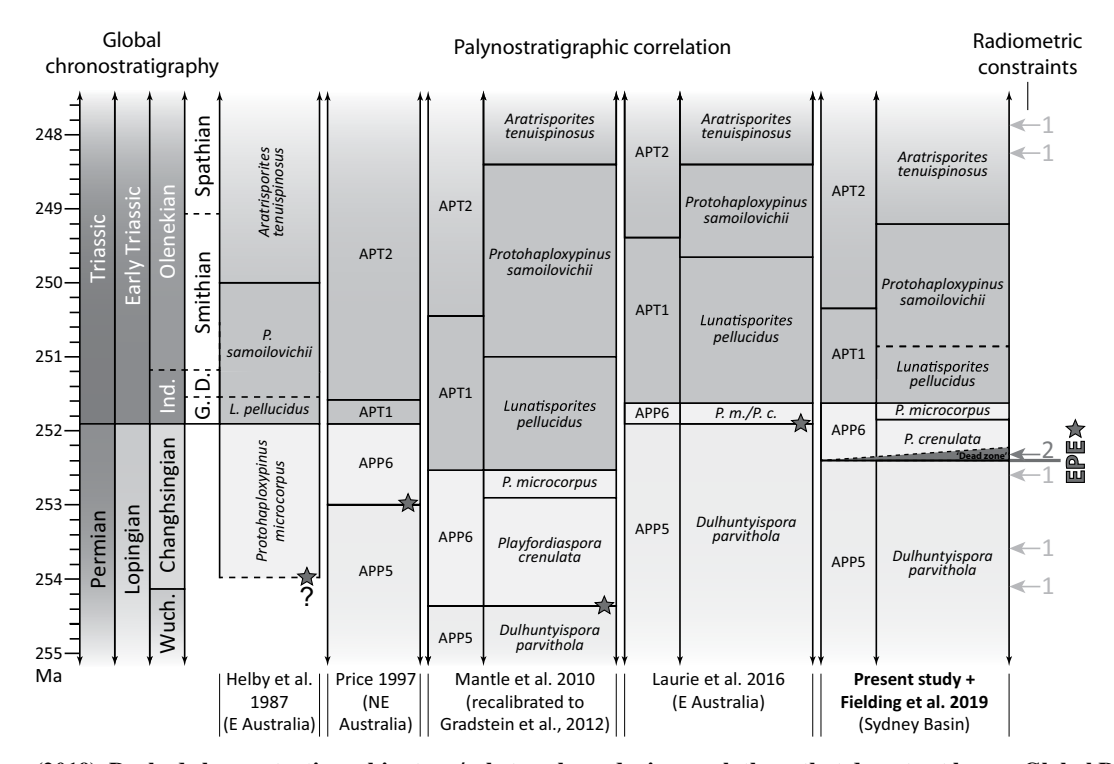


Figure 1. Chart of eastern Australian palynostratigraphic schemes showing different correlations to the international timescale and contrasting placements of the Permian-Triassic boundary by various authors. Global chronostratigraphy calibrated using the following sources: Wuchiapingian (Wuch.)-Changhsingian (Cohen et al., 2013); Permian-Triassic (Burgess et al., 2014); Griesbachian (G.)-Dienerian (D.; Ovtcharova et al., 2006); Smithian-Spathian (this study); Dienerian-Smithian (= Induan [Ind.]-Olenekian; Ovtcharova et al., 2006; Gradstein et al., 2012; Cohen et al., 2013). Arrows indicate radiogenic-isotope (U-Pb zircon) age constraints within the Sydney Basin: 1—Metcalfe et (2015); 2—Fielding

(2019). Dashed chronostratigraphic stage/substage boundaries mark those that do not yet have a Global Boundary Stratotype Section and Point and lack well-constrained absolute ages. Dashed biostratigraphic zone boundaries indicate placements with relatively poor age control. "Dead zone" refers to the palynomorph-poor zone identified within the northern Sydney Basin by Vajda et al. (2020). EPE—onset of the terrestrial end-Permian mass extinction interval. Star indicates the approximate placement of the EPE for each scheme.

additional contributions from transverse river systems east- and westward has been determined from paleocurrent indices (Ward, 1972; Cowan, 1993; Tadros, 1995; Herbert, 1997a). Subsidence progressed faster to the northeast, thus accommodating a much thicker and more continuous succession in the region between Sydney and Newcastle (Herbert, 1997a).

Traditionally, a major unconformity has been inferred across much of the Sydney Basin at or near the Permian-Triassic system boundary between the Newcastle Coal Measures and the overlying Narrabeen Group (Helby, 1973; Herbert, 1980; Herbert, 1997a). However, recent radiogenic-isotope ages have demonstrated minimal to no discernible time gap at this contact in sections where the uppermost Permian has not been removed by fluvial downcutting (Metcalfe et al., 2015; Fielding et al., 2019). The welldefined lithostratigraphic contact between these units reflects an abrupt cessation of peat-forming conditions across Gondwana for several million years (Retallack et al., 1996, 2011). Above the PTB in eastern Australia, the first occurrence of minor coaly laminae is within the Terrigal Formation (Spathian: ca. 248 Ma), but significant coal deposits are not represented until accumulation of the Nymboida Coal Measures of northern New South Wales in the Middle Triassic (Retallack et al., 1993; Wells, 1995). Some authors have interpreted a prolonged change in the style of terrestrial sedimentation across Australian basins at or near the PTB (Michaelsen, 2002), with synchronous changes across other regions of Gondwana (Antarctica, Webb and Fielding, 1993; India, Sarkar et al., 2003; South Africa, Ward et al., 2000, Pace et al., 2009) and beyond (e.g., Arche and López-Gómez, 2005; Sephton et al., 2005; Newell et al., 2010). However, the nature and severity of the depositional transition in Gondwana has been disputed. For example, in Antarctica, forest-derived paleosols are common features of both upper Permian and Lower Triassic strata (Retallack and Krull, 1999), and apart from a clear lack of peat formation in the Early Triassic, the Sydney Basin reveals only limited evidence of change in fluvial sedimentation style (Fielding et al., 2019). The stratigraphic successions in the Sydney Basin examined in this study offer a near-continuous and age-constrained perspective of southern high-latitude continental depositional environments through the Lopingian to late Early Triassic.

### MATERIALS AND METHODS

### Well Cores and Sedimentology

All data in this study derive from two well cores: (1) Pacific Power Hawkesbury

Bunnerong DDH 1 (PHKB-1), central Sydney Basin (lat: 33° 58′ 17.61"S; long: 151° 13′ 43.52"E); and (2) Coalcliff Colliery DDH 27 (CCC-27), southern Sydney Basin (lat: 34° 13' 25.28"S; long: 150° 56′ 50.67"E). Core samples and plant fossils were collected from the W.B. Clarke Geoscience Centre drillcore library, Londonderry, New South Wales, Australia. Both well cores were logged for sedimentological and macropaleontological features, and these logs are presented graphically (Figs. 3 and 4). PHKB-1 was selected as the primary reference well because of its position near the synclinal axis of the Sydney Basin and its great thickness (>1260 m) of upper Permian-Lower Triassic strata. CCC-27 provides a continuous record of the PTB succession in the southeastern Sydney Basin, which can be related directly to the adjacent and laterally extensive coastal exposures at Coalcliff, New South Wales, sampled for zircon dating (Fielding et al., 2019). For both CCC-27 and PHKB-1, most of the strata from the uppermost coal seam (Bulli Coal) were removed for analysis soon after drilling, so these could not be documented herein.

Sedimentation rates were calculated from the ten U-Pb zircon absolute ages for the Sydney Basin by Metcalfe et al. (2015). These were correlated to PHKB-1 by Fielding et al. (2019), who recorded an additional absolute date from

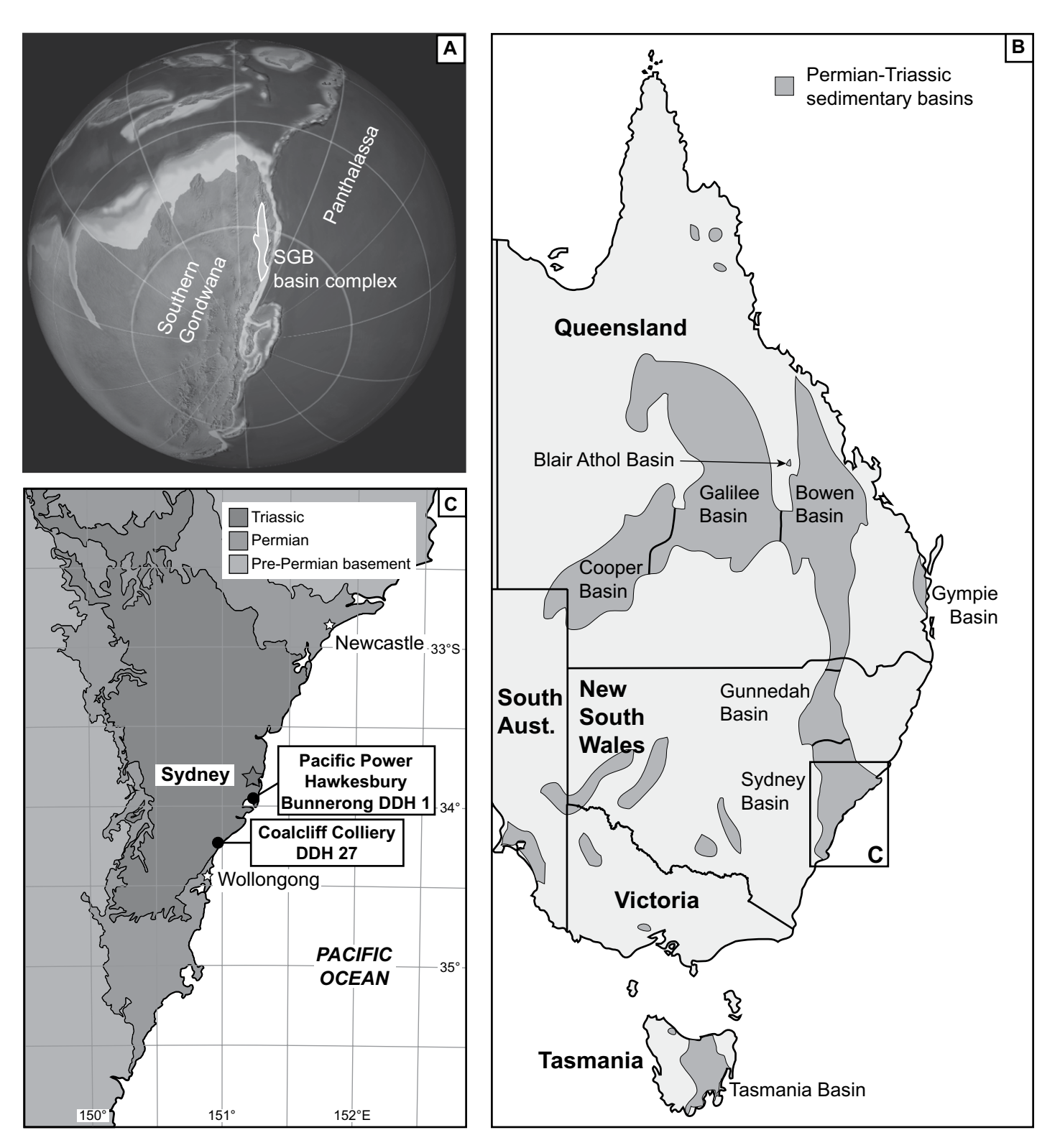


Figure 2. (A) Permian–Triassic (ca. 250 Ma) paleogeography of southern Gondwana, oblique south polar perspective; SGB—Sydney-Gunnedah-Bowen, modified from Blakey (2016). (B) Map of modern eastern Australia including the sedimentary basins active during the Permian–Triassic. (C) Generalized geological map of the Sydney Basin with source locations of well cores examined in this study, Pacific Power Hawkesbury Bunnerong DDH 1 (PHKB-1) and Coalcliff Colliery DDH 27 (CCC-27). Geology simplified from New South Wales Geological Survey 1:500,000 Special Sheet Map of the Sydney Basin (1969).

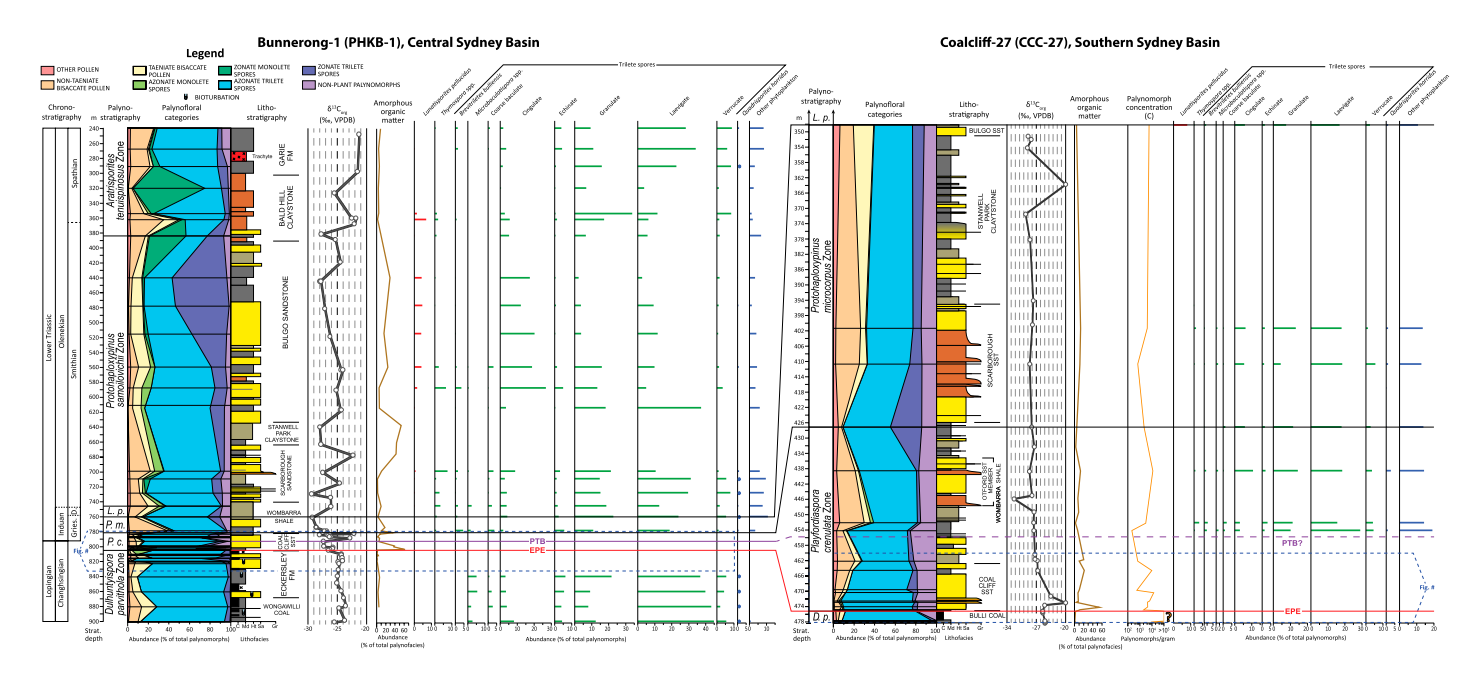


Figure 3. Broad-scale stratigraphy and correlations between the reference well Bunnerong-1 (PHKB-1, central Sydney Basin) and Coal-cliff-27 (CCC-27, southern Sydney Basin). Intervals near the terrestrial end-Permian mass extinction (EPE) for both wells are expanded in Figure 4. PTB—probable Permian—Triassic boundary; the position of this horizon for CCC-27 has not been well constrained in this study. Vertical scale of CCC-27 is exaggerated relative to PHKB-1 for clarity. "?" indicates samples for which accurate concentration values could not be displayed because they exceeded the maximum estimates permitted by the method employed herein (see Table A3; see footnote 1). Abundance columns: red—pollen; green—cryptogam spores; blue—non-plant palynomorphs. *L. p.—Lunatisporites pellucidus* Zone; C—coal; Md—mudrock; Ht—heterolithic facies (interlaminated siltstone and sandstone); Sa/SST—sandstone; Gr—conglomerate; Fm—Formation; Gries.—Griesbachian; D.—Dienerian. PHKB-1 litho-, bio-, and palynofacies and δ<sup>13</sup>C<sub>org</sub> data from Fielding et al. (2019). Chronostratigraphy updated from Fielding et al. (2019).

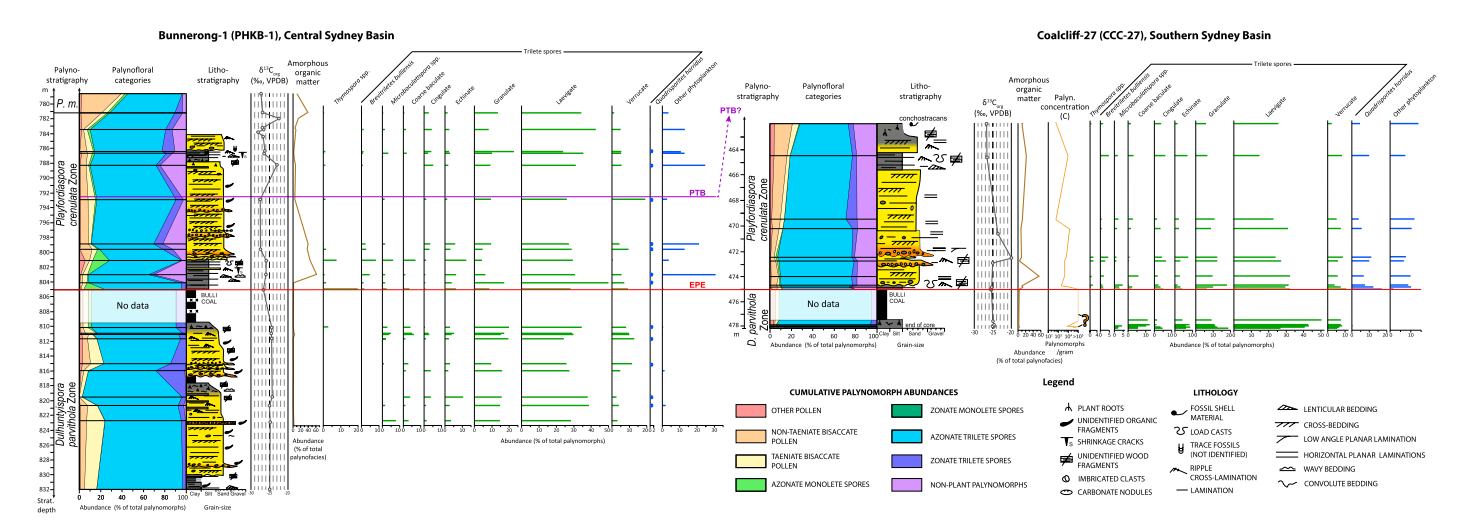


Figure 4. Stratigraphy and correlations of the terrestrial end-Permian mass extinction interval (EPE) between the reference well Bunnerong-1 (PHKB-1, central Sydney Basin) and Coalcliff-27 (CCC-27, southern Sydney Basin). See Figure 3 for the broader stratigraphic contexts of these wells. PTB—probable Permian—Triassic boundary; the position of this horizon for CCC-27 has not been well-constrained in this study. Vertical scale of CCC-27 is relatively exaggerated for clarity; no palynological data were recovered from the coal seam immediately underlying the EPE horizons of both wells because of a lack of available core for analysis. "?" indicates samples for which accurate concentration values could not be displayed because they exceeded the maximum estimates permitted by the method employed herein (see Table A3; see footnote 1). Abundance columns: green—cryptogam spores; blue—non-plant palynomorphs. *P. m.—Protohaploxypinus microcorpus*. Lithostratigraphy of both wells and biostratigraphic, palynofacies, and  $\delta^{13}C_{org}$  data of PHKB-1 from Fielding et al. (2019).

the Coal Cliff Sandstone (252.31  $\pm$  0.07 Ma). We subdivided the strata of PHKB-1 into two distinct successions based on their predominant depositional regimes. The lower stratigraphic succession (>980 m depth in PHKB-1) was deposited primarily under marine conditions (marine shelf) or peat-forming deltaic/coastal-plain settings, whereas the upper portion (<980 m depth in PHKB-1) was deposited primarily in terrestrial settings (coastal and alluvial plain; Fielding et al., 2019). Simple linear functions of sediment accumulation rates for these successions were derived assuming uniform compaction and constant deposition within each portion of the succession. Where indicated, chronostratigraphic placements of zone boundaries were estimated by interpolating these accumulation rates from the probable age of the top of the Bulli Coal (ca. 252.4 Ma), which is the uppermost bed of the Illawarra Coal Measures.

### Palynology

Seventy-eight well core samples were analyzed in this study; 52 samples from PHKB-1 and 26 from CCC-27. Palynological samples were processed at Global Geolab, Medicine Hat, Canada. Samples were digested using hydrochloric (HCl) and hydrofluoric (HF) acids to remove inorganic mineral content. Kerogen slides were produced for each sample for palynofacies analysis; organic residues were subsequently oxidized with Schulze's Solution, sieved using a 10 µm nylon mesh, then mounted on glass slides for palynomorph identification

and quantitative assessment. Index spore-pollen taxa were counted from both sieved and kerogen slides. All palynomorph images were acquired using a Zeiss Axioskop 2 Plus transmitted light microscope equipped with a Zeiss AxioCam MRc camera. All palynological figures are composite images of multiple microphotographs taken at different focal depths (see Bercovici et al., 2009); these were processed digitally with the "Auto-Blend Layers" function in Adobe Photoshop CC 2018. All palynological slides are provided with prefix "S" and housed at the Department of Palaeobiology, Naturhistoriska riksmuseet, Stockholm, Sweden. Detailed palynological count methods and productivity estimates are provided in Appendix 11. Taxonomic categories for palynomorph counts are in Table A2, and palynomorph and palynofacies count data are presented in Table A3 and Table A4, respectively.

Biostratigraphic correlations were based on palynozone definitions by Foster (1982), Helby et al. (1987), and Price (1997). Radiogenic-isotope age controls for the Sydney Basin were provided by Metcalfe et al. (2015) and Fielding et al. (2019); palynozones were calibrated to the global geochronological scheme by Laurie et al. (2016) and further developed herein (see Fig. 1).

<sup>1</sup>GSA Data Repository item 2020024, Appendix 1, Tables A1–A7, and color versions of all figures, is available at http://www.geosociety.org/datarepository/2020 or by request to editing@geosociety.org.

#### **Ordination Data Analysis**

To gauge whether differences between palynological assemblages represented discrete floristic stages or were better explained by geographic position or local depositional conditions, the quantitative palynofloral data were tested statistically by ordination analyses. The palynomorphs were categorized as outlined in Table A5 (see footnote 1). These categories were tested for (dis)similarities between palynomorph samples as a function of the following three variables: (1) palynostratigraphic zones, as a proxy of the age relative to the terrestrial end-Permian extinction (EPE); (2) sample lithofacies; and (3) geographic position (wells PHKB-1 and CCC-27). It was predicted that all three of these variables would contribute to the differences in palynomorph assemblages but that the pre-EPE and post-EPE zones would be most dissimilar.

Non-metric multidimensional scaling (nMDS) was selected for this analysis because it has long been shown to yield reliable results for ecological data (Minchin, 1987) with promising results in paleopalynological applications (e.g., Bowman et al., 2014; Slater and Wellman, 2015). NMDS ordination is a non-parametric method for discerning similarity between rank-ordered samples and provides a visual representation on a minimal number of axes (Hammer and Harper, 2006). Specifically, samples that are similar in composition plot relatively close in the projected ordination space. All nMDS scaling analyses were plotted in two dimensions (Fig. 5); the resulting stress values of the different data sets (transformed

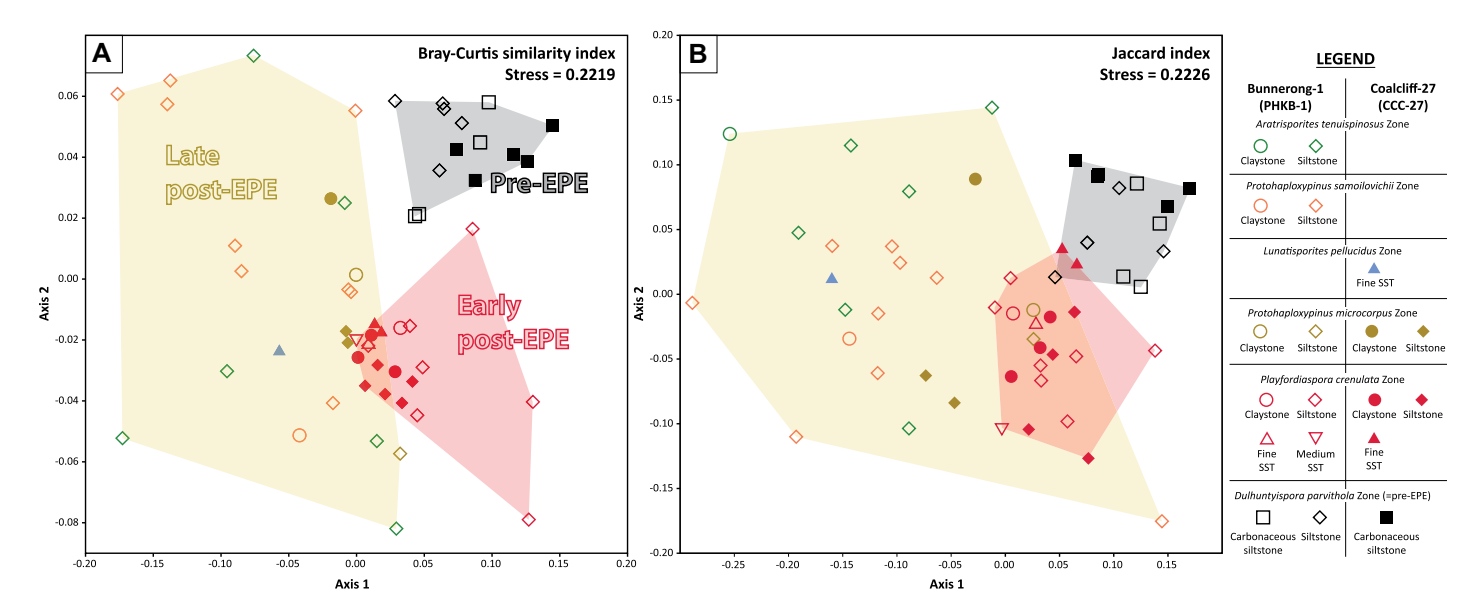


Figure 5. Non-metric multidimensional scaling (nMDS) plots of palynomorph group data. (A) Relative abundance (square root transformed); (B) presence/absence (binary). Gray-shaded area—pre-end-Permian mass extinction event (EPE) samples (= *Dulhuntyispora parvithola* Zone); red shaded area—*Playfordiaspora crenulata* Zone; yellow shaded area—other post-EPE samples. SST—sandstone; med.—medium. Note: one outlier sample was excluded from the abundance plot (S014134) for illustration in A.

abundance, untransformed abundance, and binary) were relatively low and similar (= 2.1–2.2). The replicability of these different tests suggests that the trends in the data were reliable. Ordination analyses were performed using the program Palaeontological Statistics (PAST, v.3.22; Hammer et al., 2001). Additional details of the ordination analyses are provided in Appendix 1.

#### **Stable Carbon Isotopes**

Stable carbon isotope data for bulk organic matter ( $\delta^{13}C_{org}$ ) were collected from 108 samples of PHKB-1 and 33 samples of CCC-27 (Table A6; see footnote 1). Most of the palynological samples were derived from corresponding  $\delta^{13}C_{\rm org}$ sample levels. In preparation for analysis, samples were powdered, reacted for 24 h with 1N HCl at room temperature to remove inorganic carbon, and rinsed three times in ultra-pure water. Following each rinse, the supernatant was separated by centrifugation and discarded. Samples were then dried in an oven at 40 °C and crushed using an agate mortar and pestle. Carbon isotope compositions were measured using a Costech 4010 Element Analyzer connected to a Thermo Finnigan MAT 253 stable-isotope gas-ratio mass spectrometer in the W.M. Keck Paleoenvironmental and Environmental Stable Isotope Laboratory at the University of Kansas. Carbon isotope compositions of the bulk organic matter fractions are reported in permil (%o) relative to the Vienna Peedee Belemnite standard (V-PDB). Analyses of powdered dogfish remains (DORM) certified working standards were reproducible to better than  $\pm 0.11\%$  (1 $\sigma$  SD) for  $\delta^{13}$ C.

#### RESULTS

### Sedimentology and Lithostratigraphy

The uppermost succession of the Illawarra Coal Measures in PHKB-1 (Wongawilli Coal, Eckersley Formation, Bulli Coal) consists of an array of erosionally based, single to multi-story sandstone bodies (with minor pebble conglomerate and pebbly sandstone), heterolithic (thinly interbedded to interlaminated) sandstones and siltstones, mudrocks, and coals with common light-colored beds of tuff (Fig. 3). The coals are associated with well-developed hydromorphic paleosols (Retallack, 1999). Sandstone bodies preserve heterolithic partings, some of which incorporate rhythmic interlamination of sand and mud, synaeresis cracks, and a sporadically distributed, low-diversity suite of simple trace fossils. These partings and the thicker intervals of heteroliths host various interlamination features (pinstripe, lenticular, wavy, and flaser bedding) with abundant soft-sediment deformation structures. Plant debris is also ubiquitous, ranging from large axes to macerated "coffee grounds," together with coaly traces and in situ roots. Above the uppermost coal seam (Figs. 3 and 4), facies are broadly similar but lack coal, and initially lack plant debris before it reappears after a few meters of vertical section. The coloration of mudrocks becomes steadily more pronounced above the Bulli Coal, changing from medium gray to initially light gray with increasing blue and yellow hues upward. Tuffs are also almost entirely absent and thinner above the Bulli Coal.

The erosionally based sandstone bodies are interpreted as the deposits of laterally mobile sand bed rivers on a coastal plain. Multi-story sandstone bodies suggest an aggradational pattern of sediment accumulation facilitated by channel filling and lateral migration over time. A location within the coastal backwater zone is indicated for the lower part of the Illawarra Coal Measures by the presence of synaeresis cracks, trace fossils, and rhythmically laminated heterolithic partings, which indicate some tidal modulation of fluvial outflow currents.

Although the uppermost Permian section (upper Illawarra Coal Measures) contains abundant evidence of terrestrial plant colonization of substrates, the interval immediately above the Bulli Coal seam is devoid of plant fossils, suggesting abrupt biotic change at this level. The Bulli Coal is normally overlain by a regionally extensive package (generally <5 m thick) of gray siltstones. These siltstones are absent in some localities where overlying channel sandstones have been deposited on scour surfaces that extend down to the Bulli Coal. Impressions of gymnosperm logs (possibly *Voltziopsis*) and other woody debris are locally common in lag deposits within these channel sandstones.

The pronounced coloration of mudrocks higher in the Narrabeen Group is interpreted to reflect lowering of the water table soon after deposition, leading to partial or temporary oxidation of iron-bearing minerals in coastal-plain substrates. The continued presence of synaeresis cracks and trace fossils suggests the coastal-plain setting persisted for some time into the Triassic, gradually becoming more continental upward as these features dissipate.

We estimate (compacted) sediment accumulation rates of ~63 m/m.y. for the lower succession (marine shelf/delta/coastal-plain settings) and ~108 m/m.y. for the upper succession (coastal- and alluvial-plain settings) of PHKB-1 (Fig. 6).

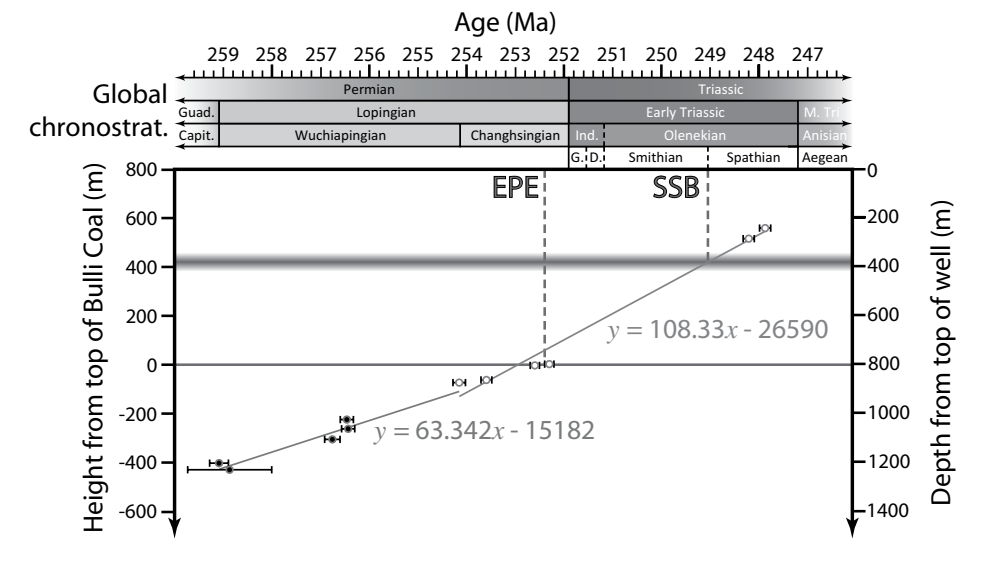


Figure 6. Scatterplot of U-Pb chemical abrasion-isotope dilution-thermal ionization mass spectrometry (CA-ID-TIMS) absolute age estimates from Metcalfe et al. (2015) and Fielding et al. (2019) and their correlative stratigraphic depths in PHKB-1. Age estimate error ranges =  $2\sigma$ . Filled circles—age estimates from strata formed in predominantly marine depositional settings (marine shelf and deltaic/coastal-plain); hollow circles—age estimates from predominantly terrestrial depositional settings (coastal and alluvial plain). Capit.—Capitanian; D.—Dienerian; G.—Griesbachian; Guad.—Guadalupian; Ind.—Induan; M. Tri.—Middle Triassic; EPE—onset of the terrestrial end-Permian mass extinction interval; SSB—estimated placement of the Smithian–Spathian boundary; chronostrat.—chronostratigraphy. For chronostratigraphic boundary calibrations, see Figure 1; additional calibrations from Cohen et al. (2013). Correlative placements of radiochronologic ages to PHKB-1, and paleoenvironmental interpretations from Fielding et al. (2019).

## Palynofloras, Macrofloras and Biostratigraphy

Six palynozones were identified in the studied succession. Representative palynofloral and macrofloral taxa for these zones are illustrated (Figs. 7–10) and the key features, stratigraphic distribution, and inferred ages of each zone are outlined below.

## Dulhuntyispora parvithola Zone (Mantle et al., 2010) = APP5 Zone (Price, 1997)

Composition. This zone has a distinctive but rather uniform palynological and macrofloral character, which distinguishes it clearly from the overlying zones. The D. parvithola Zone is characterized by: (1) a high abundance of laevigate trilete spores (Fig. 7C); (2) abundant Microbaculatispora and trilete spores with coarse baculae (Horriditriletes, Neoraistrickia, Raistrickia; Figs. 7A-7B and 7E); (3) diverse Dulhuntyispora (Price, 1983; Fig. 7F); (4) abundant pollen typical of glossopterids (Protohaploxypinus, Striatopodocarpites); and (5) a near total absence of phytoplankton. Relatively high palynomorph concentrations and organic productivity at the time of deposition are indicated by low counts of extrinsic Lycopodium spores in both palynomorph and palynofacies data sets (see Appendix 1 for productivity estimation methods). Strata assigned to this zone are also characterized by abundant macrofloral remains of glossopterid gymnosperms (Glossopteris, Figs. 8A-8F and 8H; Vertebraria, Figs. 8I-8K) and locally common representation of herbaceous sphenophytes (Paracalamites Fig. 8M; Phyllotheca Fig. 8L, Schizoneura). Charcoalrich laminae are common (Fig. 8N).

**Remarks.** The examined succession of the *D. parvithola* Zone in the two wells studied is equivalent to the upper portion of the informal APP5 biostratigraphic zone (Price, 1997), the upper *Dulhuntyispora* Assemblage Zone (Helby, 1973; Foster, 1979), or Upper Stage 5c (Price, 1983).

Stratigraphic depths of zone base. The base of this zone is at >900.22 m depth in PHKB-1 (>95.14 m below the top of the Bulli Coal) and >478.12 m depth in CCC-27 (>2.94 m below the top of the Bulli Coal); i.e., the zone base was not observed in either studied succession. This zone exceeds 95.19 m of strata in PHKB-1 and 2.97 m in CCC-27.

Estimated chronostratigraphic range. Numerous recent zircon U-Pb radiochronologic ages from tuff beds across eastern Australia have provided the *D. parvithola* Zone with the most well-constrained ages of any Permian palynostratigraphic unit in Gondwana (Laurie et al., 2016). These estimates have provided a

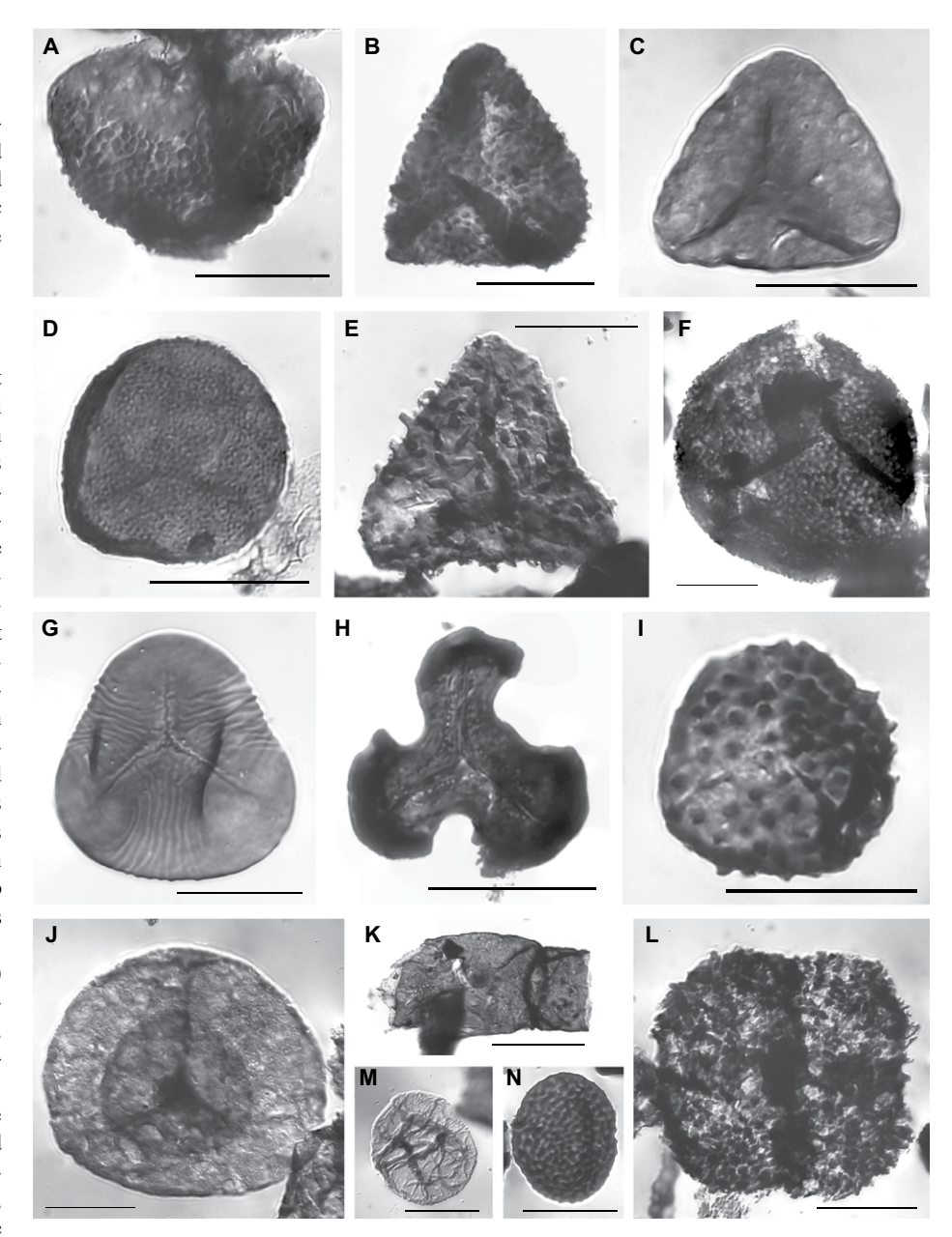


Figure 7. Characteristic palynomorphs of the *Dulhuntyispora parvithola* and *Playfordiaspora crenulata* zones, Sydney Basin, all scales = 20 μm; C, G, H, J, and M enlarged from Fielding et al. (2019), taxon authorities and specimen details are supplied in Table A7 (see footnote 1). (A–F) Common spores of the *D. parvithola* Zone; (A,B) *Microbaculatispora* sp. cf. *M. nodosa* (A, equatorial view; B, proximal view); (C) *Leiotriletes directus*; (D) *Cyclogranisporites gondwanensis*; (E) *Horriditriletes ramosus*; (F) *Dulhuntyispora parvithola*. (G–K) Index taxa of the *P. crenulata* Zone; (G) *Triplexisporites playfordii*; (H) *Triquitrites proratus*; (I) *Brevitriletes bulliensis*; (J) *Playfordiaspora crenulata*; (K) *Reduviasporonites chalastus*. (L–N) Palynomorphs with abundance spikes ("disaster taxa") within the basal *P. crenulata* Zone; (L) *Quadrisporites horridus*; (M) *Leiosphaeridia* sp.; (N) *Thymospora ipsviciensis*.

mid-Wuchiapingian age (ca. 258.0 Ma) for the lower boundary (Metcalfe et al., 2015; Ayaz et al., 2016; Phillips et al., 2018) and a Changhsingian age (ca. 252.3–252.6 Ma) for the upper boundary (Metcalfe et al., 2015; Fielding et al., 2019; Fig. 1). See the *Playfordiaspora crenulata* 

Zone section below for further discussion of the upper boundary.

#### Playfordiaspora crenulata Zone (Foster, 1982)

**Composition.** The base of this zone is identified by the first appearance data of *Triplexisporites* 

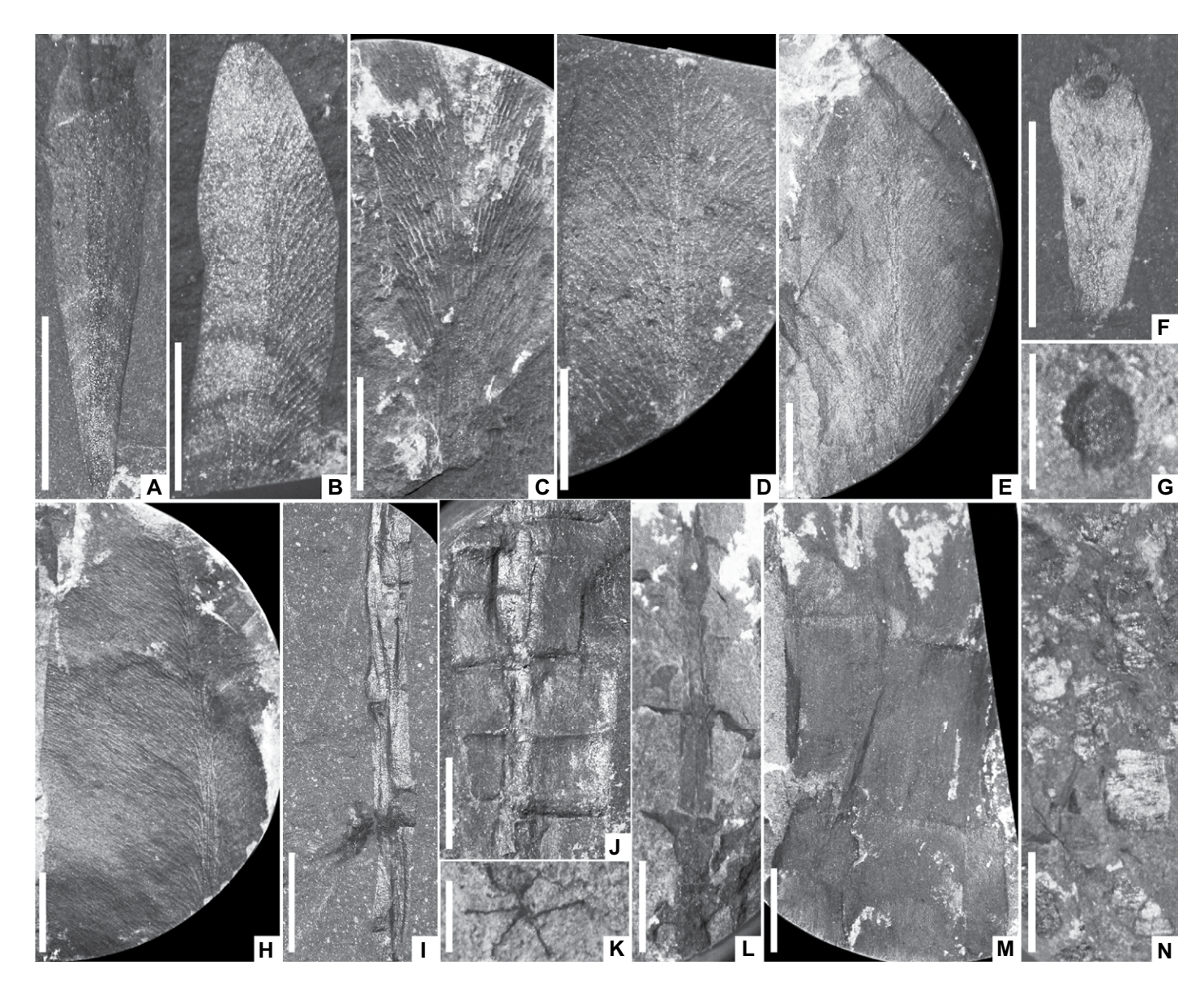


Figure 8. Permian plants from PHKB-1 (A–I, K–N) and CCC-27 (J) wells. (A) Glossopteris xiphophylla, 844.43 m. (B) Glossopteris xiphophylla, 891.68 m. (C) Glossopteris fitzroyensis, 901.70 m. (D) Glossopteris browniana, 901.32 m. (E) Glossopteris browniana, 1042.15 m. (F) Glossopterid scale leaf or microsporophyll, 1000.35 m. (G) Samaropsis sp., a possible glossopterid seed, 1039.65 m. (H) Glossopteris chevronata, 1046.37 m. (I) Lateral compression of a slender Vertebraria australis (segmented root with small subsidiary rootlets), 810.28 m. (J) Lateral compression of a broad Vertebraria australis segmented root, 477.90 m. (K) Transverse section of a Vertebraria australis segmented root, 1041.74 m. (L) Phyllotheca etheridgei (sphenophyte) lateral compression, 863.50 m. (M) Large segmented stem of Paracalamites australis (sphenophyte), 860.62 m. (N) Abundant macroscopic charcoal fragments preserved on a bedding plane, 880.35 m. Scale bars = 10 mm for all images except K (= 5 mm).

playfordii and Brevitriletes (Apiculatisporis) bulliensis in both wells (Figs. 7G and 7I). The palynological record of this boundary is further characterized by: (1) a significant reduction in coarse baculate trilete spores (e.g., Horriditriletes spp., Neoraistrickia spp., Raistrickia spp.); (2) local abundance spikes of the fern spore Thymospora spp. (PHKB-1 only; Fig. 7N) or the alga Quadrisporites horridus (CCC-27 only; Fig. 7L); (3) anomalously high abundances of

amorphous organic matter (AOM); and (4) a reduction in plant productivity, as indicated by a relative decrease in palynomorph concentrations in both the strict palynomorph and palynofacies counts. Non-marine algal cysts are abundant in the lower 2 m of this zone in both wells.

The last occurrence of *D. parvithola* is recorded within the *P. crenulata* Zone, but these specimens are fragmentary and have surface textures indicative of pyrite damage. Within

PHKB-1, this degradation style is typical of specimens from the preceding *D. parvithola* Zone (Fielding et al., 2019). Their occurrence within the *P. crenulata* Zone may be a consequence of reworking from the underlying *D. parvithola* Zone. Extrinsic *Lycopodium* spores added to the samples during processing have a very wide range of abundances within the upper portion of this zone, indicating highly fluctuating plant and phytoplankton productivity.

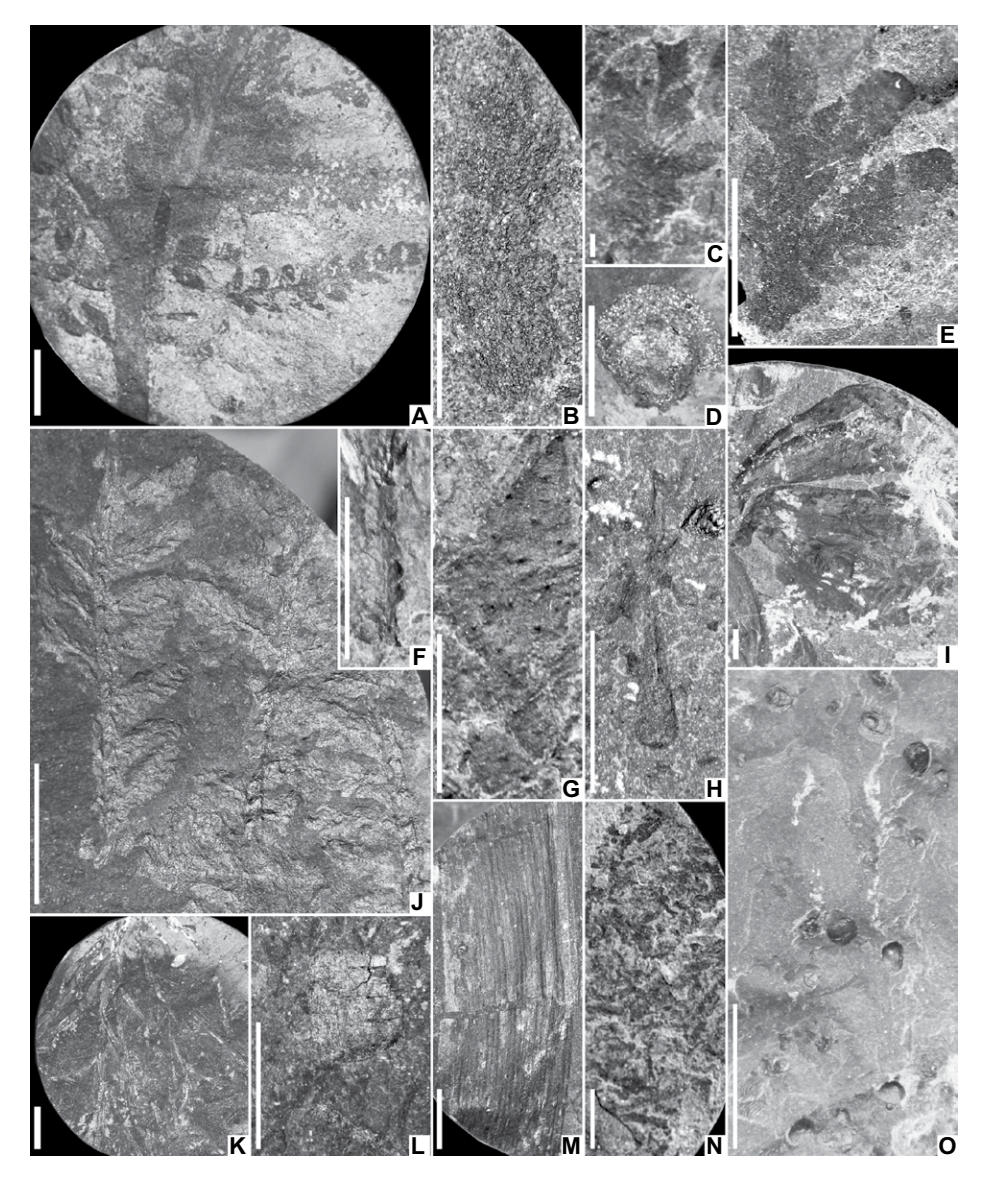


Figure 9. Triassic fossils from PHKB-1 (A, B, D-H, K-O) and CCC-27 (C, I) wells. (A) Portion of *Dicroidium zuberi*, 353.70 m. (B) *Dicroidium zuberi* pinna, 370.53 m. (C) *Cladophlebis* sp. pinna fragment, 445.61 m. (D) Seed or cupule, 324.49 m. (E) *Lepidopteris madagascariensis*, 362.00 m. (F) Diminutive fern pinna, 779.60 m. (G) Pleuromeian lycophyte axis with spirally arranged microphyll scars, 495.72 m. (H) Lycopsid microphyll, 503.55 m. (I) Detached *Pleuromeian* sporophylls, 460.49 m. (J) *Lepidopteris callipteroides*, 362.60 m. (K) Branching roots, 354.15 m. (L) Charcoal fragments, 614.35 m. (M) *Neocalamites* sp., 365.20 m. (N) Debris of lycopsid or conifer leaves, 451.26 m. (O) Scattered spinicaudatan carapaces, 459.25 m. Scale bars = 10 mm for all images except E (= 5 mm).

The base of this zone is also marked by the last occurrence of fossils with unambiguous glossopterid affinity (e.g., Glossopteris, Vertebraria). Within the broader Sydney Basin, the first occurrences of the peltaspermalean leaf taxon Lepidopteris callipteroides (Fig. 9J) and the conifer Voltziopsis africana, together with persistent examples of Schizoneura gondwanensis (a sphenophyte taxon that survived the EPE), are recorded in this zone (Retallack, 1980, 2002; Vajda et al.,

2020). Macrofossils are otherwise scarce in this interval apart from fine woody debris, charcoal fragments, and a few unidentifiable roots.

**Remarks.** The *D. parvithola–P. crenulata* zone boundary is equivalent to the APP5–APP6 boundary of Price (1997). In both of the examined successions, large portions of the uppermost coal seam (Bulli Coal) were removed for analysis soon after drilling; consequently, the base of this zone might extend into the upper-

most part of the Bulli Coal, as has been reported in the Bowen Basin (Foster, 1982). However, the Bulli Coal appears to be of consistent botanical composition throughout, being dominated by glossopterid remains (Diessel, 1992) typical of those occurring throughout the *D. parvithola* Zone; hence, we consider the *D. parvithola–P. crenulata* boundary to be best placed at the top of this coal.

In two sections of the Sydney Basin (Frazer Beach, and Snapper Point), the index taxa for the *P. crenulata* Zone were not observed until ~1.5 m above the uppermost Permian coal (Mishra et al., 2019; Vajda et al., 2020; Fig. 1). This ~1.5 m interval was identified as a post-EPE "dead zone" and is characterized by a high abundance of coalified and charcoalified phytoclasts and a near-total absence of palynomorphs. This "dead zone" is not present across the entire basin, or may be overlooked where sampling is too widely spaced, as no directly correlative interval was identified within CCC-27 or PHKB-1.

Stratigraphic distribution. Assemblages assigned to this zone occur in samples immediately above the Bulli Coal in both wells studied (Vajda et al., 2020; Mishra et al., in press). The depths to the base of this zone (top of the Illawarra Coal Measures) are 805.08 m (in PHKB-1) and 475.18 m (in CCC-27). Despite evidence of erosion at the base of some sandstone bodies within this interval, the P. crenulata Zone has a preserved thickness of 24 m in PHKB-1 and 48 m in CCC-27, consistently thicker than the 7 m type succession of this zone in the Bowen Basin, Queensland (Foster, 1982). Lithostratigraphically, this zone encompasses the Coal Cliff Sandstone in the central part of the basin (PHKB-1) but correlates to both the Coal Cliff Sandstone and the Wombarra Shale southwards (CCC-27), suggesting that these rock units are at least partially time-transgressive.

Estimated chronostratigraphic range. Previously, the age of the Dulhuntyispora parvithola-Playfordiaspora crenulata boundary in eastern Australia was considered within the Wuchiapingian (Mantle et al., 2010) or close to the PTB (Changhsingian-Griesbachian boundary; Laurie et al., 2016; Fig. 1). Recent radiogenic-isotope ages from the Sydney Basin tightly constrain the D. parvithola-P. crenulata zonal boundary to a maximum of  $252.6 \pm 0.04$  Ma (Metcalfe et al., 2015) and a minimum of  $252.31 \pm 0.07 \text{ Ma}$ (Fielding et al., 2019). These new radiochronologic age constraints place the D. parvithola-P. crenulata zone boundary firmly within the Changhsingian Stage (upper Lopingian). This is a chronostratigraphic position intermediate between the above-mentioned biostratigraphic schemes (Mantle et al., 2010; Laurie et al., 2016). Furthermore, a preliminary U-Pb

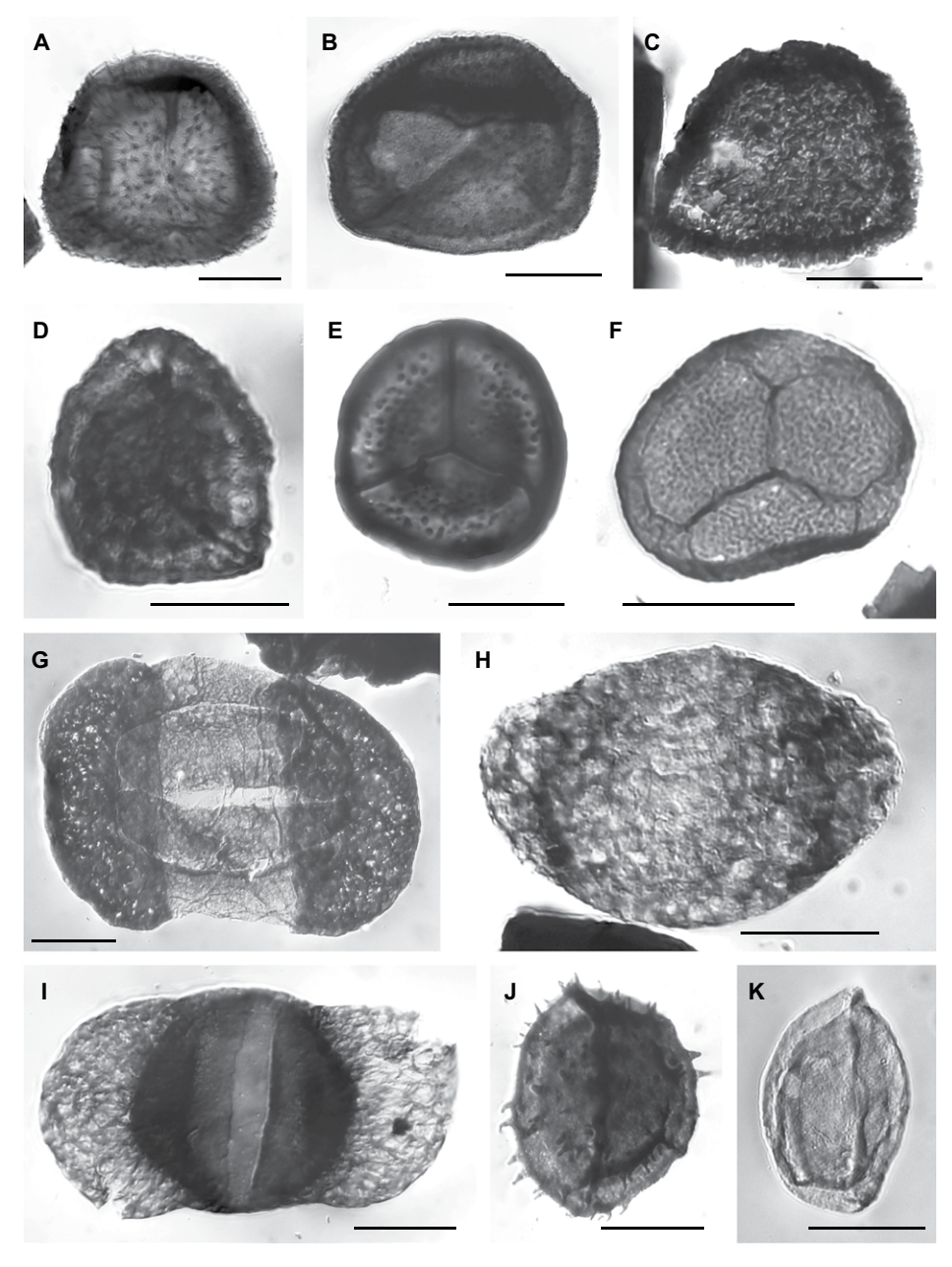


Figure 10. Characteristic palynomorphs of the *Protohaploxypinus microcorpus*, *Lunatisporites pellucidus*, *P. samoilovichii*, and *Aratrisporites tenuispinosus* zones, Sydney Basin, all scales = 20 μm, A, D, E, G and J enlarged from Fielding et al. (2019), taxon authorities and specimen details are supplied in Table A7 (see footnote 1). (A–D) Index taxa of the *P. microcorpus* Zone; (A) *Lundbladispora springsurensis*; (B) *Lundbladispora* sp. A (*sensu* Foster, 1979, 1982); (C, D) *Rewanispora foveolata*. (E–G) Index taxa of the *L. pellucidus* Zone; (E) *Limatulasporites limatulus*; (F) *Limatulasporites* sp. cf. *L. fossulatus*; (G) *Lunatisporites pellucidus*. (H–K) Index taxa of the *P. samoilovichii* and *A. tenuispinosus* zones; (H) *Pteruchipollenites gracilis*; (I) *Alisporites (Falcisporites) australis*; (J) *Aratrisporites tenuispinosus*; (K) *A. plicatus*.

radiochronologic age indicates an earliest Triassic (Griesbachian) age for the upper *P. crenulata* Zone (Fielding et al., 2019).

Early attempts to tie the spore-pollen biostratigraphy to the global time scale tended to place the PTB above the *Protohaploxypinus microcor*-

pus-equivalent zones (Helby, 1973; Foster, 1979, 1982; Helby et al., 1987; Price, 1997; Mantle et al., 2010) and, in some cases, within or above the *Lunatisporites pellucidus*-equivalent zones (Foster, 1979, 1982; Mantle et al., 2010; Fig. 1). Recalibration of the zones by Laurie et al. (2016)

to the radioisotopic geochronology (Metcalfe et al., 2015) interpreted the P. microcorpus Zone, and hence the overlying L. pellucidus Zone, to be above the PTB (presently dated to  $251.902 \pm 0.0241$ ; Burgess et al., 2014). The additional age constraints outlined above support a higher position of the PTB relative to the EPE, a pattern also expressed in the PTB-type section in southern China (e.g., Jin et al., 2000). However, the Sydney Basin absolute ages revealed a much longer discrepancy (~400 k.y.) between the terrestrial EPE and PTB than in the marine record, suggesting an early onset of vegetation turnover at high southern latitudes (Fielding et al., 2019). Collectively, these data suggest: (1) the base of this zone correlates to the EPE; and (2) this zone encompasses the PTB (Fig. 1).

In summary, we interpret this zone to range from the upper Changhsingian to lower Induan (?lower Griesbachian) based on lower-boundary U-Pb calibrations (Metcalfe et al., 2015; Fielding et al., 2019) and age estimates of the upper boundary from inferred sediment accumulation rates in the basin (Laurie et al., 2016; this study).

## Protohaploxypinus microcorpus *Zone (Foster, 1982)*

Composition. We identified the first appearances of index taxa unique to the P. microcorpus Zone, specifically Rewanispora foveolata and Lundbladispora springsurensis (Figs. 10A and 10C-10D), in both wells examined. We also identified the first appearance of Lundbladispora sp. A (sensu Foster, 1979), a rare index taxon for this zone (Foster, 1982), but only within the P. microcorpus Zone of CCC-27 (Fig. 10B). The first appearances of two additional index species, Playfordiaspora crenulata and Triquitrites proratus (Figs. 7H and 7J), were identified within this zone; however, these taxa were very rare. Consequently, their stratigraphic ranges possibly extend into the underlying P. crenulata Zone within the Sydney Basin, as suggested by other successions in eastern Australia (Helby, 1973; Foster, 1979; Helby et al., 1987) and greater Gondwana (e.g., Pakistan: Balme, 1970; Prince Charles Mountains, Antarctica: Lindström and McLoughlin, 2007). Leiospherid acritarchs and AOM remain abundant throughout this interval, but total palynomorph concentrations were low. The first appearances of Lepidopteris callipteroides (peltasperm) fragments (Fig. 9J) and voltzialean conifer remains (Fig. 90) were identified within PHKB-1 at or near the base of the P. microcorpus Zone.

**Remarks.** The *Protohaploxypinus microcorpus* Zone has proven elusive in some studies owing to the probable diachronous distribution of some index taxa (e.g., Price, 1997). As per previous authors (Mantle et al., 2010; Laurie

et al., 2016), we identify the *P. microcorpus* Zone as equivalent to the upper portion of zone APP6 (*sensu* Price, 1997), but the recognition of the above-mentioned, zone-specific index taxa (*Rewanispora foveolata* and *Lundbladispora springsurensis*) has enabled the differentiation of this zone from the preceding *P. crenulata* Zone in both wells studied (cf., Laurie et al., 2016). Further investigation may reveal that this zone, as defined by Foster (1982), has only regional (e.g., basin-wide) utility.

Stratigraphic distribution. Lacking any absolute age constraints within the P. microcorpus Zone, a short chronostratigraphic range for this zone has been inferred from its relatively small stratigraphic thickness within the wells investigated in our study, in other Sydney Basin wells studied (Helby et al., 1987), and in other eastern Australian Basins (Foster, 1982). This study constrains the base of the P. microcorpus Zone to 781.18 m in PHKB-1 (23.9 m above the top of the Bulli Coal) and 427.1 m in CCC-27 (48.08 m above the top of the Bulli Coal), giving zone thicknesses of ~20-25 m in PHKB-1 and 75-80 m in CCC-27. Although this zone is more extensive in the studied wells than in some other successions, this thickness is broadly consistent with previous studies of this zone in the Bowen Basin (Foster, 1982). The lithostratigraphic units encompassing this zone in the southern part of the basin (CCC-27; Scarborough Sandstone and Stanwell Park Claystone) differ from those in the central part of Sydney Basin (PHKB-1; lower Wombarra Shale). This suggests that these rock units are slightly time-transgressive across the basin, consistent with the pattern observed for the rock units correlated with the underlying *P. crenulata* Zone.

Estimated chronostratigraphic range. We interpret this zone to be restricted to the ?lower Induan (Griesbachian; Fig. 1) based on previous studies (Laurie et al., 2016) and estimates of depositional rates within the Triassic succession in the Sydney Basin (this study).

### Lunatisporites pellucidus Zone (Foster, 1982)

Composition. The base of this zone is identified by the first occurrence of Lunatisporites pellucidus (Fig. 10G) and important accessory taxa: Limatulasporites spp. (e.g., L. limatulus; Figs. 10E–10F) and Kraeuselisporites saeptatus (Foster, 1982). The species richness and abundance of zonate trilete spores, which is typical of lycophytes, increases in this zone, but there is a relative decrease in non-taeniate bisaccate pollen, e.g., Alisporites (or Falcisporites; Fig. 10I) and Pteruchipollenites (Fig. 10H). In other characteristics, this zone is very similar to the preceding P. microcorpus Zone.

**Remarks.** The Lunatisporites pellucidus Zone corresponds to the lower APT1 Zone of Price

(1997) and, previously, had been considered the lowermost zone of the Triassic (Helby, 1973; Helby et al., 1987; Price, 1997). Helby et al. (1987, p. 8) defined the base of this zone as the "oldest common occurrence of Lunatisporites pellucidus," whereas other palynostratigraphic studies of eastern Australia (Foster, 1982; Price, 1997) employed a more objective criterion: the first appearance datum of L. pellucidus as one of the markers for the base of this zone. To avoid ambiguity, the latter, more concrete definition was employed herein. Sparse palynological sampling, rare macrofloral remains, and a lack of absolute age controls preclude detailed interpretations of the duration and temporal patterns of floral change within this zone in the wells studied. A higher resolution study of these successions will likely place the P. microcorpus-L. pellucidus Zone boundary stratigraphically lower than indicated herein because it is highly unlikely that any recorded first (or last) appearance datum is genuinely the lowest (or highest) occurrence of a taxon in a given region, an axiom to consider in all biostratigraphic research. This is especially relevant to successions with low sampling densities.

Stratigraphic distribution. The base of this zone is registered at 760.09 m in PHKB-1 (44.99 m above the top of the Bulli Coal) and 348.19 m in CCC-27 (126.99 m above the top of the Bulli Coal). The zone is 14.47 m thick in PHKB-1 but of uncertain thickness in CCC-27 as the top was not defined. The L. pellucidus Zone is much thicker in the type section in the northern Sydney Basin (152 m; Helby et al., 1987) and has an estimated thickness of >250 m within the lower Rewan Formation of the Bowen Basin, Queensland (de Jersey, 1970; Foster, 1982). This zone correlates to the upper Wombarra Shale in the central portion of the basin (in PHKB-1), but southwards, the lower boundary of this zone commences at or near the base of the Bulgo Sandstone (in CCC-27). This is consistent with the diachronous pattern identified for the underlying lithostratigraphic units.

Estimated chronostratigraphic range. The zone is inferred to range from the ?lower Induan (?upper Griesbachian) to ?lower Olenekian (?lower Smithian; Fig. 1) based on data from Laurie et al. (2016) and inferences from average sediment accumulation rates in the basin (this study).

### Protohaploxypinus samoilovichii Zone (Foster, 1982; Helby et al., 1987)

*Composition.* This palynozone is identified in our study by the first occurrence of *Aratrisporites* (Figs. 10J–10K; Foster, 1982; Helby et al., 1987). This genus of zonate monolete spores is typically linked to pleuromeian lycophytes (e.g.,

Helby and Martin, 1965; Morbelli and Petriella, 1973). Fossils of this group become increasingly prevalent in the upper parts of the P. samoilovichii Zone, as represented by abundant pleuromeian leaf fragments, megaspores, and cingulate zonate trilete spores (e.g., Densoisporites). The pollen record of this zone is dominated by the taeniate bisaccate pollen Lunatisporites and the non-taeniate bisaccate pollen Alisporites (or Falcisporites) and Pteruchipollenites. In the leaf flora, this zone includes the first occurrence of Dicroidium (Umkomasiales; Figs. 9A-9B) in PHKB-1 at 587.47 m but cuticular fragments of this and other seed plants are sparse throughout. Charcoalified wood fragments occur consistently through this interval (Fig. 9L), attesting to the persistence of wildfires in the landscape through the Early Triassic. Spinicaudatans were recorded at several levels within the upper part of this zone in PHKB-1 (Fig. 9O), but they have not been identified to genera or species.

This zone is characterized by high inter-sample variability of AOM and trilete spore morphogroup abundances (particularly cingulate [e.g., Limatulasporites; Figs. 10E-10F], granulate [e.g., Cyclogranisporites; Fig. 7D], and laevigate [e.g., Leiotriletes; Fig. 7C forms]). In general, there is a gradual decline in abundance of taxa that flourished in the wake of the EPE, particularly the phytoplankton cysts Leiosphaeridia (Fig. 7M) and Quadrisporites (Fig. 7L) and the fern spore Thymospora (Marattiales; Balme, 1995; Lesnikowska and Willard, 1997; Fig. 7N). Furthermore, plant spore taxa that flourished prior to the EPE (e.g., Microbaculatispora, coarse baculate spores; Figs. 7A-B and 7E) decrease to negligible levels upwards through this zone.

Remarks. There is some ambiguity in the recognition of this zone in previous studies. The index taxon range chart provided by Helby et al. (1987, Fig. 5) indicates the first sparse occurrences of Aratrisporites as low as the P. microcorpus Zone, and a consistent distribution of this genus through most of the L. pellucidus Zone and the entirety of the P. samoilovichii Zone. However, this is inconsistent with their written definition of the Protohaploxypinus samoilovichii Zone, which stipulates that the base is concurrent with the first appearance of Aratrisporites spp. (Helby et al., 1987, p. 8). Herein, we have followed the latter definition of this zonal boundary, which is consistent with that of Foster (1982). Furthermore, Helby et al. (1987) reported a decline of Alisporites (Falcisporites) australis with a concomitant increase in taeniate bisaccate pollen at the base of this zone. A distinct change from non-taeniate to taeniate-dominated pollen assemblages was identified, but this was observed ~130 m above the base of this zone (614.33 m depth; sample S014124).

Stratigraphic range. The depth to the base of this zone is 745.62 m in PHKB-1 (59.46 m above the top of the Bulli Coal). The zone was not detected in the sampled portion of CCC-27. The Protohaploxypinus samoilovichii Zone has the largest observed stratigraphic range of any zone identified in this study. It is estimated to be 360 m thick in PKHB-1, extending from the upper Wombarra Shale to near the top of the Bulgo Sandstone. This is broadly consistent with the reference section for the P. samoilovichii Zone in the northern Sydney Basin described by Helby et al. (1987; ≥259 m thick) and the stratotype of the more-or-less coeval Kraeuselisporites saeptatus Zone of Western Australia (~361 m thick; Dolby and Balme, 1976).

Estimated chronostratigraphic range. Dating of the upper boundary is based on U-Pb radiochronologic ages (Metcalfe et al., 2015; Fielding et al., 2019), average sediment accumulation rates in the basin (~108 m/m.y.; Fig. 6), and a distinctive positive  $\delta^{13}C_{\text{org}}$  excursion (Fig. 3), which marks the Smithian-Spathian boundary (Galfetti et al., 2007; Zhang et al., 2015; Zhang et al., 2019; see Discussion section below). However, owing to the absence of global boundary stratotype sections and points (GSSPs) and precise geochronometric controls for the Lower Triassic substages, and the lack of a refined geochronology for the Dienerian-Smithian interval in eastern Australia, the placement of the upper and lower boundaries of this zone herein must be considered tentative. On the basis of available data, we interpret this zone to range from the ?lower Olenekian (?lower Smithian) to mid-Olenekian (upper Smithian; Fig. 1).

## Aratrisporites tenuispinosus Zone (Helby, 1973; Helby et al., 1987)

Composition. The base of this unit is identified by a marked increase in the relative abundance of Aratrisporites spp., particularly A. tenuispinosus and A. plicatus (Figs. 10J-10K). This genus constitutes up to 63% of the entire palynomorph count (at 320.1 m depth) but is generally ≤5% in most other samples. Increases in non-taeniate bisaccate pollen, particularly Alisporites (Falcisporites) and Pteruchipollenites (Figs. 10H-10I), occur near the base of this zone, and their abundances remain relatively high throughout (average abundance per sample ~20%). With these increases, there is a corresponding decrease in Lunatisporites (Fig. 10G), the dominant taeniate bisaccate pollen type of the underlying Protohaploxypinus samoilovichii Zone. As per the preceding zone, fluctuations in abundance of the primary spore groups (especially granulate and laevigate acavate trilete spores) continue through the A. tenuispinosus Zone. Unexpectedly, the polyplicate pollen

Praecolpatites spp. has a local first appearance at the base of the A. tenuispinosus Zone in PHKB-1, although this taxon has a widely accepted Permian first appearance in eastern Australia (e.g., Foster, 1979) and elsewhere in Gondwana (Antarctica: Balme and Playford, 1967; India: Venkatachala and Kar, 1968; Pakistan: Balme, 1970). These specimens likely indicate local reworking into the Lower Triassic succession. AOM levels decrease to approximately pre-EPE levels. Evidence from macrofossil leaves and cuticle mesofossils indicates the replacement of Lepidopteris by Dicroidium as the dominant foliage of seed-ferns in this interval. Isoetalean lycophyte microphylls remain abundant in this zone (Figs. 9G-9I).

**Remarks.** The marked increase in *Aratrisporites*, and the replacement of *Lunatisporites* by *Alisporites* (or *Falcisporites*) as the dominant pollen form, matches previous studies for the basal portions of this zone (Helby, 1973; Helby et al., 1987) and the correlative *Triplexisporites playfordii* Zone of Western Australia (Dolby and Balme, 1976; Helby et al., 1987).

Stratigraphic distribution. The depth to the base of the Aratrisporites tenuispinosus Zone is 383.48 m in PHKB-1 (421.6 m above the top of the Bulli Coal), where it corresponds to the base of the Bald Hill Claystone. The A. tenuispinosus Zone also extends to the top of the Garie Formation (Helby, 1973), but the upper boundary of this zone, and that of the Garie Formation, were not observed in this study. The preserved stratigraphic thickness of this zone in PHKB-1 (~145 m) is substantially greater than the Sydney Basin reference section (58 m; Helby et al., 1987). The zone was not detected in the sampled portion of CCC-27.

Estimated chronostratigraphic range. We infer a range of mid-Olenekian (upper Smithian) to lower Anisian for this zone (Fig. 1). The upper boundary was broadly correlated to marine biostratigraphic zones by Helby et al. (1987) and, thence, calibrated to the global geochronological scheme of Gradstein et al. (2012) by Mantle et al. (2010).

The age of the lower boundary of the *Aratrisporites tenuispinosus* Zone (and thus the upper boundary of the *P. samoilovichii* Zone) is partially constrained by U-Pb radiochronologic ages from two tuffs near the base of the Garie Formation in the northern Sydney Basin (248.23  $\pm$  0.13 Ma and 247.87  $\pm$  0.11 Ma; Metcalfe et al., 2015). However, between the base of the *A. tenuispinosus* Zone (upper Bulgo Sandstone within the PHKB-1 reference section) and the Garie Formation is the Bald Hill Claystone, which is dominated by light brown mudrocks of substantial thickness (~90 m) in PHKB-1 and elsewhere in the Sydney Basin (up to 110 m

thick; Emerson and Branagan, 2011). Around 100 m of strata separate the base of the *A. tenuispinosus* Zone from the level equivalent to the lowermost dated tuff in the Garie Formation. Based on the overall estimated sedimentation rate of ~108 m/m.y. for the Lower Triassic succession, we infer that this interval corresponds to around 0.9–1 m.y., or perhaps slightly more given the fine-grained nature of these strata. On this basis, we estimate that the base of the *A. tenuispinosus* Zone is close to 249.2 Ma (upper Smithian), thus significantly older than inferred by previous studies (e.g., Mantle et al., 2010).

#### **Ordination Data Analysis**

Ordination analyses of the palynological data revealed minimal overlap of the pre-EPE (= Dulhuntyispora parvithola Zone) and post-EPE (= all other zones) palynoassemblages in the ordination space (Fig. 5). This supports the prediction that there was a major shift in vegetation composition between these intervals. The only exceptions to this distinction between pre- and post-EPE assemblages were assemblages from the Playfordiaspora crenulata Zone, which overlapped to a small degree with those of the preceding D. parvithola Zone, but only within the presence-absence ordination. In contrast, the abundance data for these zones separated these assemblages into distinct areas in the ordination space. The post-EPE zones generally show a high degree of overlap, with the oldest of these, the P. crenulata Zone, being an exceptional assemblage once again. Specifically, the relative abundance data indicate that this zone is mostly distinct but shares a few palynofloral characters with other post-EPE assemblages, particularly the immediately overlying Protohaploxypinus microcorpus Zone. As such, the P. crenulata Zone likely represents a succession of distinct transitional assemblages between the classical Permian and Triassic palynofloras (the "ecosystem collapse" stage of Fig. 11).

The relatively small area of the ordination space occupied by the D. parvithola Zone assemblages in both analyses reflects a low degree of inter-sample variability, which is typical of a relatively uniform palynoflora (and parent vegetation). In contrast, the zone with the highest inter-sample abundance dissimilarity was the Aratrisporites tenuispinosus Zone, which spans a large area in the ordination space. The high inter-sample variability of the A. tenuispinosus Zone was largely the result of highly variable abundances of Aratrisporites and non-taeniate bisaccate pollen species. Emblematic of this was sample S014134 (PHKB-1, 320.1 m depth), which was an extreme outlier in the relative abundance ordination. Because this sample was not an outlier in the binary ordination (Fig. 5B), the dissimilarity of this sample was due primarily to anomalous abundances rather than disparate taxa. Specifically, this sample had an inordinately high abundance of *Aratrisporites*, comprising ~63% of the total, which is nearly twice as much as the assemblage with the next highest abundance of this genus (S014131, PHKB-1, 383.48 m depth). This sample was not illustrated in Figure 5A because it heavily compressed the remaining data points, even with transformed abundance data sets, and made visualization impractical.

Palynostratigraphic zones accounted for most of the clustering in both ordinations, whereas sample lithofacies and geographic position played only minor roles in distinguishing palynomorph content. This suggests that the stage of floral community evolution played a greater role in segregating palynomorph assemblage compositions than local depositional conditions or regional variations in the flora and supports the biozones as reflecting discrete palynofloral/vegetation phases, particularly the well-differentiated *D. parvithola* and *P. crenulata* zones.

### **Carbon Isotope Chemostratigraphy**

The  $\delta^{13}C_{org}$  trend from the uppermost Permian to the upper Lower Triassic reveals a major negative shift just above the last Permian coal. Although initially marked by a series of positive spikes in short succession, the  $\delta^{13}C_{org}$  remained depressed for much of the examined post-EPE interval. Toward the upper part of the succession, a gradual positive shift in  $\delta^{13}C_{org}$  was observed, followed by a relatively rapid stepwise increase. A zone-by-zone description of this broad trend is outlined below.

The Dulhuntyispora parvithola Zone has a relatively consistent stable carbon isotope signature, with high  $\delta^{13}C_{org}$  values throughout (-25 to -23%), but they decrease notably in the uppermost strata. Within the Playfordiaspora crenulata Zone, immediately above the Bulli Coal (which we interpret as the onset of the EPE herein), we identify overall low  $\delta^{13}C_{org}$ values (generally below -26%) but also significant fluctuations ranging from -28% to -22%. A similar  $\delta^{13}C_{org}$  pattern was not observed in CCC-27 over the same interval, which is tentatively linked to the lower sampling resolution in the CCC-27 core. The  $\delta^{13}C_{org}$  values reach a minimum within the Protohaploxypinus microcorpus Zone and remain consistently low in this interval (-30% to -27%). Within PHKB-1, the Lunatisporites pellucidus Zone marks the onset of a second but much longer phase of extreme  $\delta^{13}C_{org}$  variability between samples (-30% to -22%), a pattern that continues well into the

subsequent *Protohaploxypinus samoilovichii* Zone. A shift toward higher  $\delta^{13}C_{org}$ , followed by sustained high values, initiates shortly below the base of the *Aratrisporites tenuispinosus* Zone and is concurrent with an increase in pleuromeian lycophyte fossils (microphylls, axes, and zonate trilete and monolete spores). With one exception (375.68 m depth), the  $\delta^{13}C_{org}$  values from the *A. tenuispinosus* Zone are all consistently higher than those of the pre-EPE interval (-26% to -21%).

#### DISCUSSION

## Vegetation Changes of the Latest Permian to Early Triassic (Lopingian–Spathian)

Here, we summarize five discrete uppermost Permian (upper Lopingian) to Lower Triassic (Spathian) floristic stages within the Sydney Basin that approximately correspond to the palynozones outlined above. Each stage is supported by a combination of macrofloras, palynofloras, palynofacies, palynological ordination analyses, and non-fossil proxy data, such as chemostratigraphic and lithostratigraphic signatures. The stages have been calibrated to the global time scale following the chronostratigraphy presented in the Results (see Fig. 1). These stages are summarized graphically in Figure 11, and the details of each are presented below.

## Stable glossopterid forests (Dulhuntyispora parvithola Zone)

This stage was characterized by a highly productive glossopterid-dominated, forest-mire vegetation and dense, broad-leafed deciduous forests in humid coastal-plain environments. The macrofloras of both examined wells yield not only copious Glossopteris leaves but a continuous record of Vertebraria, a distinctive chambered root taxon with clear glossopterid affinities (Schopf, 1965; Pigg and Taylor, 1993; Decombeix et al., 2009), and only minor components of other groups, such as sphenophytes, ferns, and lycophytes (Fig. 8). Elsewhere in the Sydney Basin, strata assigned to this interval also contain sparse cordaitalean and scale-leafed conifer foliage, rare pteridosperm leaves, and the remains of various reed-like to scrambling sphenophytes, ferns, and lycophytes (Townrow, 1968; Holmes, 1995; Shi et al., 2010). A consistent vegetation type is signified by the relatively small area that the palynoassemblages of this zone occupy in the ordination space (Fig. 5). The vegetation can be equated to a stable arborescent, broad-leafed, deciduous climax community in the humid high latitudes. Despite a dominance of hygrophilic plants in the assemblages of this zone, macroscopic charcoal particles (Fig. 8N) are common and signify the regular occurrence of wildfires in the Lopingian wetlands.

The most common pollen groups throughout this interval are those typical of glossopterids (taeniate bisaccate forms such as Protohaploxypinus and Striatopodocarpites). However, it is difficult to use these grains as a measure of floristic diversity because multiple pollen morphogenera have been found within individual glossopterid sporangia, demonstrating wide intraspecific morphological variability of pollen within this group (Lindström et al., 1997). Furthermore, the occurrences of these pollen morphotypes extend well beyond the demonstrable stratigraphic and geographic ranges of definitive glossopterid macrofossils, indicating that equivalent pollen types were produced by several other plant groups (Balme, 1995). On this latter point, two of the Lower Triassic palynozones identified in this study are named for the pollen genus most commonly associated with glossopterids, Protohaploxypinus, but these zones are much younger (Griesbachian-Smithian) than any reliable record of Glossopteris. Additionally, the distribution of glossopterids appears to be restricted to Gondwana during the Lopingian (McLoughlin, 2011), but Protohaploxypinus has also been commonly associated with peltasperms at various locations in Laurasia (e.g., Gomankov and Meyen, 1986; Balme, 1995).

Similar palyno- and macrofloral assemblages in Lopingian fluvio-deltaic deposits have been recorded in continental basins across eastern Australia (Shi et al., 2010) and other regions of southern Gondwana (e.g., Antarctica, Taylor et al., 1992, Gulbranson et al., 2012, Slater et al., 2015, Miller et al., 2016; southern Africa, Prevec et al., 2009, 2010). This signifies a very wide distribution of relatively monotonous glossopteriddominated hygrophilous austral forests. Coals of this age are common across southern Gondwana, but their contents are generally homogenized and obscured by diagenesis (McLoughlin et al., 1997). The constituents of Gondwanan Permian coals are best expressed in permineralized peats distributed across eastern Australia and Antarctica. These are invariably dominated by glossopterid remains (Schopf, 1970; Gould and Delevoryas, 1977; Taylor et al., 1989; Pigg and McLoughlin, 1997; McManus et al., 2002; Holdgate et al., 2005; McLoughlin et al., 2019). Despite the extreme photoperiod regime at polar paleolatitudes, late Permian (sub-)polar forests had a very high, albeit seasonal, rate of productivity (e.g., Taylor et al., 1992; Miller et al., 2016). This high productivity is supported by the relatively high pollen absolute abundances in both wells investigated herein. This productivity appears to have remained high until the end of this zone, despite independent evidence that

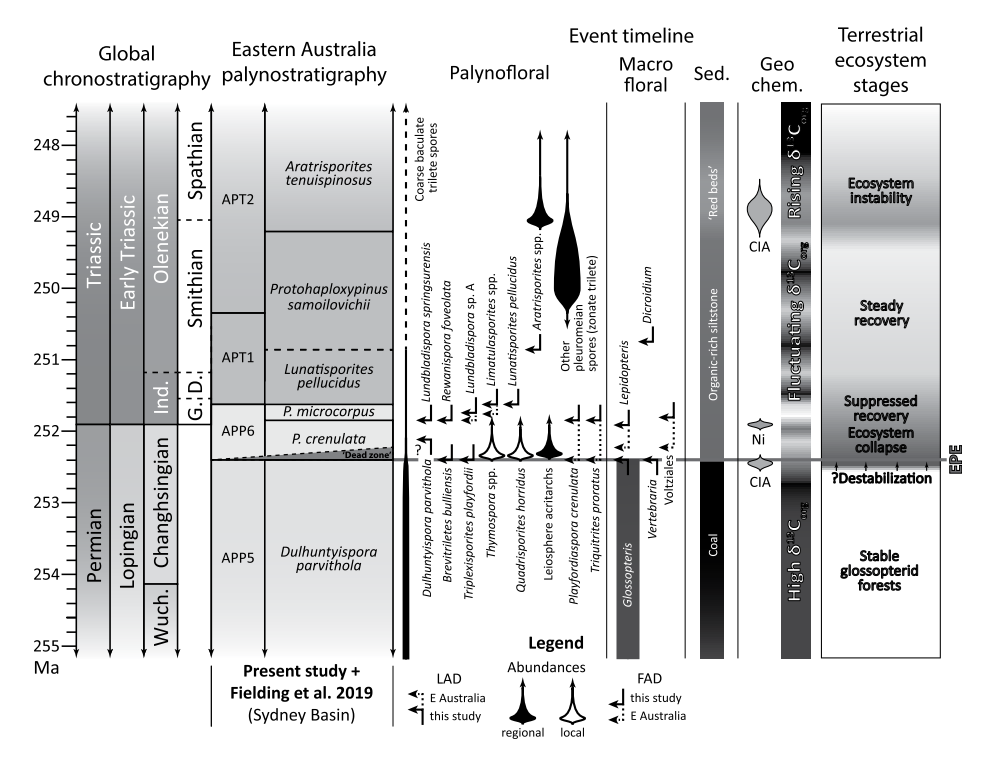


Figure 11. Timeline of Permian–Triassic floral and palynological bioevents, geochemical and sedimentological features, and stages in terrestrial ecosystem evolution, as recorded from eastern Australian basins. Geochemical, sedimentological, and macrofloral data from Fielding et al. (2019) and this study. FAD—first appearance datum; LAD—last appearance datum; CIA—chemical index of alteration; ?—distribution due to possible reworking; sed.—sedimentary facies; geochem.—geochemical. "Local" refers to an abundance trend evident in only one well herein; "regional" refers to a trend observed in both wells and/or reported from other successions of eastern Australia. Sedimentary facies column characterizes the dominant finegrained facies at the upper stratum of each fluvial facies succession. For chronostratigraphic boundary calibrations, see Figure 1. For taxon authorities, see Table A3 (see footnote 1).

the biosphere may have been under increasing environmental stress, as outlined below.

Lithologically, the top of the Bulli Coal corresponds to a coal-siltstone interface with no evidence of scouring or sediment remobilization in either of the examined wells. This suggests a widespread and abrupt (e.g., Herbert, 1997a) but conformable transition from the D. parvithola to P. crenulata zones; thus, it provides a continuous record of the initial stages of the terrestrial EPE interval in the wells studied. The Bulli Coal has a relatively high tissue preservation index and moderate to low gelification index characteristic of coals formed in forested mires (Diessel and Smyth, 1995). However, it shows a dulling-upward profile indicative of an increased proportion of oxidized macerals (inertinite) toward the top (Shibaoka and Smyth, 1975). Furthermore, chemical analyses of aluminosilicate minerals within the uppermost Lopingian strata reveal a prominent phase of chemical alteration initiating prior to the EPE (Fielding et al., 2019), as noted for probable coeval deposits in Antarctica

(Sheldon, 2006) and China (Cao et al., 2019). Additionally, a reduction in *Glossopteris* leaf size has been observed in the uppermost Permian strata of southern Africa (Anderson and Anderson, 1985; Zavada and Mentis, 1992). These lines of evidence hint at a shifting climate at high southern latitudes immediately preceding the terrestrial EPE and may indicate destabilization of the glossopterid biome near the end of its temporal range.

## Ecosystem collapse (Playfordiaspora crenulata Zone)

The synchronous collapse of the glossopterid biome across the continental settings of eastern Australia marks the cessation of Permian peatforming conditions in the south polar landscape. We interpret the *D. parvithola–P. crenulata* boundary as concurrent with the onset of the terrestrial end-Permian mass extinction interval (EPE; Figs. 1 and 3–4). The EPE in the Sydney Basin is marked by: (1) the substitution of coals by carbonaceous siltstone capping upward-fining

cyclic fluvial successions; (2) the last occurrence of glossopterids; (3) a significant and prolonged negative  $\delta^{13}C_{org}$  excursion; (4) high abundances of amorphous organic matter (AOM); and (5) a massive reduction in plant productivity. High-resolution palynofloral and palynofacies details of the immediate aftermath from additional outcrop sections are outlined elsewhere (Vajda et al., 2020), but a brief summary is included here to indicate the broad-scale changes.

The palynological records of the mudstone/ siltstone facies overlying the uppermost Permian coal ("roof shales," sensu Fielding et al., 2019) are characterized by a series of anomalous, stepwise abundance spikes. These include the fern spore Thymospora (PHKB-1 only), the freshwater alga Quadrisporites (CCC-27 only), and a combination of concurrent leiosphere acritarchs and AOM in both successions. The abundance peak of Thymospora indicates a local proliferation of opportunistic Marattiales, a fern group dominant in many late Paleozoic wet floodplain habitats (Pfefferkorn and Thomson, 1982). Freshwater algal proliferation is indicative of continuing, at least seasonally, wet conditions and a dearth of microfaunal consumers in freshwater habitats. Although the palynofloras from this zone have many features in common with younger zones, these abundance spikes result in a high degree of inter-sample variability highlighted by the wide but distinct area of the P. crenulata Zone suites in the abundance ordination plot (Fig. 5A). Although only modest gross palynofloral diversity reduction has been claimed across the EPE (Nowak et al., 2019), the dramatic changes in group representation and loss of the previously dominant taxa indicate a major biotic crisis. The immediately succeeding vegetation appears to have been dominated by opportunistic herbaceous plants and rapidly changing plant communities.

The roof shales above the Bulli Coal are of variable thicknesses (4 m in PHKB-1, 0.4 m in CCC-27) and are truncated above by a thick succession of sandstone commonly incorporating a basal conglomeratic lag of quartz pebbles and intraformational mudstone clasts. The uneven base of the sandstone/conglomerate facies suggests that, although the basal contact of the P. crenulata Zone is likely intact, a portion of the upper part of this short biozone may have been lost to erosion locally. Based on the first appearances of P. crenulata Zone index taxa, and a significant negative  $\delta^{13}C_{org}$  excursion, these roof shales likely correlate to the <25-m-thick informally named "marker mudstone" overlying the uppermost Permian coal in the Bowen and Galilee basins, Queensland (Clare, 1985; Michaelsen et al., 2000), although this mudrock unit may be slightly diachronous (Wheeler et al., 2019).

The onset of the terrestrial biotic collapse interval in eastern Australia has been constrained to between  $252.60 \pm 0.04$  Ma (Metcalfe et al., 2015) and 252.31  $\pm$  0.07 Ma (Fielding et al., 2019). In concordance with the marine record (e.g., Jin et al., 2000; Song et al., 2013), the onset of biotic collapse occurred significantly earlier than the PTB. However, these recent age constraints also suggest that the terrestrial EPE in eastern Australia occurred at least 300 k.y. before the marine extinction interval at ca.  $251.94 \pm 0.037$  Ma, as per representation in the Meishan *P-T* type section (Burgess et al., 2014). The collapse of the Glossopteris flora in the Sydney Basin is concurrent with the initiation of the primary extrusion phase of the Siberian Traps Large Igneous Province (STLIP; Burgess and Bowring, 2015), whereas the marine extinction interval has been temporally linked to massive STLIP intrusive magmatism (Burgess and Bowring, 2015; Burgess et al., 2017). Independent support for an earlier terrestrial collapse comes from apparent discrepancies in the marine and terrestrial stable carbon isotope records. Firstly, the marine  $\delta^{13}C_{carb}$  record at Meishan indicates a negative excursion at least 60 k.y. before the marine extinction interval (Burgess et al., 2014). However, diachroneity is suggested by the C-isotope signal in Iran, where the  $\delta^{13}C_{carb}$  excursion appears to have initiated during the Clarkina subcarinata conodont biozone (Korte and Kozur, 2010). This would correspond to a level between beds 15 and 20 at Meishan (Cao et al., 2009) and thus be >250 k.y. before the Chinese marine extinction interval (Bowring et al., 1998; Burgess and Bowring, 2015). Secondly, the initial negative excursion of  $\delta^{13}C_{org}$  from a terrestrial succession at Chahe, southern China (Zhang et al., 2016), has been dated at 252.30  $\pm$  0.07 Ma (Shen et al., 2011; Fig. 12). The onset of this gradual excursion is concurrent with the last occurrences of many plant taxa (Chu et al., 2016; Zhang et al., 2016). The reported age (~360 k.y. before the marine EPE) is concordant with the onset of the terrestrial EPE interval in eastern Australia; however, the zircon data from the ash bed at Chahe should be reanalyzed using the updated age model outlined by Burgess et al. (2014) for more valid comparisons to the Meishan type section. Furthermore, there is an unresolved controversy surrounding the continuity of the Chahe strata across the end-Permian interval (Bourquin et al., 2018a, b; Zhang et al., 2018). Regardless, the strata that include the first signs of the EPE (the uppermost coal bed and onset of  $\delta^{13}C_{org}$  excursion) appears to be continuous or show only minor disruption (Bourquin et al., 2018a). Thirdly, a major floral overturn has been recorded in northern Norway, which preceded the major  $\delta^{13}C_{org}$  excursion associated with the onset of marine extinctions by an interval on the order of 100 k.y. (Hochuli et al., 2010). Lastly, the start of the gradual negative  $\delta^{13}C_{org}$  decline occurs approximately within the uppermost coal laminae and at the base of the *P. crenulata* Zone in some successions of eastern Australia (e.g., Bowen Basin, Morante, 1996; Sydney Basin, Fielding et al., 2019; Fig. 12). Thus, the estimated age for the start of the terrestrial ecosystem collapse and opportunism stage is approximately concurrent with the initiation of a protracted shift in the global carbon cycle, which may have commenced hundreds of thousands of years prior to the first marine extinction pulse.

There are important limitations of the most recent  $\delta^{13}C_{org}$  studies in the Sydney Basin that have precluded their direct correlation of this ecosystem collapse interval (~P. crenulata Zone) to other chemostratigraphic signatures of the EPE and PTB. Firstly, high resolution records of  $\delta^{13}C_{org}$  from the uppermost Permian coals of Sydney Basin are largely lacking (Williams et al., 2012, 2017; Mishra et al., 2019; this study), which would confirm the nature of the carbon isotope signal leading up to the terrestrial EPE. Secondly, in southern China there is a major, rapid carbon isotope excursion with marine  $\delta^{13}C_{org}$  values of ~-5% $\circ$  (at Meishan; Cao et al., 2009) associated with the onset of the marine extinction event, very shortly (~50 k.y.) before the PTB (Burgess et al., 2014) and probable coeval terrestrial  $\delta^{13}C_{org}$  values of ~-8% (at Chahe; Zhang et al., 2016; Fig. 12). In contrast, the  $\delta^{13}C_{org}$  record of the terrestrial strata directly above the last Permian coals in the Sydney Basin (~lower P. crenulata Zone) shows two modest  $\delta^{13}C_{\rm org}$  excursions of ~-2%0 to -3%0 (Williams et al., 2017; Mishra et al., 2019). These values are generally of similar magnitude to the carbon isotope excursions concurrent with the floral ecosystem overturn recorded from the Barents Sea near Norway (Hochuli et al., 2010), which likely occurred long before the marine extinction interval and PTB. However, recent outcrop sampling has revealed a very short but prominent carbon isotope excursion (~-5%) immediately above the uppermost coal in the northern Sydney Basin (Vajda et al., 2020). The differences between the magnitudes of these  $\delta^{13}C_{org}$  excursions may be due to variations in organic components (e.g., wood fragments, miospores, AOM), which can have a demonstrable and significant impact on the secular δ<sup>13</sup>C<sub>org</sub> signal of some Permian-Triassic successions (Foster et al., 1997). Because the correlative PTB horizon is predicted to be on the order of several meters above the uppermost Permian coals (e.g., Chahe, Zhang et al., 2016; within the midst of the *P. crenulata* Zone in eastern Australia, Morante, 1996, this study; Fig. 12), this short excursion may signal an early disruption to the global carbon cycle, coeval with the collapse of terrestrial ecosystems. At present however, it is possible that the PTB interval in eastern Australia has either not yet been sampled (e.g., Williams et al., 2012, 2017) or examined at sufficiently high resolution (Morante, 1996; Retallack et al., 2011; this study) to fully characterize the  $\delta^{13}C_{\text{org}}$  signal.

There are some important differences between the Sydney Basin fossil record and other Permian-Triassic successions around the globe. For instance, Reduviasporonites, a microfossil of fungal (Eshet et al., 1995; Visscher et al., 1996; Twitchett et al., 2001) or algal (Afonin et al., 2001; Spina et al., 2015; Hochuli, 2016) origin, is extremely abundant in many localities across Gondwana and Laurasia soon after the initial phase of the EPE (Visscher et al., 1996). It has been considered an opportunistic "disaster taxon" and a key marker for the Permian-Triassic biotic collapse (see Rampino and Eshet, 2018). However, Reduviasporonites occurs in extremely low numbers in the examined successions (Fig. 7K), suggesting either: (1) Reduviasporonites did not have an abundance acme in these parts of the Sydney Basin; or (2) the relevant stratigraphic beds were not sampled in our study. The local increase in Thymospora spores is similar in magnitude and probable duration to the lycophyte spore acme in the Permian-Triassic record of East Greenland (Looy et al., 2001) and Norway (Hochuli et al., 2010), which suggests the temporary emergence of an open herbaceous flora in the aftermath of the EPE. High abundances of spinose acritarchs (e.g., Micrhystridium and Veryhachium) during the end-Permian extinction interval were found in several marine successions following the end-Permian extinction interval (Sarjeant et al., 1970; Tripathi, 1997; Twitchett et al., 2001; Payne and van de Schootbrugge, 2007), indicating a pulse of primary productivity or dearth of consumers in the oceans. In contrast to the present study in which the acritarch assemblages are dominated by smooth-walled leiospherids, spiny acritarchs are consistently more common in marine successions of the EPE (Lei et al., 2012, 2019; Shen et al., 2013).

There are scattered reports of dominant Lopingian plant groups surviving beyond the onset of terrestrial ecological collapse. Although the last record of glossopterids in Sydney Basin is more-or-less coincident with the cessation of peat-forming conditions, this group may have persisted in small numbers in disparate Gondwanan localities (Antarctica: McManus et al., 2002, Elliot et al., 2017; India: Pant and Pant, 1987; southern Africa: Gastaldo et al., 2015; see Bomfleur et al., 2018), although age controls on these successions are poor. Similarly, scattered

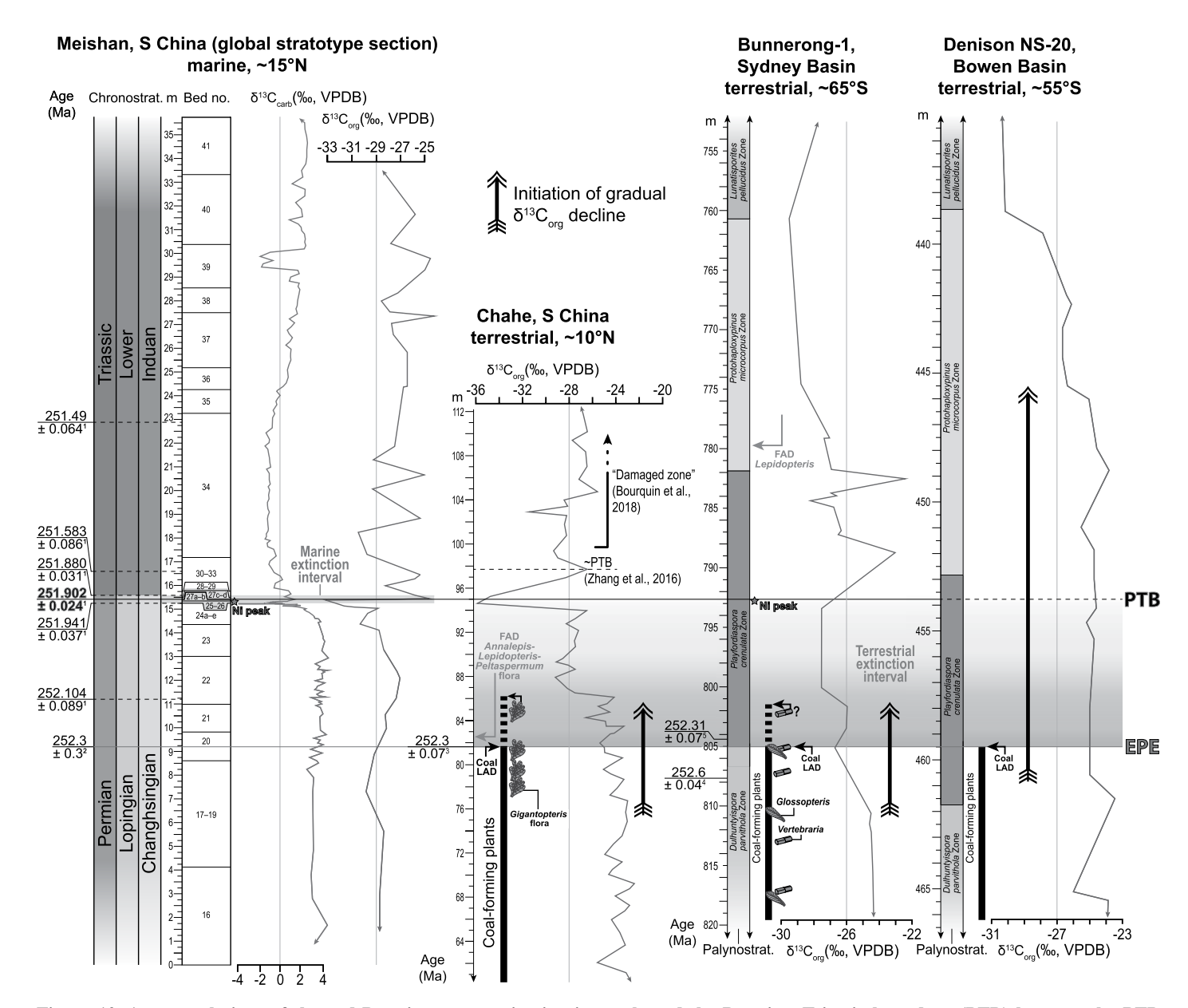


Figure 12. Age correlations of the end-Permian mass extinction intervals and the Permian–Triassic boundary (PTB) between the PTB global stratotype section (Meishan) and three terrestrial stratigraphic successions. All absolute age uncertainties are at  $2\sigma$  level; <sup>1</sup>—Burgess et al., 2014; <sup>2</sup>—Bowring et al. (1998); <sup>3</sup>—Shen et al. (2011); <sup>4</sup>—Metcalfe et al. (2015); <sup>5</sup>—Fielding et al. (2019). EPE—onset of terrestrial end-Permian mass extinction interval; PTB—Permian–Triassic boundary; FAD—first appearance datum; LAD—last appearance datum. Meishan:  $\delta^{13}C_{carb}$  from Cao et al. (2002),  $\delta^{13}C_{org}$  from Cao et al. (2009), and nickel peak placement from Kaiho et al. (2001). Chahe:  $\delta^{13}C_{org}$  from Zhang et al. (2016), and fossil distributions from Bercovici et al. (2015); ~PTB is the estimated placement of the Permian–Triassic boundary by Zhang et al. (2016); "damaged area" refers to an interval of apparent structurally deformed strata reported by Bourquin et al. (2018a). Denison NS-20 (Bowen Basin): biostratigraphy from Foster (1982), coal distribution and  $\delta^{13}C_{org}$  from Morante (1996). Paleolatitudes from Blakey (2008) and Metcalfe (2011). Updated and expanded from Fielding et al. (2019).

remains of gigantopterids, a major pteridosperm component of the Lopingian Cathaysian (east Asian) floral province, appear to post-date the onset of the terrestrial extinction interval by a brief time interval (Bercovici et al., 2015; Fig. 12). Regardless, these groups never recovered, soon became extinct, and did not produce coal deposits after the onset of the EPE.

Vertebrate remains are very sparse from the *P. crenulata* Zone, but the tracks of small therapsids have long been known from terrestrial strata of the Sydney Basin (Harper, 1915). *Lystrosaurus* has been inferred as the maker of these tracks (Retallack, 1996), a distinctive dicynodontid survivor of the EPE very commonly found in the relatively low diversity post-EPE strata of

the Karoo Basin, southern Africa (King, 1990; Damiani et al., 2004; Viglietti et al., 2013). In that region, herbaceous horsetails (Equisetales) have been inferred as the preferred diet of these small herbivores (Rayner, 1992). The paucity of equisetalean spores (e.g., *Calamospora, Laevigatosporites*) in the *P. crenulata* Zone suggests that horsetails were not abundant in the

eastern Australian landscape at the time, while herbaceous lycophyte spores are more common in strata from this interval. This supports Retallack's (1996) proposal that pleuromeian lycophytes were a more likely food source for lystrosaurids in the Sydney Basin. The highly variable spore-pollen abundances throughout the P. crenulata Zone indicate rapid changes in the flora, which would have provided considerable stress on the herbivore populations in eastern Australia and promoted the survival of those subsisting on broad diets. The occurrence of lystrosaurids in both the Sydney and Karoo Basins and the dissimilar floras of these regions also support a generalist feeding strategy for these animals. Such a strategy would have provided a distinct selective advantage over more specialized herbivores or carnivores during the end-Permian ecosystem collapse.

Other mass extinction intervals reveal fossil signatures that may be analogous to the end-Permian collapse stage recorded in the Sydney Basin. For example, the Thymospora fern spore acme is similar to the "spore spike" consistently reported for the Cretaceous-Paleogene (K-Pg) mass extinction event (e.g., Saito et al., 1986; Sweet and Braman, 1992; Vajda et al., 2001; Nichols and Johnson, 2008; Vajda and Bercovici, 2014) and the end-Triassic event (Larsson, 2009). Indeed, spikes in the abundance of fern, lycophyte, or bryophyte spores appear to be a repeated response to global crises in the terrestrial flora through Earth's history (Vajda and McLoughlin, 2007). A similar association of increased sphaeromorph acritarch and AOM abundances has also been recognized in beds spanning the marine Toarcian Oceanic Anoxic Event in Yorkshire, UK (Slater et al., 2019). These pulses were inferred to result from vegetation turnover leading to enhanced soil and bedrock erosion and increased nutrient supply to marine basins (Slater et al., 2019), a scenario likely paralleled by the end-Permian extinction interval (Sephton et al., 2005; Algeo et al., 2011).

## Suppressed Recovery (Protohaploxypinus microcorpus Zone)

The initial interval of the recovery stage shares some important characteristics with the preceding zone, reflecting a gradual transition as indicated by the partial overlap with the *P. crenulata* Zone in ordination space (Fig. 5). Specifically, primary productivity remained low as shown by low absolute palynomorph abundances and significant abundances of AOM and leiospherid acritarchs persisting into this zone, which suggest intervals of lacustrine sedimentation and extensive bacterial degradation of organic matter (Payne and van de Schootbrugge, 2007). Relatively open vegetation, dominated by peltasperm

seed-ferns, voltzialean conifers, and herbaceous sphenophytes and lycophytes, appears to have occupied the landscape throughout this interval (Fig. 9). There are sparse records of *Lepidopteris* (peltasperm seed-fern) appearing very soon after the terrestrial biotic collapse in various localities around the Sydney Basin (Retallack, 2002; Vajda et al., 2020), in East Antarctica (McLoughlin et al., 1997), and in Madagascar (Carpentier, 1935; Townrow, 1965). Opportunistic green algae (e.g., *Quadrisporites*) and fern (e.g., *Thymospora*) groups, which were highly abundant in the wake of the biotic collapse, occur only in minor abundances through this stage.

### Steady recovery (Lunatisporites pellucidus— Protohaploxypinus samoilovichii Zones)

This interval signals the emergence of conifers and corystosperm seed-ferns as dominant constituents of the Triassic floral biome. Peltasperms (Lepidopteris; Figs. 9E and 9J) persist through this interval, but they are progressively relegated to subsidiary components of the flora. Initially, the dominant pollen types were the bisaccate non-taeniate forms Alisporites (Falcisporites) and Pteruchipollenites, indicative of corystosperms (and/or conifers; Townrow, 1967b; Clement-Westerhof, 1974; Balme, 1995). However, these were soon replaced by the taeniate bisaccate pollen Lunatisporites (Fig. 10G), which likely represents podocarpaceous (Townrow, 1967b) or voltzialean (Townrow, 1967a) conifers. The latter group is considered a more likely parent plant group because of the abundant voltzialean leaf compressions found in coeval strata (Retallack, 1980). In contrast, taeniate bisaccate pollen of probable peltasperm affinity (Protohaploxypinus, Striatopodocarpites; Gomankov and Meyen, 1986; see Balme, 1995) persist in very low abundance. The corystosperm Dicroidium (Fig. 9B), a major component of Middle and Late Triassic Gondwanan coal deposits (Balme et al., 1995), appears shortly above the first appearance datum of Lepidopteris in the studied wells (Fig. 11) and becomes progressively more common toward the end of this recovery stage. Over the longer timeframe, there is a protracted reduction of trilete spore groups common during the Permian, such as Microbaculatispora, and the possible osmundalean Horriditriletes (Galtier and Taylor, 1994; Figs. 7A-7B and 7E).

The major fluctuations in  $\delta^{13}C_{org}$  (~-30% to ~22%) through this interval reflect severe changes to the global climate and carbon cycle commonly inferred for the Early Triassic by previous researchers (Payne et al., 2004; Payne and Kump, 2007; Retallack, 2009). Elsewhere throughout the Early Triassic, major changes in palynological suites have been recognized as coinciding with the  $\delta^{13}C_{org}$  fluctuations (Hermann

et al., 2012a). Such  $\delta^{13}C_{org}$  oscillations seem to be matched in the palynological record of Sydney Basin by sharp variations in the cingulate, granulate, and laevigate trilete spore morphogroups between samples. A short interval of depressed  $\delta^{13}C_{org}$  values was identified in the *P. samoilovichii* Zone within the Patonga Formation (a correlative of the Bald Hill Claystone) by Morante (1996). This is mirrored herein by a progressive  $\delta^{13}C_{org}$  decline in the upper *P. samoilovichii* Zone, but this part of the zone corresponds to the Bulgo Sandstone, further suggesting time-transgressive lithostratigraphic units within the Sydney Basin.

Strata correlated to the upper P. samoilovichii Zone of the Sydney Basin (Bulgo Sandstone) have yielded body fossils of a range of archosauriform amniotes (Kear, 2009) and temnospondyl amphibians (Warren, 1991; Damiani, 1999; Greco et al., 2014). However, diverse coprolites suggest an even richer vertebrate fauna than has been recovered to date from these strata (Niedźwiedzki et al., 2016). Similar diverse faunas of aquatic tetrapods and non-marine bony fish have been recovered from Lower Triassic strata of Queensland, Australia: the Rewan Group of the Bowen and Galilee basins (Thulborn, 1986; Warren, 1991; Damiani and Warren, 1996; Northwood, 1999, 2005; Warren et al., 2006). These fossil occurrences correspond to the L. pellucidus-P. samoilovichii palynozones (Metcalfe et al., 2015) and are approximately coeval or perhaps slightly older than the Bulgo Sandstone faunas. Although not yet conducive to peat accumulation, the environmental conditions of this time were stable enough to promote a thriving terrestrial ecosystem of diverse vertebrate faunas and the mixed conifer-seed fern floras less than 2 m.y. after the onset of the end-Permian extinction interval.

## Ecosystem instability (Aratrisporites tenuispinosus Zone)

The transition to this stage (mid-P. samoilovichii-A. tenuispinosus zones) is characterized by the following features: (1) a large and gradual increase in pleuromeian lycophyte fossils; (2) common spinicaudatan fossils; (3) a major, stepwise positive  $\delta^{13}C_{org}$  excursion; and later (4) the prevalence of red, ferruginous mudrock facies or "redbeds" (Bald Hill Claystone) and a concomitant increase in the chemical index of alteration (CIA; Fielding et al., 2019). In the interval immediately preceding this zone, spores of pleuromeian lycophyte affinity (Densoisporites, e.g., Grauvogel-Stamm and Lugardon, 2004; Aratrisporites, e.g., Helby and Martin, 1965; Morbelli and Petriella, 1973) emerge as the dominant palynomorphs, accompanied by abundant lycophyte axes, megaspores, and microphylls. The timing of this abundance increase is in sharp contrast to that of the pleuromeian and selaginellalean lycophyte abundance spikes of Greenland (Looy et al., 2001) and offshore Norway (Hochuli et al., 2010), which were reported to have occurred during the initial phase of the terrestrial extinction interval. Furthermore, this signature is significantly later than that of the Salt and Surghar ranges, Pakistan, which reveal the onset of a prolonged lycophyte dominated flora as early as the Dienerian (Hermann et al., 2011a). Concurrent with the increase in pleuromeian fossils, the repeated occurrence of spinicaudatans suggests a shift toward seasonal desiccation and perhaps increased salinity in ephemeral floodplain lakes (Gueriau et al., 2016).

The major positive  $\delta^{13}C_{\text{org}}$  excursion near the base of the Aratrisporites tenuispinosus Zone, and subsequent high values throughout the studied portion of this zone, are similar to the  $\delta^{13}$ C signature observed for the Smithian-Spathian boundary (SSB) from various successions of the Northern Hemisphere (e.g., Galfetti et al., 2007; Hermann et al., 2011b; Zhang et al., 2015, 2019; Lindström et al., 2019). The palynological record herein is similar to that consistently associated with the SSB; specifically, lycophyte dominated assemblages in the latest Smithian are followed by a rapid shift during the early Spathian to stable, mixed pteridophyte-gymnosperm floras (Barents Sea: Hochuli and Vigran, 2010; Pakistan: Hermann et al., 2011a, Hermann et al., 2012b; Tibet: Schneebeli-Hermann et al., 2012; northern Greenland: Lindström et al., 2019). The age of this substage boundary has not been well-constrained at present. U-Pb radiometric age determinations of zircons from tuff deposits have indicated that the SSB is older than  $250.55 \pm 0.51$  Ma (Ovtcharova et al., 2006; Galfetti et al., 2007). However, these age estimates were not derived using the updated U-Pb age model employed for the Permian-Triassic type section (Burgess et al., 2014), precluding their direct comparison with the most recent age estimates of the PTB. Importantly, these earlier methods produced large error ranges and tended to systematically overestimate the U-Pb age values (Condon et al., 2010). A ca. 248.45 Ma age for the SSB was inferred from a combination of marine biostratigraphic and magnetostratigraphic indices correlated to the global time scale (Ogg, 2012). The high-precision absolute age estimates of the Sydney Basin and deposition rates for the Lower Triassic in this study put the positive shift in  $\delta^{13}C_{\text{org}}$  at ca. 249 Ma, approximately midway between the SSB estimates in the aforementioned chronostratigraphic schemes (Ovtcharova et al., 2006; Galfetti et al., 2007; Ogg, 2012). We interpret this positive  $\delta^{13}C_{org}$ excursion as a tentative marker of the SSB in

the Sydney Basin; therefore, the base of the Aratrisporites tenuispinosus Zone is likely coincident with, or slightly below, the SSB. However, higher resolution palynological and chemostratigraphic analyses of this interval are necessary to better constrain the placement and floristic character of this event at high southern latitudes.

The emergence of herbaceous lycophytes as the dominant palynomorph group (particularly Aratrisporites), significant  $\delta^{13}C_{org}$  excursion, and coeval redbed development near the base of this zone are indicative of significant environmental changes that delayed the re-establishment of complex forest ecosystems. However, ecological and environmental interpretations of this zone are presently equivocal. Pleuromeian lycophytes, which dominate the base of this zone, have long been considered herb- to shrub-sized xerophytic or halophytic plants that flourished in regions of probable aridity and/or elevated salinity (Mägdefrau, 1931; Retallack, 1975; Ziqiang and Lixin, 1982). However, Triassic pleuromeian remains have also been found in wetland settings in some parts of southern Gondwana (central Transantarctic Mountains; Bomfleur et al., 2011). Pleuromeians, like their closest extant relatives Isoëtes (quillworts), may have preferred consistently or seasonally wet habitats, and their dominance during various intervals of the Early Triassic in various parts of the world was possibly favored by other factors. This could have included greater immunity to fluctuations in atmospheric gas concentrations (obtaining CO<sub>2</sub> via their root systems), having slow growth rates with storage of starch in a large zone of cortical tissues, occupying open landscapes free from competition, and possibly having a form of crassulacean acid metabolism (CAM) and a lycopsid photosynthetic pathway. All of these features represent specialized ecological adaptations to stressed environments.

This interval saw the starvation of coarse sediment supply (Cowan, 1993) and intensification of red-bed development (Bald Hill Claystone and equivalents) in the Sydney Basin that likely reflect destabilization of the climatic system. Redbed formation has been commonly interpreted to reflect semi-arid conditions (Van Houten, 1973) and/or strongly fluctuating watertables (Dubiel and Smoot, 1994). The development of ferruginous mudrock facies in the Lower Triassic of the Karoo Basin, southern Africa, has been attributed to increased temperature, seasonality (Smith and Botha-Brink, 2014), and either an increase (Retallack et al., 2003) or decrease (Smith and Botha-Brink, 2014) in overall precipitation. Although these facies generally constrain the range of possible depositional conditions, they are not indicative of any specific paleoenvironments without additional proxies (Sheldon, 2005).

However, in the case of the Sydney Basin, the marked increase in the CIA during this stage of ecosystem instability (Fig. 11) favors an overall increase in precipitation (Fielding et al., 2019). This likely reflects intensification of the Gondwana monsoon in the region. More humid conditions have also been inferred for the onset of Lower Triassic red paleosols of Antarctica (Retallack and Krull, 1999). Importantly, as per the lycophyte abundance increase outlined above, the onset of redbed development appears to have occurred at disparate times across southern Gondwana. Ferruginous mudstone facies have been dated to near the inferred onset of Permian-Triassic terrestrial extinctions in the Karoo Basin (Ward et al., 2005; Smith and Botha-Brink, 2014; Gastaldo et al., 2015) and some regions of the Transantarctic Mountains (e.g., Collinson et al., 1994). In other Antarctic successions, the first ferruginous mudrocks occur much higher in the Lower Triassic successions, in some cases hundreds of meters above the last evidence of Permian floras (see McLoughlin et al., 1997; Retallack and Krull, 1999). This diachroneity of ferruginous strata and coeval pulse of lycophyte dominance are clearly indicative of shifting climatic belts across much of Pangaea that likely initiated during the late Permian (McLoughlin et al., 1997). However, further data will be required to resolve the precise climatic drivers of the sedimentary and biotic changes in the late Early Triassic.

This interval of ecosystem instability initiated with rapid fluctuations in palynomorph assemblages caused by blooms of specialist lycophytes. However, following this interval of lycophyte dominance, the spore-pollen record of the A. tenuispinosus Zone reflects the establishment of a complex fern-gymnosperm recovery flora, with assemblages similar in composition and abundance to those of the L. pellucidus-P. samoilovichii zones. The high inter-sample variability of this zone is reflected by the large area it occupies in the ordination space (Fig. 5). Toward the end of this stage, fossil leaves of Dicroidium become much more common in the studied bore cores and in outcrop throughout the Sydney Basin (Walkom, 1925; Retallack, 1980) and are matched by abundance increases of Alisporites (Falcisporites) and Pteruchipollenites, pollen commonly associated with corystosperms (Clement-Westerhof, 1974; Balme, 1995). In contrast, there is a corresponding reduction in all taeniate bisaccate pollen to negligible levels. We note a distinct absence of Lepidopteris (peltasperm) leaves in the cores toward the top of this zone. However, Lepidopteris madagascariensis remained a sub-dominant element in macrofloras recovered from equivalent strata in outcrop of the northern Sydney Basin and the neighboring Lorne Basin (Holmes and Ash, 1979; Retallack, 1980). This seems to indicate the initial re-commencement of floral ecosystem recovery after the Smithian–Spathian event.

#### **CONCLUSIONS**

The southern high-latitude continental strata of the Sydney Basin record a near-continuous succession of sedimentary, geochemical, and floristic changes from the late Permian (Wuchiapingian) to late Early Triassic (late Olenekian). Recent absolute dating of tuffs has refined the timing of several discrete floristic stages through this interval. Most of the late Permian was characterized by a stable, low diversity mire and broad-leafed forest flora dominated by deciduous glossopterid gymnosperms. This stable ecosystem abruptly collapsed between deposition of two ash beds dated at 252.3 Ma and 252.6 Ma. This event marked the rapid demise of the glossopterid biome across southern Gondwana. The collapse, equated to the terrestrial end-Permian mass extinction event, occurred up to several hundred thousand years before the chronostratigraphic Permian-Triassic Boundary. The collapse is concurrent with the initiation of: (1) the primary phase of Siberian Traps Large Igneous Province extrusive magmatism and (2) a gradual stable carbon isotope shift toward lower values in terrestrial successions around the world, which likely signifies a long-term shift in the global carbon cycle punctuated by one or more short, sharp excursions. In the wake of this collapse, the flora was characterized by very low productivity and successive abundance spikes of opportunistic fungi, algae, and fern "disaster taxa."

Ecosystem recovery occurred through several successive palynozones and is expressed by stepwise appearances of macrofossils belonging to several prominent Mesozoic gymnosperm groups (peltasperms, voltzialean conifers, and corystosperms). This recovery phase is supported by the emergence of a diverse and ecologically complex vertebrate fauna across eastern Australia in contrast with the depauperate vertebrate record in the immediate aftermath of the EPE. However, recovery was hampered by conditions that were prohibitive to the reestablishment of productive wetlands or forests, despite early emergence of the plant groups (e.g., peltasperms, corystosperms) that became the primary peat-formers of the Middle to Late Triassic of Gondwana. In addition to the absence of coals, environmental stressors through the Early Triassic are reflected by persistent anoxic/dysoxic aqueous conditions and a fluctuating stable carbon isotope record that likely indicates an unstable global climate.

The establishment of a new, complex coniferpteridosperm climax flora was interrupted by a major phase of abiotic stress in the region initiating approximately 2 m.y. after the PTB (ca. 250 Ma; mid-Smithian). This was indicated by a marked rise of pleuromeian lycophytes with specialized ecophysiological traits and a stepwise positive shift in stable carbon isotopes. This was followed by the accumulation of thick packages of ferruginous mudrocks, an increase in chemical weathering, and a major overturn of the palynofloras shortly before the Smithian-Spathian boundary (SSB), the first such stable carbon and palynological records of this boundary from southern Gondwana. The age of the SSB was estimated as ca. 249 Ma by interpolating the sediment accumulation rates from radiogenicisotope age anchor-points within the Sydney Basin. The specific environmental changes that triggered this environmental transition late in the Early Triassic are presently unclear, but they were likely linked to prolonged climate change and shifting climatic belts across southern Gondwana. Similar changes have been identified in post-EPE successions the world over but at discrepant intervals. The high southern latitudes were likely the last region on Earth to develop these environmental conditions. In summary, the loss of the Permian climax glossopterid floras represents a major collapse in primary productivity and ecological complexity from which the terrestrial vegetation did not recover until late in the Early Triassic.

### ACKNOWLEDGMENTS

This research was funded by collaborative research grants from the National Science Foundation (EAR-1636625 to CRF and TDF). Funding was also received from the Swedish Research Council (grant 2015-4264 to VV, and grants 2014-5234 and 2018-04527 to SM). The authors thank Sam Slater for assistance with the ordination analyses, and Arne Winguth, Cornelia Winguth, Malcolm Bocking, and James Crowley for their input, which provided additional geochronologic and paleoclimatic context. Special thanks to John Laurie for discussions regarding Australian biostratigraphic schemes. Assistance with sample collection was provided by Mark Ryland and the staff at the Londonderry Drillcore Library, NSW, Australia. We are grateful to Rob Strachan for editing the manuscript and Benjamin Bomfleur and one anonymous reviewer for their constructive reviews, which greatly improved the manuscript.

### REFERENCES CITED

- Afonin, S.A., Barinova, S.S., and Krassilov, V.A., 2001, A bloom of *Tympanicysta* Balme (green algae of zygnematalean affinities) at the Permian-Triassic boundary: Geodiversitas, v. 23, p. 481–487.
- Agnew, D., Bocking, M., Brown, K., Ives, M., Johnson, D., Howes, M., Preston, B., Rigby, R., Warbrooke, P., and Weber, C.R., 1995, Sydney Basin—Newcastle Coalfield, in Ward, C.R., Harrington, H.J., Mallett, C.W., and Beeston, J.W., eds., Geology of Australian Coal Basins: Sydney, Geological Society of Australia, Coal Geology Group, Special Publication 1, p. 197–212.

- Algeo, T.J., Chen, Z.Q., Fraiser, M.L., and Twitchett, R.J., 2011, Terrestrial-marine teleconnections in the collapse and rebuilding of Early Triassic marine ecosystems: Palaeogeography, Palaeoclimatology, Palaeoecology, v. 308, p. 1–11, https://doi.org/10.1016/ j.palaeo.2011.01.011.
- Alroy, J., Aberhan, M., Bottjer, D.J., Foote, M., Fürsich, F.T., Harries, P.J., Hendy, A.J.W., Holland, S.M., Ivany, L.C., Kiessling, W., Kosnik, M.A., Marshall, C.R., McGowan, A.J., Miller, A.I., Olszewski, T.D., Patzkowsky, M.E., Peters, S.E., Villier, L., Wagner, P.J., Bonuso, N., Borkow, P.S., Brenneis, B., Clapham, M.E., Fall, L.M., Ferguson, C.A., Hanson, V.L., Krug, A.Z., Layou, K.M., Leckey, E.H., Nürnberg, S., Powers, C.M., Sessa, J.A., Simpson, C., Tomašových, A., and Visaggi, C.C., 2008, Phanerozoic trends in the global diversity of marine invertebrates: Science, v. 321, p. 97–100, https://doi.org/10.1126/science.1156963.
- Anderson, J.M., and Anderson, H.M., 1985, Palaeoflora of Southern Africa: Prodromus of South African Megafloras Devonian to Lower Cretaceous: Rotterdam, AA Balkema, 423 p.
- Arche, A., and López-Gómez, J., 2005, Sudden changes in fluvial style across the Permian–Triassic boundary in the eastern Iberian Ranges, Spain: Analysis of possible causes: Palaeogeography, Palaeoclimatology, Palaeoecology, v. 229, p. 104–126, https://doi.org/10.1016/ j.palaeo.2005.06.033.
- Ayaz, S.A., Amelin, Y., Nicoll, R.S., Esterle, J.S., and Martin, M.A., 2016, Age of the Yarrabee and accessory tuffs: Implications for the upper Permian sediment-accumulation rates across the Bowen Basin: Australian Journal of Earth Sciences, v. 63, p. 843–856, https://doi.org/10 .1080/08120099.2016.1255254.
- Balme, B.E., 1969, The Permian-Triassic boundary in Australia: Geological Society of Australia Special Publication, v. 2, p. 99–112.
- Balme, B.E., 1970, Palynology of Permian and Triassic strata in the Salt Range and Surghar Range, West Pakistan, in Kummel, B., and Teichert, C., eds., Stratigraphic Boundary Problems—Permian and Triassic of West Pakistan: Lawrence, University of Kansas Special Publication, v. 4, p. 305–453.
- Balme, B.E., 1995, Fossil in situ spores and pollen grains: An annotated catalogue: Review of Palaeobotany and Palynology, v. 87, p. 81–323, https://doi.org/10.1016/0034-6667(95)93235-X.
- Balme, B.E., and Playford, G., 1967, Late Permian plant microfossils from the Prince Charles Mountains, Antarctica: Revue de Micropaleontologie, v. 10, p. 179–192.
- Balme, B.E., Kershaw, A.P., and Webb, J.A., 1995, Floras of Australian coal measures, with notes on their associated Mesozoic faunas, in Ward, C.R., Harrington, H.J., Mallett, C.W., and Beeston, J.W., eds., Geology of Australian Coal Basins: Sydney, Geological Society of Australia, Coal Geology Group, p. 41–62.
- Bamberry, W.J., Hutton, A.J., and Jones, B.G., 1995, The Permian Illawarra Coal Measures, southern Sydney Basin, Australia: A case study of deltaic sedimentation, in Postma, G., and Oti, M.N., eds., Geology of Deltas: Rotterdam, AA Balkema, p. 153–166.
- Benton, M.J., 1995, Diversification and extinction in the history of life: Science, v. 268, p. 52–58, https://doi .org/10.1126/science.7701342.
- Benton, M.J., and Newell, A.J., 2014, Impacts of global warming on Permo-Triassic terrestrial ecosystems: Gondwana Research, v. 25, p. 1308–1337, https://doi.org/10.1016/j.gr.2012.12.010.
- Bercovici, A., and Vajda, V., 2016, Terrestrial Permian–Triassic boundary sections in South China: Global and Planetary Change, v. 143, p. 31–33, https://doi.org/10.1016/j.gloplacha.2016.05.010.
- Bercovici, A., Hadley, A., and Villanueva-Amadoz, U., 2009, Improving depth of field resolution for palynological photomicrography: Palaeontologia Electronica, v. 12, no. 12.2.5 T.
- Bercovici, A., Cui, Y., Forel, M.-B., Yu, J., and Vajda, V., 2015, Terrestrial paleoenvironment characterization across the Permian-Triassic boundary in South China: Journal of Asian Earth Sciences, v. 98, p. 225–246, https://doi.org/10.1016/j.jseaes.2014.11.016.
- Blakey, R.C., 2008, Gondwana paleogeography from assembly to breakup—A 500 m.y. odyssey, *in* Fielding,

- C.R., Frank, T.D., and Isbell, J.L., eds., Resolving the Late Paleozoic Ice Age in Time and Space: Geological Society of America Special Paper 441, p. 1–28, https://doi.org/10.1130/2008.2441(01).
- Blakey, R.C., 2016, Global Paleogeography and Tectonics in Deep Time: Colorado Plateau Geosystems: https://deeptimemaps.com/global-series-details/.
- Bomfleur, B., Krings, M., Taylor, E.L., and Taylor, T.N., 2011, Macrofossil evidence for pleuromeialean lycophytes from the Triassic of Antarctica: Acta Palaeontologica Polonica, v. 56, p. 195–203, https://doi .org/10.4202/app.2010.0022.
- Bomfleur, B., Blomenkemper, P., Kerp, H., and McLoughlin, S., 2018, Polar regions of the Mesozoic-Paleogene greenhouse world as refugia for relict plant groups, in Krings, M., Harper, C.J., Cuneo, N.R., and Rothwell, G.W., eds., Transformative Paleobotany: Papers to Commemorate the Life and Legacy of Thomas N. Taylor: Cambridge, Academic Press, p. 593–611, https:// doi.org/10.1016/B978-0-12-813012-4.00024-3.
- Bond, D.P.G., and Wignall, P.B., 2014, Large igneous provinces and mass extinctions: An update, in Keller, G., and Kerr, A.C., eds., Volcanism, Impacts, and Mass Extinctions: Causes and Effects: Geological Society of America Special Paper 505, p. 28, https://doi.org/10.1130/2014.2505(02).
- Bourquin, S., Rossignol, C., Jolivet, M., Poujol, M., Broutin, J., and Yu, J., 2018a, Terrestrial Permian-Triassic boundary in southern China: New stratigraphic, structural and palaeoenvironment considerations: Palaeogeography, Palaeoclimatology, Palaeoecology, v. 490, p. 640–652, https://doi.org/10.1016/j.palaeo.2017.11.055.
- Bourquin, S., Rossignol, C., Jolivet, M., Poujol, M., Broutin, J., and Yu, J., 2018b, Reply to the comment on "Terrestrial Permian-Triassic boundary in southern China: New stratigraphic, structural and palaeoen-vironment considerations" by H. Zhang, Z. Feng, J. Ramezanik, S-Z Shen: Palaeogeography, Palaeoclimatology, Palaeoecology, v. 506, p. 257–259, https://doi.org/10.1016/j.palaeo.2018.02.021.
- Bowman, V.C., Francis, J.E., Askin, R.A., Riding, J.B., and Swindles, G.T., 2014, Latest Cretaceous—earliest Paleogene vegetation and climate change at the high southern latitudes: Palynological evidence from Seymour Island, Antarctic Peninsula: Palaeogeography, Palaeoclimatology, Palaeoecology, v. 408, p. 26–47, https://doi. org/10.1016/j.palaeo.2014.04.018.
- Bowring, S.A., Erwin, D.H., Davidek, K., Wang, W., Jin, M.W., and Martin, Y.G., 1998, U/Pb zircon geochronology and tempo of the end-Permian mass extinction: Science, v. 280, p. 1039–1045, https://doi.org/10.1126/ science.280.5366.1039.
- Brakel, A.T., 1986, Global sea-level change as a method of correlating the Late Permian coal measures in the Sydney, Gunnedah and Bowen basins, eastern Australia: BMR Journal of Australian Geology and Geophysics, v. 10, p. 17–22.
- Brand, U., Posenato, R., Came, R., Affek, H., Angiolini, L., Azmy, K., and Farabegoli, E., 2012, The end-Permian mass extinction: A rapid volcanic CO<sub>2</sub> and CH<sub>4</sub>-climatic catastrophe: Chemical Geology, v. 322–323, p. 121–144, https://doi.org/10.1016/j.chemgeo.2012.06.015.
- Brunker, R.L., and Rose, G., 1969, Sydney Basin Geological Maps (1st edition): Sydney, Geological Survey of New South Wales, scale 1:500,000.
- Burgess, S.D., and Bowring, S.A., 2015, High-precision geochronology confirms voluminous magmatism before, during, and after Earth's most severe extinction: Science Advances, v. 1, e1500470, https://doi.org/10.1126/ sciadv.1500470.
- Burgess, S.D., Bowring, S., and Shen, S.-z., 2014, Highprecision timeline for Earth's most severe extinction: Proceedings of the National Academy of Sciences of the United States of America, v. 111, p. 3316–3321, https://doi.org/10.1073/pnas.1317692111 (correction: http://dx.doi.org/10.1073/pnas.1403228111).
- Burgess, S.D., Muirhead, J.D., and Bowring, S.A., 2017, Initial pulse of Siberian Traps sills as the trigger of the end-Permian mass extinction: Nature Communications, v. 8, no. 164, https://doi.org/10.1038/s41467-017-00083-9.

- Cao, C., Wang, W., and Jin, Y., 2002, Carbon isotope excursions across the Permian-Triassic boundary in the Meishan section, Zhejiang Province, China: Chinese Science Bulletin, v. 47, p. 1125–1129, https://doi.org/10.1360/02tb9252.
- Cao, C., Love, G.D., Hays, L.E., Wang, W., Shen, S., and Summons, R.E., 2009, Biogeochemical evidence for euxinic oceans and ecological disturbance presaging the end-Permian mass extinction event: Earth and Planetary Science Letters, v. 281, p. 188–201, https:// doi.org/10.1016/j.epsl.2009.02.012.
- Cao, Y., Song, H., Algeo, T.J., Chu, D., Du, Y., Tian, L., Wang, Y., and Tong, J., 2019, Intensified chemical weathering during the Permian-Triassic transition recorded in terrestrial and marine successions: Palaeogeography, Palaeoclimatology, Palaeoecology, v. 519, p. 166–177, https://doi.org/10.1016/j.palaeo.2018.06.012.
- Carpentier, A., 1935, Études paléobotaniques sur le groupe de la Sakoa et le groupe de la Sakamena (Madagascar): Annales Géologiques du Service des mines de Madagascar, v. 5, p. 7–32.
- Cascales-Miñana, B., Diez, J.B., Gerrienne, P., and Cleal, C.J., 2016, A palaeobotanical perspective on the great end-Permian biotic crisis: Historical Biology, v. 28, p. 1066–1074, https://doi.org/10.1080/08912963.201 5.1103237.
- Chu, D., Yua, J., Tong, J., Benton, M.J., Song, H., Huang, Y., Song, T., and Tiana, L., 2016, Biostratigraphic correlation and mass extinction during the Permian– Triassic transition in terrestrial-marine siliciclastic settings of South China: Global and Planetary Change, v. 146, p. 67–88, https://doi.org/10.1016/ j.gloplacha.2016.09.009.
- Clare, R.C., 1985, Geology of the Newlands mine area, Bowen Basin Coal Symposium: Rockhampton, Geological Society of Australia, p. 284–292.
- Clement-Westerhof, J.A., 1974, In situ pollen from gymnospermous cones from the Upper Permian of the Italian Alps—A preliminary account: Review of Palaeobotany and Palynology, v. 17, p. 63–73, https://doi.org/10.1016/0034-6667(74)90092-X.
- Cohen, K.M., Finney, S.C., Gibbard, P.L., and Fan, J.-X., 2013, The ICS International Chronostratigraphic Chart: Episodes, v. 36, p. 199–204, https://doi.org/10.18814/ epiiugs/2013/v36i3/002.
- Collinson, J.W., Isbell, J.L., Elliot, D.H., Miller, M.F., Miller, J.M.G., and Veevers, J.J., 1994, Permian-Triassic Transantarctic Basin, in Veevers, J.J., and Powell, C.M., eds., Permian-Triassic Pangean Basins and Foldbelts along the Panthalassan Margin of Gondwanaland: Geological Society of America Memoir 184, p. 173–222.
- Condon, D.J., McLean, N., Noble, S.R., and Bowring, S.A., 2010, Isotopic composition (<sup>238</sup>U/<sup>235</sup>U) of some commonly used uranium reference materials: Geochimica et Cosmochimica Acta, v. 74, p. 7127–7143, https://doi .org/10.1016/j.gca.2010.09.019.
- Cowan, E.J., 1993, Longitudinal fluvial drainage patterns within a foreland basin-fill: Permo-Triassic Sydney Basin, Australia: Sedimentary Geology, v. 85, p. 557–577, https://doi.org/10.1016/0037-0738(93)90102-B.
- Cui, Y., and Kump, L.R., 2015, Global warming and the end-Permian extinction event: Proxy and modeling perspectives: Earth-Science Reviews, v. 149, p. 5–22, https:// doi.org/10.1016/j.earscirev.2014.04.007.
- Damiani, R.J., 1999, Giant temnospondyl amphibians from the Early to Middle Triassic Narrabeen Group of the Sydney Basin, New South Wales, Australia: Alcheringa, v. 23, p. 87–109, https://doi.org/10.1080/03115519908619324.
- Damiani, R.J., and Warren, A.A., 1996, A new look at members of the Superfamily Brachyopoidea (Amphibia, Temnospondyli) from the Early Triassic of Queensland and a preliminary analysis of braehyopoid relationships: Alcheringa, v. 20, p. 277–300, https://doi .org/10.1080/03115519608619472.
- Damiani, R.J., Neveling, J., Modesto, S.P., and Yates, A.M., 2004, Barendskraal, a diverse amniote locality from the *Lystrosaurus* assemblage zone: Early Triassic of South Africa: Palaeontologia Africana, v. 39, p. 53–62.
- de Jersey, N.J., 1970, Early Triassic miospores from the Rewan Formation: Geological Survey of Queensland Publications, v. 345, p. 1–29.

- Decombeix, A.L., Taylor, E.L., and Taylor, T.N., 2009, Secondary growth in Vertebraria roots from the Late Permian of Antarctica: A change in developmental timing: International Journal of Plant Sciences, v. 170, p. 644–656, https://doi.org/10.1086/597784.
- Diessel, C.F.K., 1992, Coal-bearing Depositional Systems: Berlin, Springer, 721 p., https://doi.org/10.1007/978-3-642-75668-9.
- Diessel, C.F.K., and Smyth, M., 1995, Petrographic constituents of Australian coals, in Ward, C.R., Harrington, H.J., Mallett, C.W., and Beeston, J.W., eds., Geology of Australian Coal Basins: Sydney, Geological Society of Australia, Coal Geology Group, Special Publication 1, p. 63–81.
- Dolby, J.H., and Balme, B.E., 1976, Triassic palynology of the Carnarvon Basin, Western Australia: Review of Palaeobotany and Palynology, v. 22, p. 105–168, https:// doi.org/10.1016/0034-6667(76)90053-1.
- Dubiel, R.F., and Smoot, J.P., 1994, Criteria for interpreting paleoclimate from red beds—A tool for Pangean reconstructions, in Embry, A.F., Beauchamp, B., and Glass, B.J., eds., Pangea: Global Environments and Resources: Calgary, Canadian Society of Petroleum Geologists Memoirs 17, p. 295–310.
- Elliot, D.H., Fanning, C.M., Isbell, J.L., and Hulett, S.R.W., 2017, The Permo-Triassic Gondwana sequence, central Transantarctic Mountains, Antarctica: Zircon geochronology, provenance, and basin evolution: Geosphere, v. 13, p. 155–178, https://doi.org/10.1130/GES01345.1.
- Emerson, D.W., and Branagan, D.F., 2011, The Narrabeen Group in the east-central Sydney Basin: Physical properties and interpretation: Exploration Geophysics, v. 42, p. 258–274, https://doi.org/10.1071/EG11011.
- Eshet, Y., Rampino, M.R., and Visscher, H., 1995, Fungal event and palynological record of ecological crisis and recovery across the Permian-Triassic boundary: Geology, v. 23, p. 967–970, https://doi.org/10.1130/0091-7613(1995)023<0967:FEAPRO>2.3.CO;2.
- Esmeray-Senlet, S., Miller, K.G., Sherrella, R.M., Senlet, T., Vellekoop, J., and Brinkhuis, H., 2017, Iridium profiles and delivery across the Cretaceous/Paleogene boundary: Earth and Planetary Science Letters, v. 457, p. 117–126, https://doi.org/10.1016/j.epsl.2016.10.010.
- Fielding, C.R., Frank, T.D., Vajda, V., McLoughlin, S., Mays, C., Tevyaw, A.P., Winguth, A., Winguth, C., Nicoll, R.S., Bocking, M., and Crowley, J.L., 2019, Age and pattern of the southern high-latitude continental end-Permian extinction constrained by multiproxy analysis: Nature Communications, v. 10, no. 385, https://doi.org/10.1038/s41467-018-07934-z.
- Foster, C.B., 1979, Permian plant microfossils of the Blair Athol Coal Measures, Baralaba coal measures, and basal Rewan Formation of Queensland: Geological Survey of Queensland Publications, v. 372, p. 1–244.
- Foster, C.B., 1982, Spore-pollen assemblages of the Bowen Basin, Queensland (Australia): Their relationship to the Permian/Triassic boundary: Review of Palaeobotany and Palynology, v. 36, p. 165–183, https://doi .org/10.1016/0034-6667(82)90016-1.
- Foster, C.B., Logan, G.A., Summons, R.E., Gorter, J.D., and Edwards, D.S., 1997, Carbon isotopes, kerogen types and the Permian-Triassic boundary in Australia: Implications for exploration: APPEA Journal, v. 37, p. 472–489, https://doi.org/10.1071/AJ96028.
- Galfetti, T., Bucher, H., Ovtcharova, M., Schaltegger, U., Brayard, A., Brühwiler, T., Goudemand, N., Weissert, H., Hochuli, P.A., Cordey, F., and Guodun, K., 2007, Timing of the Early Triassic carbon cycle perturbations inferred from new U–Pb ages and ammonoid biochronozones: Earth and Planetary Science Letters, v. 258, p. 593–604, https://doi.org/10.1016/j.epsl.2007.04.023.
- Galtier, J., and Taylor, T.N., 1994, The first record of ferns from the Permian of Antarctica: Review of Palaeobotany and Palynology, v. 83, p. 227–239, https://doi .org/10.1016/0034-6667(94)90071-X.
- Gastaldo, R.A., Kamo, S.L., Neveling, J., Geissman, J.W., Bamford, M., and Looy, C.V., 2015, Is the vertebratedefined Permian–Triassic boundary in the Karoo Basin, South Africa, the terrestrial expression of the end-Permian marine event?: Geology, v. 43, p. 939–942, https:// doi.org/10.1130/G37040.1.
- Gomankov, A.V., and Meyen, S.V., 1986, Tatarinovaya flora (soslav i rasprostranenie v pozdnei permi Evrazi)

- [Tatarian flora (composition and distribution in the late Permian of Eurasia)]: Trudy Akademia Nauk SSSR, v. 401, p. 1–174.
- Gould, R.E., and Delevoryas, T., 1977, The biology of Glossopteris: Evidence from petrified seed-bearing and pollen-bearing organs: Alcheringa, v. 1, p. 387–399, https://doi.org/10.1080/03115517708527774.
- Gradstein, F.M., Ogg, J.G., Schmitz, M.D., and Ogg, G.M., 2012, The Geologic Time Scale 2012: London, Elsevier, 1144 p.
- Grauvogel-Stamm, L., and Lugardon, B., 2004, The spores of the Triassic lycopsid *Pleuromeia sternbergii* (Münster) Corda: Morphology, ultrastructure, phylogenetic implications, and chronostratigraphic inferences: International Journal of Plant Sciences, v. 165, p. 631–650, https://doi.org/10.1086/386562.
- Greco, F., Kear, B., Campione, N.E., and Niedźwiedzki, G., 2014, An Olenekian high-latitude vertebrate assemblage from the Sydney Basin, Australia: Testing Gondwanan faunal segregation in the earliest Triassic, 74th Annual Meeting of the Society of Vertebrate Paleontology, November 5–8: Berlin, Germany, p. 141.
- Grice, K., Twitchett, R.J., Alexander, R., Foster, C.B., and Looy, C., 2005, A potential biomarker for the Permian– Triassic ecological crisis: Earth and Planetary Science Letters, v. 236, p. 315–321, https://doi.org/10.1016/ j.epsl.2005.05.008.
- Gueriau, P., Rabet, N., Clément, G., Lagebro, L., Vannier, J., Briggs, D.E.G., Charbonnier, S., Olive, S., and Béthoux, O., 2016, A 365-million-year-old freshwater community reveals morphological and ecological stasis in branchiopod crustaceans: Current Biology, v. 26, p. P383–P390, https://doi.org/10.1016/ j.cub.2015.12.039.
- Gulbranson, E.L., Isbell, J.L., Taylor, E.L., Ryberg, P.E., Taylor, T.N., and Flaig, P.P., 2012, Permian polar forests: Deciduousness and environmental variation: Geobiology, v. 10, p. 479–495, https://doi.org/10.1111/j.1472-4669.2012.00338.x.
- Hammer, Ø., and Harper, D.A.T., 2006, Paleontological Data Analysis: Oxford, Blackwell, 351 p.
- Hammer, Ø., Harper, D.A.T., and Ryan, P.D., 2001, PAST: Paleontological statistics software package for education and data analysis: Palaeontologia Electronica, v. 4, no. 4, p. 1–9.
- Harper, L.E., 1915, Geology and mineral resources of the southern coal-field: Geological Memoir of the Geological Survey of New South Wales 7, p. 1–410.
- Helby, R., 1973, Review of Late Permian and Triassic palynology of New South Wales: Geological Society of Australia Special Publication 4, p. 141–155.
- Helby, R.J., and Martin, A.R.H., 1965, Cylostrobus gen. nov., cones of lycopsidean plants from the Narrabeen Group (Triassic) of New South Wales: Australian Journal of Botany, v. 13, p. 389–404, https://doi.org/10.1071/ BT9650389.
- Helby, R., Morgan, R., and Partridge, A.D., 1987, A palynological zonation of the Australian Mesozoic: Memoirs of the Association of Australasian Palaeontologists, v. 4, p. 1–94.
- Herbert, C., 1980, Depositional development of the Sydney Basin, in Herbert, C., and Helby, R., eds., A Guide to the Sydney Basin: Sydney, Geological Survey of New South Wales, Geological Survey of New South Wales Bulletin, v. 26, p. 11–52.
- Herbert, C., 1997a, Sequence stratigraphic analysis of Early and Middle Triassic alluvial and estuarine facies in the Sydney Basin, Australia: Australian Journal of Earth Sciences, v. 44, p. 125–143, https://doi .org/10.1080/08120099708728299.
- Herbert, C., 1997b, Relative sea level control of deposition in the Late Permian Newcastle Coal Measures of the Sydney Basin, Australia: Sedimentary Geology, v. 107, p. 167–187, https://doi.org/10.1016/S0037-0738(96)00027-9.
- Hermann, E., Hochuli, P.A., Bucher, H., Brühwiler, T., Hautmann, M., Ware, D., and Roohi, G., 2011a, Terrestrial ecosystems on North Gondwana following the end-Permian mass extinction: Gondwana Research, v. 20, p. 630–637, https://doi.org/10.1016/j.gr.2011.01.008.
- Hermann, E., Hochuli, P.A., Méhay, S., Bucher, H., Brühwiler, T., Ware, D., Hautmann, M., Roohi, G.,

- ur-Rehman, K., and Yaseen, A., 2011b, Organic matter and palaeoenvironmental signals during the Early Triassic biotic recovery: The Salt Range and Surghar Range records: Sedimentary Geology, v. 234, p. 19–41, https:// doi.org/10.1016/j.sedgeo.2010.11.003.
- Hermann, E., Hochuli, P.A., Bucher, H., Brühwiler, T., Hautmann, M., Ware, D., Weissert, H., Roohi, G., Yaseen, A., and Khalil-ur-Rehman, 2012a, Climatic oscillations at the onset of the Mesozoic inferred from palynological records from the North Indian Margin: Journal of the Geological Society, v. 169, p. 227–237, https://doi.org/10.1144/0016-76492010-130.
- Hermann, E., Hochuli, P.A., Bucher, H., and Roohi, G., 2012b, Uppermost Permian to Middle Triassic palynology of the Salt Range and Surghar Range, Pakistan: Review of Palaeobotany and Palynology, v. 169, p. 61–95, https://doi.org/10.1016/j.revpalbo.2011.10.004
- Hill, R.S., Truswell, E.M., McLoughlin, S., and Dettmann, M.E., 1999, Evolution of the Australian flora: Fossil evidence, in Orchard, A.E., ed., Flora of Australia. Vol. 1: Melbourne, CSIRO Publishing, p. 251–320.
  Hochuli, P.A., 2016, Interpretation of "fungal spikes" in
- Hochuli, P.A., 2016, Interpretation of "fungal spikes" in Permian–Triassic boundary sections: Global and Planetary Change, v. 144, p. 48–50, https://doi.org/10.1016/ i.gloplacha.2016.05.002.
- Hochuli, P.A., and Vigran, J.O., 2010, Climate variations in the Boreal Triassic — Inferred from palynological records from the Barents Sea: Palaeogeography, Palaeoclimatology, Palaeoecology, v. 290, p. 20–42, https:// doi.org/10.1016/j.palaeo.2009.08.013.
- Hochuli, P.A., Hermann, E., Vigran, J.O., Bucher, H., and Weissert, H., 2010, Rapid demise and recovery of plant ecosystems across the end-Permian extinction event: Global and Planetary Change, v. 74, p. 144–155, https://doi.org/10.1016/ j.gloplacha.2010.10.004.
- Holdgate, G.R., McLoughlin, S., Drinnan, A.N., Finkelman, R.B., Willett, J.C., and Chiehowsky, L.A., 2005, Inorganic chemistry, petrography and palaeobotany of Permian coals in the Prince Charles Mountains, East Antarctica: International Journal of Coal Geology, v. 63, p. 156–177, https://doi.org/10.1016/j.coal.2005.02.011.
- Holmes, W.B.K., 1995, The Late Permian megafossil flora from Cooyal, New South Wales, Australia: Birbal Sahni Centenary Volume, p. 123–152.
- Holmes, W.B.K., and Ash, S.R., 1979, An Early Triassic megafossil flora from the Lorne Basin, New South Wales: Proceedings of the Linnean Society of New South Wales, v. 103, p. 48–70.
- Hounslow, M.W., and Nawrocki, J., 2008, Palaeomagnetism and magnetostratigraphy of the Permian and Triassic of Spitsbergen: A review of progress and challenges: Polar Research, v. 27, p. 502–522, https://doi.org/10.1111/ j.1751-8369.2008.00075.x.
- Jin, Y.G., Wang, Y., Wang, W., Shang, Q.H., Cao, C.Q., and Erwin, D.H., 2000, Pattern of marine mass extinction near the Permian-Triassic boundary in South China: Science, v. 289, p. 432–436, https://doi.org/10.1126/ science.289.5478.432.
- Kaiho, K., Kajiwara, Y., Nakano, T., Miura, Y., Kawahata, H., Tazaki, K., Ueshima, M., Chen, Z., and Shi, G.R., 2001, End-Permian catastrophe by a bolide impact: Evidence of a gigantic release of sulfur from the mantle: Geology, v. 29, p. 815–818, https://doi.org/10.1130/0091-7613(2001)029<0815:EPCBAB>2.0.CO;2.
- Kear, B.P., 2009, Proterosuchid archosaur remains from the Early Triassic Bulgo Sandstone of Long Reef, New South Wales: Alcheringa, v. 33, p. 331–337, https://doi .org/10.1080/03115510903270944.
- King, G.M., 1990, The Dicynodonts: A Study in Palaeobiology: London, Chapman & Hall, 233 p.
- Korte, C., and Kozur, H.W., 2010, Carbon-isotope stratigraphy across the Permian-Triassic boundary: A review: Journal of Asian Earth Sciences, v. 39, p. 215–235, https://doi.org/10.1016/j.jseaes.2010.01.005.
- Labandeira, C.C., 2005, The fossil record of insect extinction: New approaches and future directions: American Entomologist, v. 51, p. 14–29, https://doi.org/10.1093/ ae/51.1.14.
- Larsson, L.M., 2009, Palynostratigraphy of the Triassic–Jurassic transition in southern Sweden: GFF, v. 131, p. 147–163, https://doi.org/10.1080/11035890902924828.

- Laurie, J.R., Bodorkos, S., Nicoll, R.S., Crowley, J.L., Mantle, D.J., Mory, A.J., Wood, G.R., Backhouse, J., Holmes, E.K., Smith, T.E., and Champion, D.C., 2016, Calibrating the middle and Late Permian palynostratigraphy of Australia to the geologic time-scale via U-Pb zircon CA-ID-TIMS dating: Australian Journal of Earth Sciences, v. 63, p. 701-730, https://doi.org/10.1080/08 120099.2016.1233456.
- Lei, Y., Servais, T., Feng, Q., and He, W., 2012, The spatial (nearshore-offshore) distribution of latest Permian phytoplankton from the Yangtze Block, South China: Palaeogeography, Palaeoclimatology, Palaeocology, v. 363–364, p. 151–162, https://doi.org/10.1016/j.palaeo.2012.09.010.
- Lei, Y., Shen, J., Algeo, T.J., Servais, T., Feng, Q., and Yu, J., 2019, Phytoplankton (acritarch) community changes during the Permian-Triassic transition in South China: Palaeogeography, Palaeoclimatology, Palaeoecology, v. 519, p. 84–94, https://doi.org/10.1016/ j.palaeo.2018.09.033.
- Lesnikowska, A.D., and Willard, D.A., 1997, Two new species of *Scolecopteris* (Marattiales), sources of *Torispora securis* Balme and *Thymospora thiessenii* (Kosanke) Wilson et Venkatachala: Review of Palaeobotany and Palynology, v. 95, p. 211–225, https://doi.org/10.1016/S0034-6667(96)00035-8.
- Lindström, S., and McLoughlin, S., 2007, Synchronous palynofloristic extinction and recovery after the end-Permian event in the Prince Charles Mountains, Antarctica: Implications for palynofloristic turnover across Gondwana: Review of Palaeobotany and Palynology, v. 145, p. 89–122, https://doi.org/10.1016/ j.revpalbo.2006.09.002.
- Lindström, S., McLoughlin, S., and Drinnan, A.N., 1997, Intraspecific variation of taeniate bisaccate pollen within Permian glossopterid sporangia, from the Prince Charles Mountains, Antarctica: International Journal of Plant Sciences, v. 158, p. 673–684, https:// doi.org/10.1086/297479.
- Lindström, S., Bjerager, M., Alsen, P., Sanei, H., and Bojesen-Koefoed, J., 2019, The Smithian–Spathian boundary in North Greenland: Implications for extreme global climate changes: Geological Magazine, https://doi.org/10.1017/S0016756819000669.
- Looy, C.V., Twitchett, R.J., Dilcher, D.L., van Konijnenburg-van Cittert, J.H.A., and Visscher, H., 2001, Life in the end-Permian dead zone: Proceedings of the National Academy of Sciences of the United States of America, v. 98, p. 7879–7883, https://doi.org/10.1073/ pnas.131218098.
- Mägdefrau, K., 1931, Zur Morphologie und phylogenetischen Bedeutung der fossilen Pflanzengattung Pleuromeia: Beihefte zum Botanischen Centralblatt 2, v. 48, p. 119–140.
- Mantle, D.J., Kelman, A.P., Nicoll, R.S., and Laurie, J.R., 2010, Australian Biozonation Chart 2010. Part 1: Australian and Selected International Biozonation Schemes Tied to the GTS 2004 Geological Timescale: Canberra, Geoscience Australia.
- McElwain, J.C., and Punyasena, S.W., 2007, Mass extinction events and the plant fossil record: Trends in Ecology & Evolution, v. 22, p. 548–557, https://doi.org/10.1016/j.tree.2007.09.003.
- McElwain, J.C., Beerling, D.J., and Woodward, F.I., 1999, Fossil plants and global warming at the Triassic–Jurassic boundary: Science, v. 285, p. 1386–1390, https://doi.org/10.1126/science.285.5432.1386.
- McElwain, J.C., Wade-Murphy, J., and Hesselbo, S.P., 2005, Changes in carbon dioxide during an oceanic anoxic event linked to intrusion into Gondwana coals: Nature, v. 435, p. 479–482, https://doi.org/10.1038/nature03618
- McLoughlin, S., 2011, *Glossopteris*—insights into the architecture and relationships of an iconic Permian Gondwanan plant: Journal of the Botanical Society of Bengal, v. 65, p. 1–14.
- McLoughlin, S., Lindström, S., and Drinnan, A.N., 1997, Gondwanan floristic and sedimentological trends during the Permian-Triassic transition: New evidence from the Amery Group, northern Prince Charles Mountains, East Antarctica: Antarctic Science, v. 9, p. 281–298, https://doi.org/10.1017/S0954102097000370.

- McLoughlin, S., Maksimenko, A., and Mays, C., 2019, A new high-paleolatitude late Permian permineralized peat flora from the Sydney Basin, Australia: International Journal of Plant Sciences, v. 180, p. 513–539, https://doi.org/10.1086/702939.
- McManus, H.A., Taylor, E.L., Taylor, T.N., and Collinson, J.W., 2002, A petrified *Glossopteris* flora from Collinson Ridge, central Transantarctic Mountains: Late Permian or Early Triassic?: Review of Palaeobotany and Palynology, v. 120, p. 233–246, https://doi.org/10.1016/S0034-6667(02)00078-7.
- Mei, S.-I., Zhang, K.-x., and Wardlaw, B.R., 1998, A refined succession of Changhsingian and Griesbachian neogondolellid conodonts from the Meishan section, candidate of the Global Stratotype Section and Point of the Permian–Triassic boundary: Palaeogeography, Palaeoclimatology, Palaeoecology, v. 143, p. 213–226, https://doi .org/10.1016/S0031-0182(98)00112-6.
- Metcalfe, I., 2011, Palaeozoic-Mesozoic history of SE Asia, in Hall, R., Cottam, M., and Wilson, M., eds., The SE Asian Gateway: History and Tectonics of Australia-Asia Collision: Geological Society, London, Special Publication 355, p. 7–35.
- Metcalfe, I., and Nicoll, R.S., 2007, Conodont biostratigraphic control on transitional marine to non-marine Permian–Triassic boundary sequences in Yunnan–Guizhou, China: Palaeogeography, Palaeoclimatology, Palaeoecology, v. 252, p. 56–65, https://doi.org/10.1016/j.palaeo.2006.11.034.
- Metcalfe, I., Crowley, J.L., Nicoll, R.S., and Schmitz, M., 2015, High-precision U-Pb CA-TIMS calibration of Middle Permian to Lower Triassic sequences, mass extinction and extreme climate-change in eastern Australian Gondwana: Gondwana Research, v. 28, p. 61–81, https://doi.org/10.1016/j.gr.2014.09.002.
- Michaelsen, P., 2002, Mass extinction of peat-forming plants and the effect on fluvial styles across the Permian-Triassic boundary, northern Bowen Basin, Australia: Palaeogeography, Palaeoclimatology, Palaeoecology, v. 179, p. 173–188, https://doi.org/10.1016/S0031-0182(01)00413-8.
- Michaelsen, P., Henderson, R.A., Crosdale, P.J., and Mikkelsen, S.O., 2000, Facies architecture and depositional dynamics of the Upper Permian Rangal Coal Measures, Bowen Basin, Australia: Journal of Sedimentary Research, v. 70, p. 879–895, https://doi.org/10.1306/2DC4093F-0E47-11D7-8643000102C1865D.
- Miller, M.F., Knepprath, N.E., Cantrill, D.J., Francis, J.E., and Isbell, J.L., 2016, Highly productive polar forests from the Permian of Antarctica: Palaeogeography, Palaeoclimatology, Palaeoecology, v. 441, p. 292–304, https://doi.org/10.1016/j.palaeo.2015.06.016.
- Minchin, P., 1987, An evaluation of the relative robustness of techniques for ecological ordination, in Prentice, I.C., and van der Maarel, E., eds., Theory and Models in Vegetation Science: Dordrecht, Springer, Advances in Vegetation Science, v. 8, p. 89–107.
- Mishra, S., Jha, N., Stebbins, A., Brookfield, M., and Hannigan, R., 2019, Palaeoenvironments, flora, and organic carbon and nitrogen isotope changes across the non-marine Permian-Triassic boundary at Wybung Head, Australia: Palaeogeography, Palaeoclimatology, Palaeoecology, v. 534, p. 109292, https://doi.org/10.1016/j.palaeo.2019.109292.
- Morante, R., 1996, Permian and Early Triassic isotopic records of carbon and strontium in Australia and a scenario of events about the Permian-Triassic boundary: Historical Biology, v. 11, p. 289–310, https://doi .org/10.1080/10292389609380546.
- Morbelli, M.A., and Petriella, B., 1973, "Austrostrobus ornatum" nov. gen. et sp. cono petrificado de Lycopsida del Triasico de Santa Cruz (Argentina): Revista del Museo de La Plata, Nueva Serie: Sección Paleontología, v. 7, p. 279–289.
- Newell, A.J., Sennikov, A.G., Benton, M.J., Molostovskaya, I.I., Golubev, V.K., Minikh, A.V., and Minikh, M.G., 2010, Disruption of playa-lacustrine depositional systems at the Permo-Triassic boundary: Evidence from Vyazniki and Gorokhovets on the Russian Platform: Journal of the Geological Society, v. 167, p. 695–716, https://doi.org/10.1144/0016-76492009-103.

- Nichols, D.J., and Johnson, K.R., 2008, Plants and the K-T Boundary: Cambridge, Cambridge University Press, 280 p., https://doi.org/10.1017/CBO9780511535536.
- Niedźwiedzki, G., Bajdek, P., Owocki, K., and Kear, B.P., 2016, An Early Triassic polar predator ecosystem revealed by vertebrate coprolites from the Bulgo Sandstone (Sydney Basin) of southeastern Australia: Palaeogeography, Palaeoclimatology, Palaeoecology, v. 464, p. 5–15, https://doi.org/10.1016/ j.palaeo.2016.04.003.
- Northwood, C., 1999, Actinopterygians from the Early Triassic Arcadia Formation, Queensland, Australia: Memoirs of the Queensland Museum, v. 43, p. 787–796.
- Northwood, C., 2005, Early Triassic coprolites from Australia and their palaeobiological significance: Palaeontology, v. 48, p. 49–68, https://doi.org/10.1111/j.1475-4983.2004.00432.x.
- Nowak, H., Schneebeli-Hermann, E., and Kustatscher, E., 2019, No mass extinction for land plants at the Permian-Triassic transition: Nature Communications, v. 10, no. 384, https://doi.org/10.1038/s41467-018-07945-w.
- Ogg, J.G., 2012, Triassic, in Gradstein, F.M., Ogg, J.G., Schmitz, M.D., and Ogg, G.M., eds., The Geologic Time Scale 2012: London, Elsevier, p. 681–730, https:// doi.org/10.1016/B978-0-444-59425-9.00025-1.
- Ovtcharova, M., Bucher, H., Schaltegger, U., Galfetti, T., Brayard, A., and Guex, J., 2006, New Early to Middle Triassic U–Pb ages from South China: Calibration with ammonoid biochronozones and implications for the timing of the Triassic biotic recovery: Earth and Planetary Science Letters, v. 243, p. 463–475, https://doi.org/10.1016/j.epsl.2006.01.042.
- Pace, D.W., Gastaldo, R.A., and Neveling, J., 2009, Early Triassic aggradational and degradational landscapes of the Karoo Basin and evidence for climate oscillation following the P-Tr event: Journal of Sedimentary Research, v. 79, p. 316–331, https://doi.org/10.2110/ jsr.2009.036.
- Pant, D.D., and Pant, R., 1987, Some Glossopteris leaves from Indian Triassic beds: Palaeontographica Abteilung B, v. 205, p. 165–178.
- Payne, J.L., and Clapham, M.E., 2012, End-Permian mass extinction in the oceans: An ancient analog for the twenty-first century?: Annual Review of Earth and Planetary Sciences, v. 40, p. 89–111, https://doi. org/10.1146/annurev-earth-042711-105329.
- Payne, J.L., and Kump, L.R., 2007, Evidence for recurrent Early Triassic massive volcanism from quantitative interpretation of carbon isotope fluctuations: Earth and Planetary Science Letters, v. 256, p. 264–277, https:// doi.org/10.1016/j.epsl.2007.01.034.
- Payne, J., and van de Schootbrugge, B., 2007, Life in Triassic oceans: Links between benthic and planktonic recovery and radiation, in Falkowski, P.G., and Knoll, A.H., eds., The Evolution of Primary Producers in the Sea: New York, Academic Press, p. 165–189, https://doi.org/10.1016/B978-012370518-1/50010-2.
- Payne, J.L., Lehrmann, D.J., Wei, J., Orchard, M.J., Schrag, D.P., and Knoll, A.H., 2004, Large perturbations of the carbon cycle during recovery from the end-Permian extinction: Science, v. 305, p. 506–509, https://doi .org/10.1126/science.1097023.
- Pfefferkorn, H.W., and Thomson, M., 1982, Changes in dominance patterns in Upper Carboniferous plantfossil assemblages: Geology, v. 10, p. 641–644, https:// doi.org/10.1130/0091-7613(1982)10<641:CIDPIU>2. 0 CO:2
- Phillips, L.J., Crowley, J.L., Mantle, D.J., Esterle, J.S., Nicoll, R.S., McKellar, J.L., and Wheeler, A., 2018, U-Pb geochronology and palynology from Lopingian (upper Permian) coal measure strata of the Galilee Basin, Queensland, Australia: Australian Journal of Earth Sciences, v. 65, p. 153–173, https://doi.org/10.1080/08 120099.2018.1418431.
- Pigg, K.B., and McLoughlin, S., 1997, Anatomically preserved Glossopteris leaves from the Bowen and Sydney basins, Australia: Review of Palaeobotany and Palynology, v. 97, p. 339–359, https://doi.org/10.1016/S0034-6667(97)00007-9.
- Pigg, K.B., and Taylor, T.N., 1993, Anatomically preserved Glossopteris stems with attached leaves from the central Transantarctic Mountains, Antarctica: American

- Journal of Botany, v. 80, p. 500–516, https://doi.org/10.1002/j.1537-2197.1993.tb13833.x.
- Prevec, R., Labandeira, C.C., Neveling, J., Gastaldo, R.A., Looy, C.V., and Bamford, M., 2009, Portrait of a Gondwanan ecosystem: A new late Permian fossil locality from KwaZulu-Natal, South Africa: Review of Palaeobotany and Palynology, v. 156, p. 454–493, https://doi .org/10.1016/j.revpalbo.2009.04.012.
- Prevec, R., Gastaldo, R.A., Neveling, J., Reid, S.B., and Looy, C.V., 2010, An autochthonous glossopterid flora with latest Permian palynomorphs and its depositional setting in the *Dicynodon* Assemblage Zone of the southern Karoo Basin, South Africa: Palaeogeography, Palaeoclimatology, Palaeoecology, v. 292, p. 391–408, https://doi.org/10.1016/j.palaeo.2010.03.052.
- Price, P.L., 1983, A Permian palynostratigraphy for Queensland, in Murray, C.G., ed., Proceedings of the Symposium on the Permian Geology of Queensland: Brisbane, Geological Society of Australia, Queensland Division, p. 155–212.
- Price, P.L., 1997, Permian to Jurassic palynostratigraphic nomenclature of the Bowen and Surat basins, in Green, P.M., ed., The Surat and Bowen Basins, Southeast Queensland: Brisbane, Australia, Queensland Department of Mines and Energy, p. 137–178.
- Rampino, M.R., and Eshet, Y., 2018, The fungal and acritarch events as time markers for the latest Permian mass extinction: An update: Geoscience Frontiers, v. 9, p. 147–154, https://doi.org/10.1016/j.gsf.2017.06.005.
- Raup, D.M., and Sepkoski, J.J., 1982, Mass extinctions in the marine fossil record: Science, v. 215, p. 1501–1503, https://doi.org/10.1126/science.215.4539.1501.
- Rayner, R.J., 1992, Phyllotheca: The pastures of the Late Permian: Palaeogeography, Palaeoclimatology, Palaeoecology, v. 92, p. 31–40, https://doi.org/10.1016/0031-0182(92)90133-P.
- Retallack, G.J., 1975, The life and times of a Triassic lycopod: Alcheringa, v. 1, p. 3–29, https://doi.org/10.1080/03115517508619477.
- Retallack, G.J., 1980, Late Carboniferous to Middle Triassic megafossil floras from the Sydney Basin, in Helby, R., and Herbert, C., eds., Geology of the Sydney Basin, New South Wales Geological Survey Bulletin, v. 26, p. 384–430.
- Retallack, G.J., 1996, Early Triassic therapsid footprints from the Sydney Basin, Australia: Alcheringa, v. 20, p. 301– 314, https://doi.org/10.1080/03115519608619473.
- Retallack, G.J., 1999, Post-apocalyptic greenhouse paleoclimate revealed by earliest Triassic paleosols in the Sydney Basin, Australia: Geological Society of America Bulletin, v. 111, p. 52–70, https:// doi.org/10.1130/0016-7606(1999)111<0052:PGPRBE >2.3.CO:2.
- Retallack, G.J., 2002, Lepidopteris callipteroides, an earliest Triassic seed fern of the Sydney Basin, southeastern Australia: Alcheringa, v. 26, p. 475–500, https://doi.org/10.1080/03115510208619538.
- Retallack, G.J., 2009, Greenhouse crises of the past 300 million years: Geological Society of America Bulletin, v. 121, p. 1441–1455, https://doi.org/10.1130/ B26341.1.
- Retallack, G.J., and Krull, E.S., 1999, Landscape ecological shift at the Permian-Triassic boundary in Antarctica: Australian Journal of Earth Sciences, v. 46, p. 785–812, https://doi.org/10.1046/j.1440-0952.1999.00745.x.
- Retallack, G.J., Renne, P.R., and Kimbrough, D.L., 1993, New radiometric ages for Triassic floras of southeast Gondwana, in Lucas, S.G., and Morales, M., eds., The Nonmarine Triassic: Albuquerque, New Mexico Museum of Natural History, New Mexico Museum of Natural History and Science Bulletin, v. 3, p. 415–418.
- Retallack, G.J., Veevers, J.J., and Morante, R., 1996, Global coal gap between Permian—Triassic extinction and Middle Triassic recovery of peat-forming plants: Geological Society of America Bulletin, v. 108, p. 195–207, https://doi.org/10.1130/0016-7606(1996)108<0195:GCGBPT >2.3.CO;2.
- Retallack, G.J., Smith, R.M.H., and Ward, P.D., 2003, Vertebrate extinction across Permian–Triassic boundary in Karoo Basin, South Africa: Geological Society of America Bulletin, v. 115, p. 1133–1152, https://doi.org/10.1130/B25215.1.

- Retallack, G.J., Jahren, A.H., Sheldon, N.D., Chakrabarti, R., Metzger, C.A., and Smith, R.M.H., 2005, The Permian–Triassic boundary in Antarctica: Antarctic Science, v. 17, p. 241–258, https://doi.org/10.1017/ S0954102005002658.
- Retallack, G.J., Sheldon, N.D., Carr, P.F., Fanning, M., Thompson, C.A., Williams, M.L., Jones, B.G., and Hutton, A., 2011, Multiple Early Triassic greenhouse crises impeded recovery from Late Permian mass extinction: Palaeogeography, Palaeoclimatology, Palaeoecology, v. 308, p. 233–251, https://doi.org/10.1016/ j.palaeo.2010.09.022.
- Saito, T., Yamanoi, T., and Kaiho, K., 1986, End-Cretaceous devastation of terrestrial flora in the boreal Far East: Nature, v. 323, p. 253–255, https://doi.org/10.1038/323253a0.
- Sarjeant, W.A.S., Kummel, B., and Teichert, C., 1970, Acritarchs and tasmanitids from the Chhidru Formation, uppermost Permian of West Pakistan, Stratigraphical Boundary Problems: Permian and Triassic of West Pakistan: Lawrence, University of Kansas, Department of Geology, Special Publication 4, p. 277–304.
- Sarkar, A., Yoshioka, H., Ebihara, M., and Naraoka, H., 2003, Geochemical and organic carbon isotope studies across the continental Permo-Triassic boundary of Raniganj Basin, eastern India: Palaeogeography, Palaeoclimatology, Palaeoecology, v. 191, p. 1–14, https:// doi.org/10.1016/S0031-0182(02)00636-3.
- Schneebeli-Hermann, E., Hochuli, P.A., Bucher, H., Goudemand, N., Brühwiler, T., and Galfetti, T., 2012, Palynology of the Lower Triassic succession of Tulong, South Tibet—Evidence for early recovery of gymnosperms: Palaeogeography, Palaeoclimatology, Palaeoecology, v. 339–341, p. 12–24, https://doi.org/10.1016/j.palaeo.2012.04.010.
- Schneebeli-Hermann, E., Hochuli, P.A., and Bucher, H., 2017, Palynofloral associations before and after the Permian– Triassic mass extinction, Kap Stosch, East Greenland: Global and Planetary Change, v. 155, p. 178–195, https://doi.org/10.1016/j.gloplacha.2017.06.009.
- Schopf, J.M., 1965, Anatomy of the axis in Vertebraria, in Hadley, J.B., ed., Geology and Paleontology of the Antarctic: Washington, D.C., American Geophysical Union, Antarctic Research Series, v. 6, p. 217–228.
- Schopf, J.M., 1970, Petrified peat from a Permian coal bed in Antarctica: Science, v. 169, p. 274–277, https://doi .org/10.1126/science.169.3942.274.
- Schulte, P., Alegret, L., Arenillas, I., Arz, J.A., Barton, P.J., Bown, P.R., Bralower, T.J., Christeson, G.L., Claeys, P., Cockell, C.S., Collins, G.S., Deutsch, A., Goldin, T.J., Goto, K., Grajales-Nishimura, J.M., Grieve, R.A.F., Gulick, S.P.S., Johnson, K.R., Kiessling, W., Koeberl, C., Kring, D.A., MacLeod, K.G., Matsui, T., Melosh, J., Montanari, A., Morgan, J.V., Neal, C.R., Nichols, D.J., Norris, R.D., Pierazzo, E., Ravizza, G., Rebolledo-Vieyra, M., Reimold, W.U., Robin, E., Salge, T., Speijer, R.P., Sweet, A.R., Urrutia-Fucugauchi, J., Vajda, V., Whalen, M.T., and Willumsen, P.S., 2010, The Chicxulub asteroid impact and mass extinction at the Cretaceous-Paleogene Boundary: Science, v. 327, p. 1214–1218, https://doi.org/10.1126/science.1177265.
- Sephton, M.A., Looy, C.V., Brinkhuis, H., Wignall, P.B., Leeuw, J.W.d., and Visscher, H., 2005, Catastrophic soil erosion during the end-Permian biotic crisis: Geology, v. 33, p. 941–944, https://doi.org/10.1130/G21784.1.
- Sheldon, N.D., 2005, Do red beds indicate paleoclimatic conditions?: A Permian case study: Palaeogeography, Palaeoclimatology, Palaeoecology, v. 228, p. 305–319, https://doi.org/10.1016/j.palaeo.2005.06.009.
- Sheldon, N.D., 2006, Abrupt chemical weathering increase across the Permian–Triassic boundary: Palaeogeography, Palaeoclimatology, Palaeoecology, v. 231, p. 315– 321, https://doi.org/10.1016/j.palaeo.2005.09.001.
- Shen, J., Lei, Y., Algeo, T.J., Feng, Q., Servais, T., Yu, J., and Zhou, L., 2013, Volcanic effects on microplankton during the Permian-Triassic transition (Shangsi and Xinmin, South China): Palaios, v. 28, p. 552–567, https:// doi.org/10.2110/palo.2013.p13-014r.
- Shen, S.-z., Crowley, J.L., Wang, Y., Bowring, S.A., Erwin, D.H., Sadler, P.M., Cao, C.-q., Rothman, D.H., Henderson, C.M., Ramezani, J., Zhang, H., Shen, Y., Wang, X.-d., Wang, W., Mu, L., Li, W.-z., Tang, Y.-g.,

- Liu, X.-l., Liu, L.-j., Zeng, Y., Jiang, Y.-f., and Jin, Y.-g., 2011, Calibrating the End-Permian mass extinction: Science, v. 334, p. 1367–1372, https://doi.org/10.1126/science.1213454.
- Shi, G.R., Waterhouse, J.B., and McLoughlin, S., 2010, The Lopingian of Australasia: A review of biostratigraphy, correlations, palaeogeography and palaeobiogeography: Geological Journal, v. 45, p. 230–263, https://doi .org/10.1002/gi.1213.
- Shibaoka, M., and Smyth, M., 1975, Coal petrology and the formation of coal seams in some Australian sedimentary basins: Economic Geology and the Bulletin of the Society of Economic Geologists, v. 70, p. 1463–1473, https://doi.org/10.2113/gsecongeo.70.8.1463.
- Slater, S.M., and Wellman, C.H., 2015, A quantitative comparison of dispersed spore/pollen and plant megafossil assemblages from a Middle Jurassic plant bed from Yorkshire, UK: Paleobiology, v. 41, p. 640–660, https://doi.org/10.1017/pab.2015.27.
- Slater, B.J., McLoughlin, S., Hilton, J., 2012, Animal-plant interactions in a Middle Permian permineralised peat of the Bainmedart Coal Measures, Prince Charles Mountains, Antarctica: Palaeogeography Palaeoclimatology Palaeoecology, v. 363-364, p. 109–126.
- Slater, B.J., McLoughlin, S., and Hilton, J., 2015, A high-latitude Gondwanan lagerstätte: The Permian permineralised peat biota of the Prince Charles Mountains, Antarctica: Gondwana Research, v. 27, p. 1446–1473, https://doi.org/10.1016/j.gr.2014.01.004.
- Slater, S.M., Twitchett, R.J., Danise, S., and Vajda, V., 2019, Substantial vegetation response to Early Jurassic global warming with impacts on oceanic anoxia: Nature Geoscience, v. 12, p. 462–467, https://doi.org/10.1038/ s41561-019-0349-z.
- Smith, R.M.H., and Botha-Brink, J., 2014, Anatomy of a mass extinction: Sedimentological and taphonomic evidence for drought-induced die-offs at the Permo-Triassic boundary in the main Karoo Basin, South Africa: Palaeogeography, Palaeoclimatology, Palaeoecology, v. 396, p. 99–118, https://doi.org/10.1016/ j.palaeo.2014.01.002.
- Song, H., Wignall, P.B., Tong, J., and Yin, H., 2013, Two pulses of extinction during the Permian–Triassic crisis: Nature Geoscience, v. 6, p. 52–56, https://doi .org/10.1038/ngeo1649.
- Song, H., Wignall, P.B., Chu, D., Tong, J., Sun, Y., Song, H., He, W., and Tian, L., 2014, Anoxia/high temperature double whammy during the Permian-Triassic marine crisis and its aftermath: Scientific Reports, v. 4, no. 4132, https://doi.org/10.1038/srep04132.
- Spina, A., Cirilli, S., Utting, J., and Jansonius, J., 2015, Palynology of the Permian and Triassic of the Tesero and Bulla sections (Western Dolomites, Italy) and consideration about the enigmatic species *Redu*viasporonites chalastus: Review of Palaeobotany and Palynology, v. 218, p. 3–14, https://doi.org/10.1016/ j.revpalbo.2014.10.003.
- Stanley, S.M., 2016, Estimates of the magnitudes of major marine mass extinctions in earth history: Proceedings of the National Academy of Sciences of the United States of America, v. 113, p. E6325–E6334, https://doi .org/10.1073/pnas.1613094113.
- Steinthorsdottir, M., Jeram, A.J., and McElwain, J.C., 2011, Extremely elevated CO<sub>2</sub> concentrations at the Triassic/ Jurassic boundary: Palaeogeography, Palaeoclimatology, Palaeoecology, v. 308, p. 418–432, https://doi.org/10.1016/j.palaeo.2011.05.050.
- Stephenson, M.H., 2018, Permian palynostratigraphy: A global overview, in Lucas, S.G., and Shen, S.Z., eds., The Permian Timescale: Geological Society, London, Special Publication 450, p. 321–347.
- Suan, G., Mattioli, E., Pittet, B., Lécuyer, C., Suchéras-Marx, B., Duarte, L.V., Philippe, M., Reggiani, L., and Martineau, F., 2010, Secular environmental precursors to Early Toarcian (Jurassic) extreme climate changes: Earth and Planetary Science Letters, v. 290, p. 448–458, https://doi.org/10.1016/j.epsl.2009.12.047.
- Sweet, A.R., and Braman, D.R., 1992, The K-T boundary and the contiguous strata in western Canada: Interactions between paleoenvironments and palynological assemblages: Cretaceous Research, v. 13, p. 31–79, https://doi.org/10.1016/0195-6671(92)90027-N.

- Tadros, N.Z., 1995, Sydney-Gunnedah Basin overview, in Ward, C.R., Harrington, H.J., Mallett, C.W., and Beeston, J.W., eds., Geology of Australian Coal Basins: Sydney, Geological Society of Australia, Coal Geology Group, Special Publication 1, p. 163–175.
- Taylor, E.L., Taylor, T.N., and Collinson, J.W., 1989, Depositional setting and paleobotany of Permian and Triassic permineralized peat from the central Transantarctic Mountains, Antarctica: International Journal of Coal Geology, v. 12, p. 657–679, https://doi .org/10.1016/0166-5162(89)90068-2.
- Taylor, E.L., Taylor, T.N., and Cuneo, N.R., 1992, The present is not the key to the past: A polar forest from the Permian of Antarctica: Science, v. 257, p. 1675–1677, https://doi.org/10.1126/science.257.5077.1675.
- Taylor, G.K., Tucker, C., Twitchett, R.J., Kearsey, T., Benton, M.J., Newell, A.J., Surkov, M.V., and Tverdokhlebov, V.P., 2009, Magnetostratigraphy of Permian/Triassic boundary sequences in the Cis-Urals, Russia: No evidence for a major temporal hiatus: Earth and Planetary Science Letters, v. 281, p. 36–47, https://doi .org/10.1016/j.epsl.2009.02.002.
- Thulborn, R.A., 1986, Early Triassic tetrapod faunas of southeastern Gondwana: Alcheringa, v. 10, p. 297–313, https://doi.org/10.1080/03115518608619160.
- Townrow, J.A., 1965, On Lepidopteris madagascariensis Carpentier (Peltaspermaceae): Journal and Proceedings of the Royal Society of New South Wales, v. 98, p. 203–214.
- Townrow, J.A., 1967a, On Voltziopsis, a southern conifer of Lower Triassic age: Papers and Proceedings of the Royal Society of Tasmania, v. 101, p. 173–188.
- Townrow, J.A., 1967b, On Rissikia and Mataia, podocarpaceous conifers from the lower Mesozoic of southern lands: Papers and Proceedings of the Royal Society of Tasmania, v. 101, p. 103–138.
- Townrow, J.A., 1968, A fossil *Selaginella* from the Permian of New South Wales: Journal of the Linnean Society: Botany, v. 61, p. 13–23.
- Tripathi, A., 1997, Representation of acritarchs across the Permian–Triassic boundary in India: The Palaeobotanist, v. 46, p. 112–117.
- Twitchett, R.J., Looy, C.V., Morante, R., Visscher, H., and Wignall, P.B., 2001, Rapid and synchronous collapse of marine and terrestrial ecosystems during the end-Permian biotic crisis: Geology, v. 29, p. 351–354, https://doi .org/10.1130/0091-7613(2001)029<0351:RASCOM>2 .0.CO;2.
- Vajda, V., and Bercovici, A., 2014, The global vegetation pattern across the Cretaceous–Paleogene mass extinction interval: A template for other extinction events: Global and Planetary Change, v. 122, p. 29–49, https://doi. org/10.1016/j.gloplacha.2014.07.014.
- Vajda, V., and McLoughlin, S., 2007, Extinction and recovery patterns of the vegetation across the Cretaceous–Palaeogene boundary—A tool for unravelling the causes of the end-Permian mass-extinction: Review of Palaeobotany and Palynology, v. 144, p. 99–112, https://doi .org/10.1016/j.revpalbo.2005.09.007.
- Vajda, V., Raine, J.I., and Hollis, C.J., 2001, Indication of global deforestation at the Cretaceous-Tertiary boundary by New Zealand fern spike: Science, v. 294, p. 1700–1702, https://doi.org/10.1126/science.1064706.
- Vajda, V., McLoughlin, S., Mays, C., Frank, T., Fielding, C.R., Tevyaw, A., Lehsten, V., Bocking, M., Nicoll, R.S., 2020, End-Permian (252 Mya) deforestation, wildfires and flooding—an ancient biotic crisis with lessons for the present: Earth and Planetary Science Letters, v. 529, https://doi.org/10.1016/j.epsl.2019.115875.
- van de Schootbrugge, B., and Gollner, S., 2013, Altered primary production during mass-extinction events, in Bush, A.M., Pruss, S.B., and Payne, J.L., eds., Ecosystem Paleobiology and Geobiology: Bethesda, The Paleontological Society, The Paleontological Society Papers, v. 19, p. 87–114.
- Van Houten, F.B., 1973, Origin of red beds: A review—1961–1972: Annual Review of Earth and Planetary Sciences, v. 1, p. 39–61, https://doi.org/10.1146/annurev.ea.01.050173.000351.
- Veevers, J.J., 2006, Updated Gondwana (Permian-Cretaceous) earth history of Australia: Gondwana Re-

- search, v. 9, p. 231–260, https://doi.org/10.1016/j.gr.2005.11.005.
- Venkatachala, B.S., and Kar, R.K., 1968, Palynology of the Karanpura sedimentary Basin, Bihar, India–Barakar Stage at Badam: The Palaeobotanist, v. 16, p. 56–90.
- Viglietti, P.A., Smith, R.M.H., and Compton, J.S., 2013, Origin and palaeoenvironmental significance of Lystrosaurus bonebeds in the earliest Triassic Karoo Basin, South Africa: Palaeogeography, Palaeoclimatology, Palaeoecology, v. 392, p. 9–21, https://doi .org/10.1016/j.palaeo.2013.08.015.
- Visscher, H., Brinkhuis, H., Dilcher, D.L., Elsik, W.C., Eshet, Y., Looy, C.V., Rampino, M.R., and Traverse, A., 1996, The terminal Paleozoic fungal event: Evidence of terrestrial ecosystem destabilization and collapse: Proceedings of the National Academy of Sciences of the United States of America, v. 93, p. 2155–2158, https://doi.org/10.1073/pnas.93.5.2155.
- Walkom, A.B., 1925, Fossil plants from the Narrabeen Stage of the Hawkesbury Series: Proceedings of the Linnean Society of New South Wales, v. 50, p. 214–224.
- Ward, C.R., 1972, Sedimentation in the Narrabeen Group, southern Sydney Basin, New South Wales: Journal of the Geological Society of Australia, v. 19, p. 393–409, https://doi.org/10.1080/00167617208728809.
- Ward, P.D., Montgomery, D.R., and Smith, R., 2000, Altered river morphology in South Africa related to the Permian–Triassic extinction: Science, v. 289, p. 1740–1743, https://doi.org/10.1126/science.289.5485.1740.
- Ward, P.D., Botha, J., Buick, R., Kock, M.O.D., Erwin, D.H., Garrison, G.H., Kirschvink, J.L., and Smith, R., 2005, Abrupt and gradual extinction among Late Permian land vertebrates in the Karoo Basin, South Africa: Science, v. 307, p. 709–714, https://doi.org/10.1126/ science.1107068.
- Warren, A., 1991, Australian fossil amphibians, in Vickers-Rich, P., Monaghan, J.M., Baird, R.F., and Rich, T.H., eds., Vertebrate Palaeontology of Australasia: Lilydale, Pioneer Design Studio, p. 569–590.
- Warren, A.A., Damiani, R.J., and Yates, A.M., 2006, The South African stereospondyl *Lydekkerina huxleyi*

- (Tetrapoda, Temnospondyli) from the Lower Triassic of Australia: Geological Magazine, v. 143, p. 877–886, https://doi.org/10.1017/S0016756806002524.
- Waschbusch, P., Korsch, R.J., and Beaumont, C., 2009, Geodynamic modelling of aspects of the Bowen, Gunnedah, Surat and Eromanga basins from the perspective of convergent margin processes: Australian Journal of Earth Sciences, v. 56, p. 309–334, https:// doi.org/10.1080/08120090802698661.
- Webb, J.A., and Fielding, C.R., 1993, Permo-Triassic sedimentation within the Lambert Graben, northern Prince Charles Mountains, Antarctica, in Finlay, R.H., Unrug, R., Banks, M.R., and Veevers, J.J., eds., Gondwana Eight: Rotterdam, AA Balkema, p. 357–369.
- Wells, A.T., 1995, Nymboida, Red Cliff and Evans Head Coal Measures, New South Wales, in Ward, C.R., Harrington, H.J., Mallett, C.W., and Beeston, J.W., eds., Geology of Australian Coal Basins: Sydney, Geological Society of Australia, Coal Geology Group, Special Publication 1, p. 529–532.
- Wheeler, A., Wetering, N.V.d., Esterle, J.S., and Götz, A.E., 2019, Palaeoenvironmental changes recorded in the palynology and palynofacies of a Late Permian Marker Mudstone (Galilee Basin, Australia): Palaeoworld, (in press).
- Williams, M.L., Jones, B.G., and Carr, P.F., 2012, Geochemical consequences of the Permian–Triassic mass extinction in a non-marine succession, Sydney Basin, Australia: Chemical Geology, v. 326–327, p. 174–188, https://doi.org/10.1016/j.chemgeo.2012.07.021.
- Williams, M.L., Jones, B.G., and Carr, P.F., 2017, The interplay between massive volcanism and the local environment: Geochemistry of the Late Permian mass extinction across the Sydney Basin, Australia: Gondwana Research, v. 51, p. 149–169, https://doi.org/10.1016/j.gr.2017.07.015.
- Yin, H., Xie, S., Luo, G., Algeo, T.J., and Zhang, K., 2012, Two episodes of environmental change at the Permian–Triassic boundary of the GSSP section Meishan: Earth-Science Reviews, v. 115, p. 163–172, https://doi. org/10.1016/j.earscirev.2012.08.006.

- Zavada, M.S., and Mentis, M.T., 1992, Plant-animal interaction: The effect of Permian megaherbivores on the glossopterid flora: American Midland Naturalist, v. 127, p. 1–12, https://doi.org/10.2307/2426316.
- Zhang, H., Cao, C.-q., Liu, X.-l., Mu, L., Zheng, Q.-f., Liu, F., Xiang, L., Liu, L.-j., and Shen, S.-z., 2016, The terrestrial end-Permian mass extinction in South China: Palaeogeography, Palaeoclimatology, Palaeoecology, v. 448, p. 108–124, https://doi.org/10.1016/ j.palaeo.2015.07.002.
- Zhang, H., Feng, Z., Ramezani, J., and Shen, S.-z., 2018, Comments on "Terrestrial Permian-Triassic boundary in southern China: New stratigraphic, structural and palaeoenvironment considerations" by Bourquin et al. (2018): Palaeogeography, Palaeoclimatology, Palaeoecology, v. 506, p. 254-256, https://doi.org/10.1016/ j.palaeo.2018.02.019.
- Zhang, L., Zhao, L., Chen, Z.-Q., Algeo, T.J., Li, Y., and Cao, L., 2015, Amelioration of marine environments at the Smithian–Spathian boundary, Early Triassic: Biogeosciences, v. 12, p. 1597–1613, https://doi.org/10.5194/ bg-12-1597-2015.
- Zhang, L., Orchard, M.J., Brayard, A., Algeo, T.J., Zhao, L., Chen, Z.-Q., and Lyu, Z., 2019, The Smithian/Spathian boundary (late Early Triassic): A review of ammonoid, conodont, and carbon-isotopic criteria: Earth-Science Reviews, v. 195, p. 7–36, https://doi.org/10.1016/ j.earscirev.2019.02.014.
- Ziqiang, W., and Lixin, W., 1982, A new species of the lycopsid *Pleuromeia* from the Early Triassic of Shanxi, China, and its ecology: Palaeontology, v. 25, p. 215–225.

SCIENCE EDITOR: ROB STRACHAN ASSOCIATE EDITOR: BRIAN PRATT

Manuscript Received 10 May 2019 Revised Manuscript Received 4 September 2019 Manuscript Accepted 14 October 2019

Printed in the USA